RECLAMATION
Managing Water in the West

Report DSO-2013-02

Extreme Floods in a Changing Climate

Dam Safety Technology Development Program

1. REPORT DATE *09-30-2013*	2. REPORT TYPE Research	3. DATES COVERED *(From - To)*

4. TITLE AND SUBTITLE	5a. CONTRACT NUMBER
Extreme Floods in a Changing Climate	
	5b. GRANT NUMBER
	5c. PROGRAM ELEMENT NUMBER

6. AUTHOR(S)	5d. PROJECT NUMBER
Godaire, J., J. Caldwell, N. Novembre, T. Harden, V. Sankovich	
	5e. TASK NUMBER
	5f. WORK UNIT NUMBER

7. PERFORMING ORGANIZATION NAME(S) AND ADDRESS(ES)	8. PERFORMING ORGANIZATION REPORT NUMBER
US Bureau of Reclamation P.O. Box 25007 Denver Federal Center Denver, CO 80225	DSO-2013-02

9. SPONSORING/MONITORING AGENCY NAME(S) AND ADDRESS(ES)	10. SPONSOR/MONITOR'S ACRONYM(S)
Bureau of Reclamation, Dam Safety Office P.O. Box 25007 Denver, CO 80225	11. SPONSOR/MONITOR'S REPORT NUMBER(S) DSO-2013-02

12. DISTRIBUTION/AVAILABILITY STATEMENT
Available from National Technical Information Service, 5285 Port Royal Road, Springfield, VA 22161

13. SUPPLEMENTARY NOTE

14. ABSTRACT
This study explored the potential connection between extreme floods, streamflow and climate change. The analyses concluded that relationships do exist between records of fluvial deposition and shifts in climate in that less fluvial deposition (or lower streamflow) is occurring during periods of drier climate and more fluvial deposition (or higher streamflow) is occurring during periods of wetter climate in the Sierra Nevada of central California. This relationship can be defined on a broad scale for about the last 1,000 years. Paleofloods that have been documented along rivers in the Sierra Nevada appear to fall within both dry and wet periods in the paleoclimate record. Paleofloods that have been documented in the southwestern U.S. in the Colorado River Basin appear to occur within specific wet or dry periods, depending on the geographic location.

15. SUBJECT TERMS
    climate change, floods, paleofloods, hydroclimatology, meteorology, paleoclimate, hydrology

16. SECURITY CLASSIFICATION OF: **None**			17. LIMITATION OF ABSTRACT	18. NUMBER OF PAGES	19a. NAME OF RESPONSIBLE PERSON Jeanne Godaire
a. REPORT	b. ABSTRACT	a. THIS PAGE			19b. TELEPHONE NUMBER *(Include area code)* 303-445-3164

Report DSO-2013-02

Extreme Floods in a Changing Climate

Dam Safety Technology Development Program

Prepared by:

Jeanne Godaire
Jason Caldwell
Nicole Novembre
Tessa Harden
Victoria Sankovich

MISSION STATEMENTS

The U.S. Department of the Interior protects America's natural resources and heritage, honors our cultures and tribal communities, and supplies the energy to power our future.

The mission of the Bureau of Reclamation is to manage, develop, and protect water and related resources in an environmentally and economically sound manner in the interest of the American public.

BUREAU OF RECLAMATION
Dam Safety Technology Development Program
Seismotectonics and Geophysics Group, 86-68330

DSO-2013-02

Extreme Floods in a Changing Climate

_____   9/23/2013
Prepared by: Jeanne E. Godaire, M.S.   Date
Geomorphologist, Seismotectonics and Geophysics Group, 86-68330
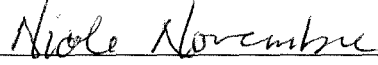
_____   9/25/2013
Prepared by: Jason Caldwell, Ph.D.   Date
Meteorologist, Flood Hydrology and Consequences Group, 86-68250

_____   9/25/2013
Prepared by: Nicole Novembre, P.E., M.S.   Date
Hydraulic Engineer, Flood Hydrology and Consequences Group, 86-68250

_____   9/24/2013
Prepared by: Tessa Harden, Ph.D.   Date
Geomorphologist, Seismotectonics and Geophysics Group, 86-68330

_____   9/25/2013
Prepared by: Victoria Sankovich, M.S.   Date
Meteorologist, Flood Hydrology and Consequences Group, 86-68250

_____   9/23/13
Peer review: Ralph E. Klinger, Ph.D.   Date
Quaternary Geologist, Seismotectonics and Geophysics Group, 86-68330

REVISIONS		Prepared	Checked	Technical approval	Peer review
Date	Description				
3/2013	Draft Report	X			
4/2013	Draft Report				X
9/2013	Final Report	X			

CONTENTS

List of Tables

List of Figures

iv

EXECUTIVE SUMMARY

This report completes a 2-year study of linkages between extreme floods and climate. During this project, radiocarbon data were compiled for regions in the State of California and compared to paleoclimate proxies and reconstructions to determine whether any patterns existed between extreme floods and changes in climate. The Sierra Nevada was the main focus of the analyses since many large floods happen in this region and impact a large portion of the State of California. The analyses concluded that relationships do exist between records of fluvial deposition and shifts in climate in that less fluvial deposition (or lower streamflow) is occurring during periods of drier climate and more fluvial deposition (or higher streamflow) is occurring during periods of wetter climate. This relationship can be defined on a broad scale for about the last 1,000 years. Beyond this point, the resolution of paleoclimate data appears to be too coarse in many cases to compare to the radiocarbon data; in addition, more radiocarbon ages may be needed to better define periods of deposition and landform stability. In any case, the implications for the future are that a drier climate over an extended period will result in smaller annual volumes delivered to Reclamation reservoirs. Therefore, droughts similar to the Medieval Climatic Anomaly (A.D. 950-1250; 1000-700 Cal yr BP) will undoubtedly negatively impact Reclamation's water supply.

Paleofloods that have been documented along rivers in the Sierra Nevada appear to fall within both dry and wet periods in the paleoclimate record and therefore suggest that these broad changes in climate may not be able to predict whether extreme floods will happen or not, but rather it is the short term fluctuations in meteorological phenomena within larger climate shifts that will drive extreme floods and if/where they will increase in severity, or frequency. This project also funded research in the Upper Colorado River Basin, which was conducted by the University of Arizona and other collaborators. Research is ongoing in that basin and is focusing on the area of transition between basins where extreme floods are related to El Niño conditions and those where extreme floods are related to La Niña conditions. So far, this research has found that paleofloods fall within dry periods such as the Medieval Climatic Anomaly are related to the positive phase of the PDO and have a poorly defined relationship with ENSO. This is in contrast to previous research in the Lower Colorado River Basin by Ely (1993; 1997), where extreme floods appear to fall within wet intervals and are closely associated with El Niño .

Many questions remain unanswered regarding how climate change will impact water supply and extreme floods at Reclamation facilities. This project takes an alternate tact to model simulations of runoff by exploring the relationships between fluvial sedimentation, paleofloods and climate in the recent geologic past. This project has provided an important step in the understanding of this relationship and recommends study in other regions to complement model projections, which still retain considerable uncertainty.

1 INTRODUCTION

Climate change has become an important topic in recent decades because of its anticipated effects on water supply and a variety of other environmental issues. Water supply is of critical concern to Reclamation as well as water managers and the general population in the western U.S. The possibility for greater and more frequent extreme floods is a related issue, with potential impacts on water storage facilities and their operation. The likelihood of changes in basin hydrology has also spurred research on how storm patterns and durations will change given various projections of climate change.

Ongoing hydrologic and climate change research suggests that changes in climate will affect the timing, magnitudes, volume and frequency of peak flows on rivers. Although much of this research still relies on Global Circulation Models (GCMs), which lack the topographic resolution to accurately model the mountainous western states, it is likely that the changes in flood regimes in the future will affect dam operations. Many of these models project annual volumes, but lack information regarding extreme events. In many areas of the western U.S., the connections between extreme floods and shifts in climate are still not well understood.

Reclamation has been collecting paleoflood data for approximately 15 years for various projects related to flood hazards at Reclamation facilities. These data provide a physical record of flooding that extends beyond the historical record and that can provide a long-term perspective on flood potential. An inherent component of paleoflood data collection is radiometric dating, which provides age control for flood deposits and stream terraces along rivers. This age control is important for understanding the timing of floods and how they may be related to shifts in climate through the Holocene.

1.1 Study goals

This study was structured to explore the potential connection between extreme floods and climate change. Does the paleoflood chronology in the western U.S. indicate increased frequency and magnitude during specific, long-term climate shifts, and do those floods correlate well with the long-term, climate record? To answer this question, this study will: (1) compile and analyze a portion of paleoflood chronologies from data collected by Reclamation personnel over about the last 15 years in the State of California; and (2) collaborate with researchers outside of Reclamation who are working on the development of similar paleoflood chronologies in the Colorado River basin.

The State of California encompasses a wide variation in climate, ranging from semi-arid deserts to high elevation temperate regions over relatively short distances. Large moisture fluxes from the Pacific Ocean are capable of providing abundant precipitation to generate large floods. These floods may be derived from

rainfall, snowmelt, or a combination of the two. Reclamation Dams are located in many areas in California and a considerable amount of paleoflood data have been collected for flood hazard studies related to these dams. Radiometric dating has been used extensively in paleoflood studies in the state of California along rivers that have Bureau of Reclamation facilities. This dataset can be utilized in order to investigate the study question in areas where paleoflood data have been collected (Figure 1-1). While radiocarbon ages were plotted for all basins with paleoflood studies in California, the Sierra Nevada region was the focus of the study because it is a region where extreme floods are recorded and it contained the largest number of radiocarbon ages to analyze.

Radiometric dating as well as other numerical dating techniques has been utilized in the Colorado River basin to explore similar questions. The results of studies by outside researchers are summarized here. These studies were partially funded by the Bureau of Reclamation through the Cooperative Ecosystem Studies Unit (CESU) program.
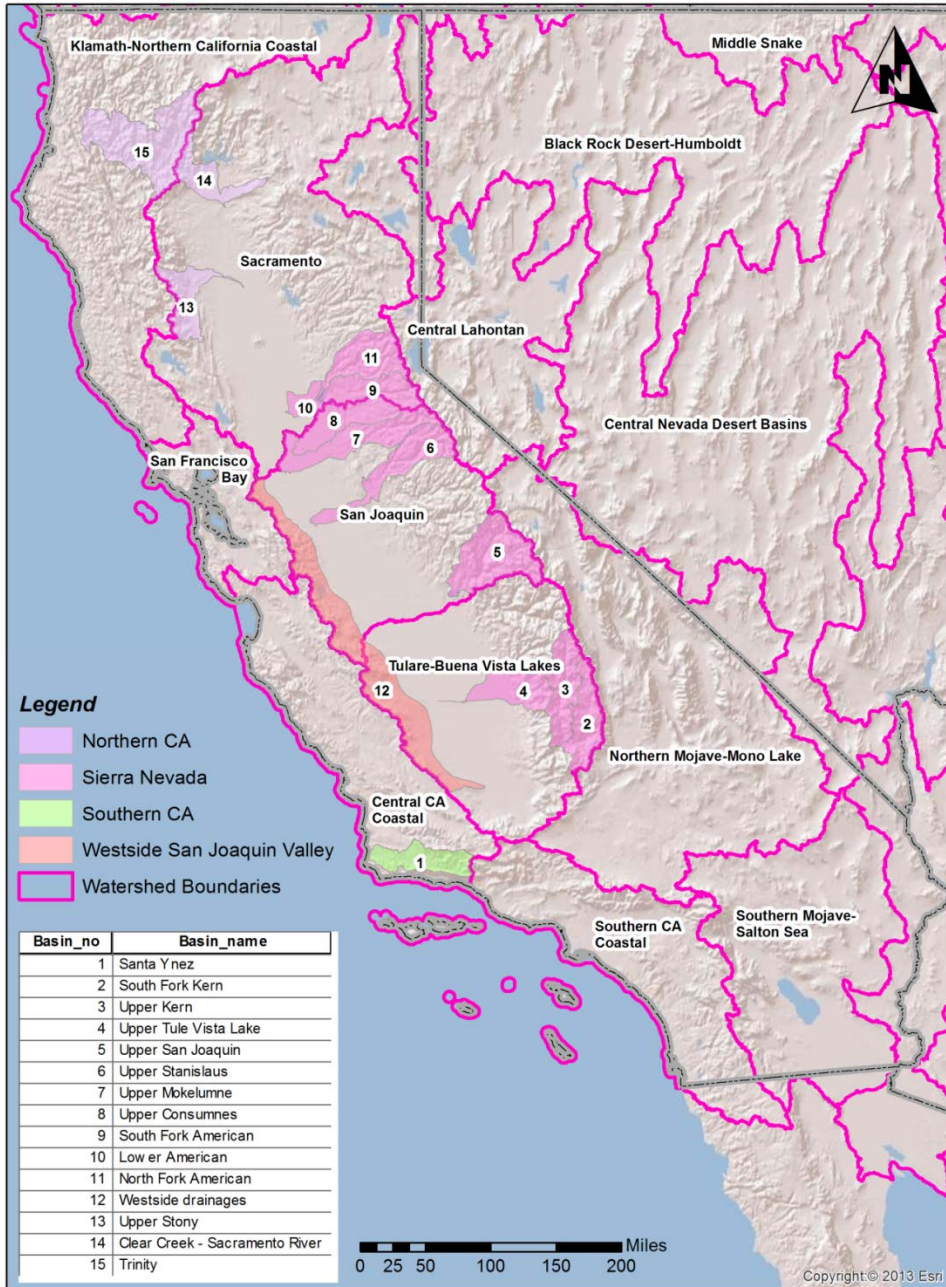
Figure 1-1. Study area locations within the state of California.

1.2 Report Organization

This report is organized into chapters. Chapter 2 discusses the methods used to develop paleoflood and non-exceedance data. Chapter 3 discusses the results of the study and includes discussions of Case study 1 in the Sierra Nevada region of California and Case study 2, which is a summary of individual paleoflood studies in the Colorado River Basin that were conducted by the University of Arizona and affiliated researchers. These studies were partially funded through the

Reclamation Dam Safety Office. Chapter 4 summarizes the results of the study. References and Attachments are provided at the end of the document.

2 METHODOLOGY

2.1 Paleoflood Data

Several methodologies have been utilized at Reclamation to develop the necessary paleoflood information for input to flood frequency analysis. One widely used technique in the study of paleofloods uses the fine-grained sedimentological record that accumulates in backwater areas (slackwater) to construct a detailed history of past floods (e.g., Patton and others, 1979; Kochel and Baker, 1988) (Figure 2-1). This technique can be extremely useful in characterizing the frequency of large floods, but can fall victim to the inherent assumption that a sequence of slackwater sediments represents a complete and continuous record of floods at a particular site. In addition, the physical setting of a backwater site may not be ideally suited for reconstructing or accurately estimating the peak discharge for the flood that is associated with a particular sequence of slackwater deposits in hydraulic models. This problem can often be aided with more elaborate hydraulic modeling (e.g., Denlinger and others, 2002).

Another methodology uses the age of a terrace surface that lacks clear evidence of recent inundation, erosion and deposition, or alternatively displays evidence for long-term stability, to establish an upper limit to flooding (Figure 2-1). This non-exceedance approach can be extremely useful in flood hazard assessment because geomorphic and stratigraphic information derived from the terrace surface can provide an upper limit or bound on the age and magnitude of extreme floods (Levish, 2002). Rather than constructing a detailed record of past floods, the non-exceedance approach focuses on identifying a non-exceedance bound. Establishing a non-exceedance bound is accomplished by identifying terrace surfaces that serve as limits for the paleostage of large floods and estimating ages for those terraces (Figure 2-1). These bounds do not represent actual floods, but instead provide physical limits to peak flood stage over some measured time interval. Simply stated, a non-exceedance bound is a maximum stage that has not been exceeded in the time period since the terrace surface stabilized. The maximum stage can be used to estimate peak discharge given some knowledge of the channel characteristics. It is not necessary to develop evidence of specific paleofloods using this methodology. The greatest value is in determining the discharge for a flood that has not been exceeded over the time interval represented by the preserved stable landscape.

Stable terrace surfaces are simply flood plains that have been abandoned due to either stream incision and/or channel migration. Once abandoned, the surface characteristics of the terrace begin to change recognizably with time. An abandoned terrace surface will tend to lose all evidence of having been inundated and become more planar and smoother with time. Once stabilized, soil will begin

to form on the terrace deposits. Thus, stable terrace surfaces are the field expression for the stage of non-inundation or non-exceedance and are a direct indication for the physical upper limit of floods along a stream through time. The geometric characteristics of the channel and terrace surfaces define the channel conveyance. The minimum overtopping depth required for the initiation of large scale erosion of and/or deposition on the stable terrace surface is certainly dependent on sediment size and degree of inundation, but can be evaluated formally in terms of shear stress or stream power (e.g., Parker, 1978; Andrews, 1984; Baker and Costa, 1987). This information can also be derived directly from empirical data for historical floods. Ultimately the depth of flow associated with a non-exceedance bound is that which is sufficient to cause modification of the overtopped terrace surface. Through step-backwater modeling or other one- or two-dimensional modeling techniques (e.g., Webb and Jarrett, 2002), a peak discharge for a non-exceedance bound can be easily derived from stage. In flood frequency analyses, a non-exceedance bound includes both an age and peak discharge and is defined as the time interval (age of the terrace surface) during which the flood stage and associated modeled peak discharge has not been exceeded.

Paleoflood discharge estimates made for Reclamation hydrologic hazard studies utilize one of three different methodologies: 1) a slope-conveyance calculation through a single cross section, 2) a one-dimensional (1D) step-backwater hydraulic model through multiple cross sections (e.g., HEC-RAS), or 3) a two-dimensional (2D) depth-averaged hydraulic model (e.g., SRH-2D; Lai, 2009).
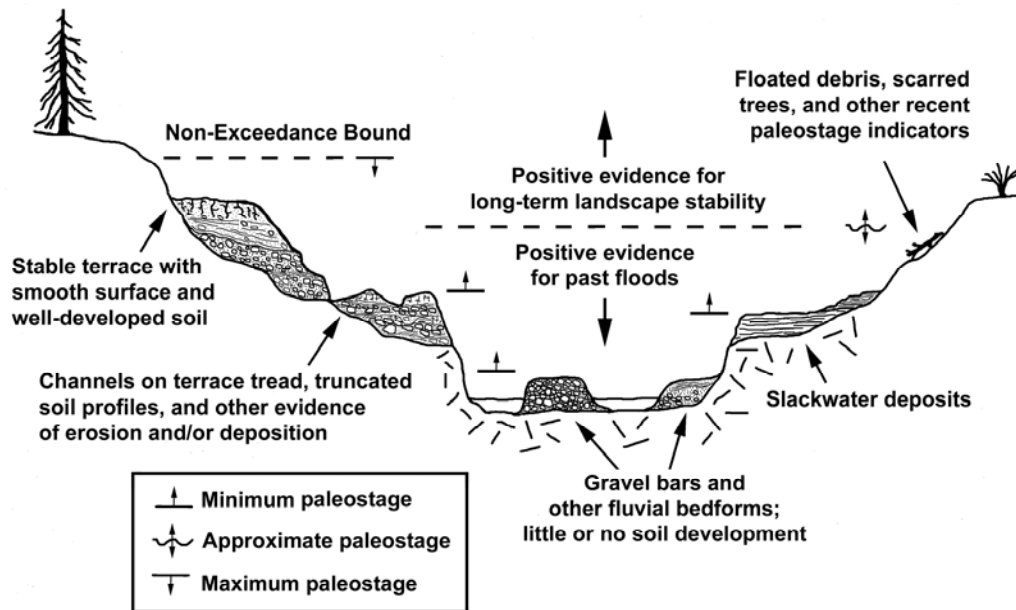
Figure 2-1. Idealized channel cross-section illustrating the concept of a non-exceedance bound

12

and the fluvial landforms and related deposits important to paleoflood studies.
To determine the age of the slackwater or terrace deposits, soils formed on the deposits are described following methodology of the U.S. Department of Agriculture (Soil Survey Division Staff, 1993), and Soil Survey terminology from Birkeland (1999). Sedimentological properties in the deposits are described using terminology from Boggs (1995). To obtain quantitative information about the ages of the various deposits, organic material, most commonly detrital charcoal, is collected from the soils and submitted for macrobotanical identification. A subset of these samples for each study are selected for AMS radiocarbon analysis to determine a numerical age. In some cases, shell, wood and pollen can also be used to develop the age of a deposit.

Geomorphic surfaces adjacent to a stream define a maximum possible channel geometry, over the time period represented by the age of the surfaces, through which a maximum discharge can be modeled. The ages associated with the geomorphic surfaces that form bounds for flood magnitude are almost always minimum ages because of the problems related to determining the precise time when a particular surface was abandoned. The result is an estimate of the maximum discharge during the minimum time interval since stabilization. Discharge estimates are most likely larger than actual past floods due to vertical and lateral erosion subsequent to the time of surface stabilization, resulting in apparently larger cross sections and discharges (Levish, 2002).

The ages used to develop both paleoflood and non-exceedance estimates can be analyzed in this study because they record periods of flooding, erosion or sedimentation along rivers in California. Both slackwater deposits and stream terraces provide evidence of flooding. The majority of slackwater deposits are found in confined bedrock canyon settings where bedrock obstructions, expansions or contractions create hydraulic settings suitable for the formation of slackwater deposits. Junctions at minor tributaries, where large floods may backwater into the tributary mouths also provide settings conducive for the preservation of slackwater deposits. Studies that focus on slackwater deposits are typically investigating extreme floods, or paleofloods that are equal or greater in magnitude than the largest historical floods in a particular basin. Stream terraces are located both within bedrock canyons and in unconfined alluvial settings along rivers. These terraces are often of different ages and positions above the modern river channel. Stream terraces provide a record of overbank flooding that in some cases can be related to extreme floods and in other cases is a record of more frequent floods. In cases where flood deposits overlie buried soils, these floods can typically be related to a rare flood. Hydraulic modeling of the discharge associated with the stage of the stream terrace often bears this out. Other stream terraces may simply record a period of floodplain formation followed by incision or migration, thus causing the surface to become isolated from river processes. In any case, these deposits record a period of time in which fluvial systems are actively depositing sediment along their courses. While it may be difficult to calculate a discharge associated with deposition, the deposits may be used to infer that streams are actively reworking and depositing sediment along their channels,

which suggests that rivers have abundant water supply in a relative sense and that floods are frequent enough to inundate overbank areas. Periods where overbank areas are infrequently inundated allow for soil formation on fluvial deposits. Therefore, soils are interpreted to represent period of surface stability and lower streamflow. Radiocarbon data record the timing of fluvial deposition in stream terraces or slackwater deposits along rivers and can therefore be used to develop a chronology of overbank flooding and landform stability.

2.2 Paleoflood database

The paleoflood database exists as a repository for data developed during hydrologic hazard studies for the Dam Safety Office at Reclamation. It contains a variety of information that can also be used as a vehicle for conducting regional paleoflood hydrology and climate change research. Paleohydrologic data in the database vary in the level of uncertainty based on the amount of work performed to develop the data. Typically, the data are derived from one of three levels of study:

Comprehensive Facility Review/Comprehensive Review (CFR/CR) level—this level of study typically involves one field day of data collection. Cross section data may be collected using a range finder, total station or GPS survey equipment. Between one and three cross sections are collected. Peak discharges required to inundate the terrace surfaces are calculated using the Manning equation with an estimated roughness and slope derived from 7.5' USGS topographic maps. Stratigraphy is described in excavated pits or streambank exposures and correlated regionally to other terraces with estimated ages to develop an age for the terrace surface or flood deposit.

Issue Evaluation (IE) level—The IE level of study is probably the most variable in terms of the quantity and quality of data collected. While a more consistent approach is currently underway, the level of detail for IE studies has varied considerably in the past. This has ranged from calculating cross section conveyance to 2D hydraulic models for peak discharge estimates and from regional soils correlation to radiocarbon analysis for age estimates. The current level of study requires detailed topography from either photogrammetry or LiDAR and either 1-D or 2-D hydraulic modeling. Quantitative age estimates from multiple sites, either detailed descriptions of soils pits or bank exposures, are also required. One to two study reaches are typically investigated at the IE level.

Corrective Action Study (CAS) level—paleoflood data is collected in the greatest detail for a CAS. A 2-D hydraulic model is developed for each study reach from detailed topography, which is derived from either photogrammetry or LiDAR. Detailed stratigraphic descriptions and radiocarbon ages are collected at multiple sites to ensure consistency in the results. Typically 2 to 3 study reaches are investigated, depending on the project objectives, the preservation of deposits, and whether any tributary reaches are critical to understanding the flood hazard. This level of study may also provide data for input to rainfall-runoff models. For

this application, paleoflood studies can be structured to develop information for specific areas or sub-basins in larger watersheds. Regional paleoflood studies may also be conducted as part of a CAS to make sure that any extreme events are captured that could potentially impact the river in question.

The data are organized as a geographic database in ArcGIS and includes information related to the paleoflood data such as geographic location, data collection methods, age estimates, peak discharge estimates, data quality, and related dams, rivers and publications (Figure 2-2; Table 2-1). The data are stored as a relational database that can be queried to retrieve the available data for a particular dam, location or river, for example. All data are related to a study site, which is identified by a unique name and geographic coordinates (Figure 2-3). Typically, the coordinates are located at the point where the stratigraphy was described on a particular terrace or flood deposit. This could be related to a streambank exposure or excavated soil pit. Several study sites may include the same paleoflood or non-exceedance data, since there are typically multiple sites involved in developing an estimate. Currently, over 200 sites have been entered into the database. The database will continue to be updated with new paleoflood data developed during the past 5 years and will be kept current with new data developed in the future. Any paleoflood or non-exceedance bounds entered into the database in the event table are linked to the sites through a site ID. The age and discharge estimates, a description of the bound, and the developer of the data are included in the Event table. Other information that can be added to each event if applicable include the stage associated with the discharge, the number of exceedances, the month of the flood (if historical), and any comments regarding the bound. For each event, several domains are added that provide more information about each bound. The domains are essentially tables with drop down lists of applicable descriptors that can be assigned to each event. For example, the paleostage indicators domain includes fields that describe the type of potential stage indicators that might be identified in the field while developing the paleoflood estimate. Paleostage indicators include features such as flotsam, jetsam, slackwater deposits, tree scars and others. The exception is the Publication domain, which only contains fields that can be filled in with the citation rather than with predefined values.

Radiocarbon data have been compiled and will be linked to the database through the site location. Radiocarbon data may be collected from several soil pits or exposures at a single site, so there will be additional data added that will identify the pit/exposure of origin for each radiocarbon age. For this study, radiocarbon data are critical to determining the timing of floods and the deposition of alluvium in a river system, which can then be linked to periods of changing climate through the Holocene.

Feature classes
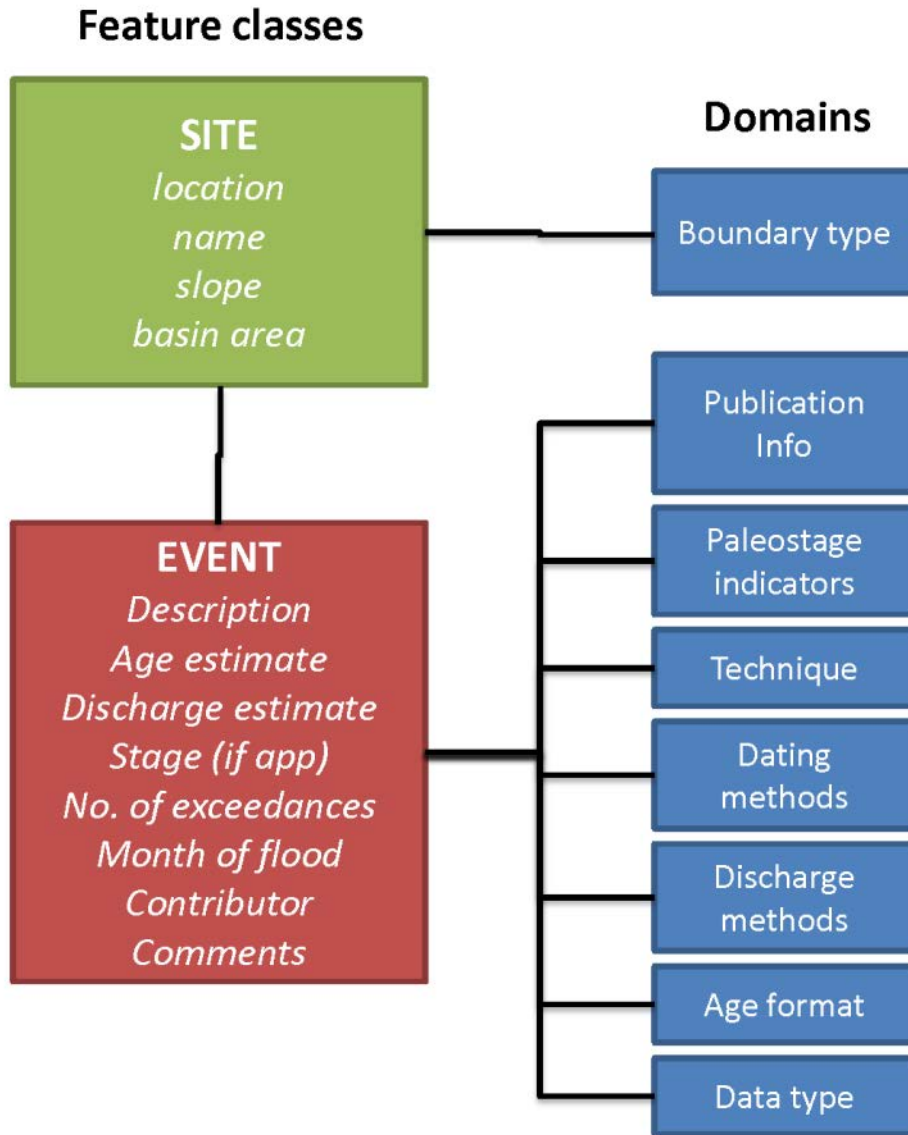
Figure 2-2. Paleoflood database relationships chart.

Table 2-1. Fields in the paleoflood database.

Domain	Description	Fields	Notes/comments
Boundary type	channel boundary type	fixed	bedrock channel
		deformable	alluvial channel
Publication info	Reference where bounds are published	Author Date Title Publisher	
Paleostage indicator	type of high water marks used to estimate the stage of the paleoflood	slackwater deposits flood-scarred trees silt lines scour lines debris lines highwater marks non-exceedance level other	
Technique	techniques used to develop the paleohydrologic bound	tractive (boulder) deposits suspended load deposits erosional/cavitation features hydraulic geometry channel pattern historic highwater marks discharge gage records precipitation records estimated observation personal communication newspaper accounts photographs dated corrasion/impact scars adventitious sprouts/inclined stem tree age ring anomalies vegetation patterns/species distribution	
Dating methods	methods used to estimate the age of the paleohydrologic bound	dendrochronology/tree ring analysis radiocarbon analysis Cesium-137 dating thermoluminescence (TL) dating stratigraphic analysis (relative age) dates based on age of	

17

Domain	Description	Fields	Notes/comments
		artifacts historical records discharge gage records precipitation records cosmogenic (3He or 21Ne) soil carbonate accumulation soil development tephrochronology other	
Discharge calc methods	methods used to estimate the discharge for the paleohydrologic bound	step-backwater method "competent" flood depths stage-rating curve slope-area method regression analysis max clast size "tractive force" bedform geometry floodplain botanical data Manning equation Chezy equation 2 dimensional modeling estimated channel conveyance other	
Age format	refers to how the age is reported	AD BC BP Cal BP Radiocarbon yrs	Gregorian calendar age "before Christ", starts at 1 BC Cal yr BP + 50 or 60 years 1950 datum uncalibrated age from laboratory
Data type	type of bound	exceedance non-exceedance threshold	one flood recorded at the stage of the bound 0 floods have exceeded the bounds' discharge more than one flood has exceeded the stage of the bound
Data quality	assessment of uncertainty in estimate	poor fair good	uncertainty = >±15% uncertainty = ±15% uncertainty = ±10%
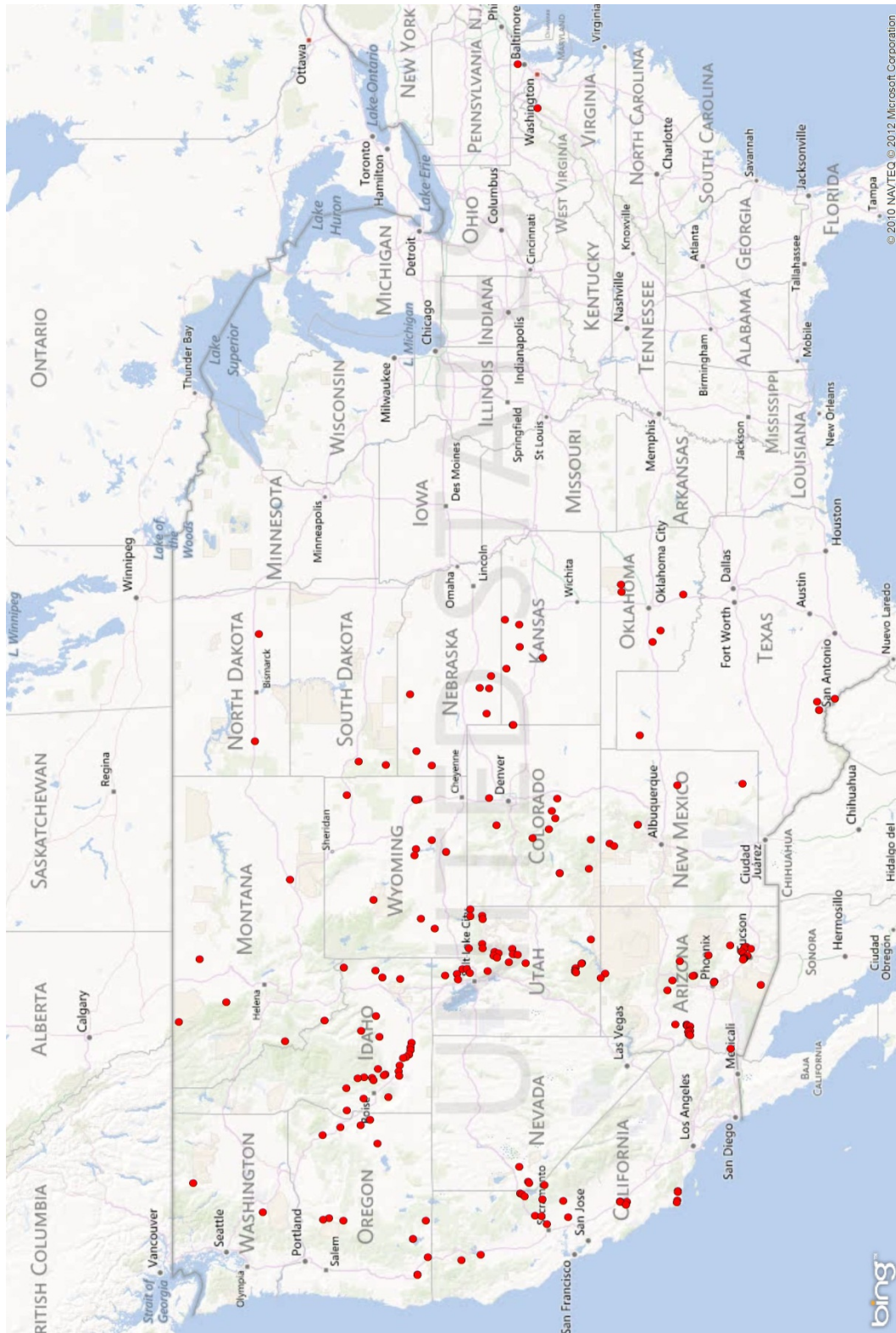
Figure 2-3. Example of paleoflood sites from the Reclamation paleoflood database.

3 CASE STUDY 1: CALIFORNIA

3.1 Extreme Precipitation and Related Flooding in California

The largest storms in California are associated with Atmospheric Rivers (ARs), a narrow corridor of concentrated moisture in the atmosphere. ARs are typically 2,000 or more kilometers in length, a few hundred kilometers wide, and in the lowest ~2.5 km of the atmosphere (Dettinger et al., 2011; Ralph et al, 2004; Ralph et al., 2005). ARs can be identified using multiple methods, including: satellite-derived integrated water vapor; raw satellite imagery; surface weather maps; and reanalysis data of winds and vapor transport (Figure 3-1). The ARs that impact the western United States are sometimes referred to as the "Pineapple Express" (PE), since they often originate over the tropical Pacific. Dettinger et al. (2011) explicitly separate the two phenomena with PEs being a subset of ARs which transport heat and moisture from the vicinity of Hawaii; however, the literature often uses these terms interchangeably. Thus, for simplicity (and depending on the particular source), this document will use AR or PE to describe the same phenomenon.

Dettinger et al. (2011) found that 20 to 50 percent of California's cool season precipitation and streamflow are contributed by AR and PE storms (Figure 3-2), with the magnitude of the streamflow events ranging from 2 to 5 times normal for the same cool season period. The extreme precipitation and flooding associated with these events lead to definitive shifts in the exceedance probabilities of floods (Dettinger et al., 2011; Dettinger, 2004). For example, Figure 3-3 shows the increased potential of daily changes in streamflow approaching 1000 m^3s^{-1} on the North Fork American River during all PE days and a preference for when the jet stream is focused near 40N latitude. Therefore, it is important to understand the mechanics (i.e., synoptic weather conditions responsible for large floods in California) and the relationships that AR/PE events have with larger scale climate patterns.
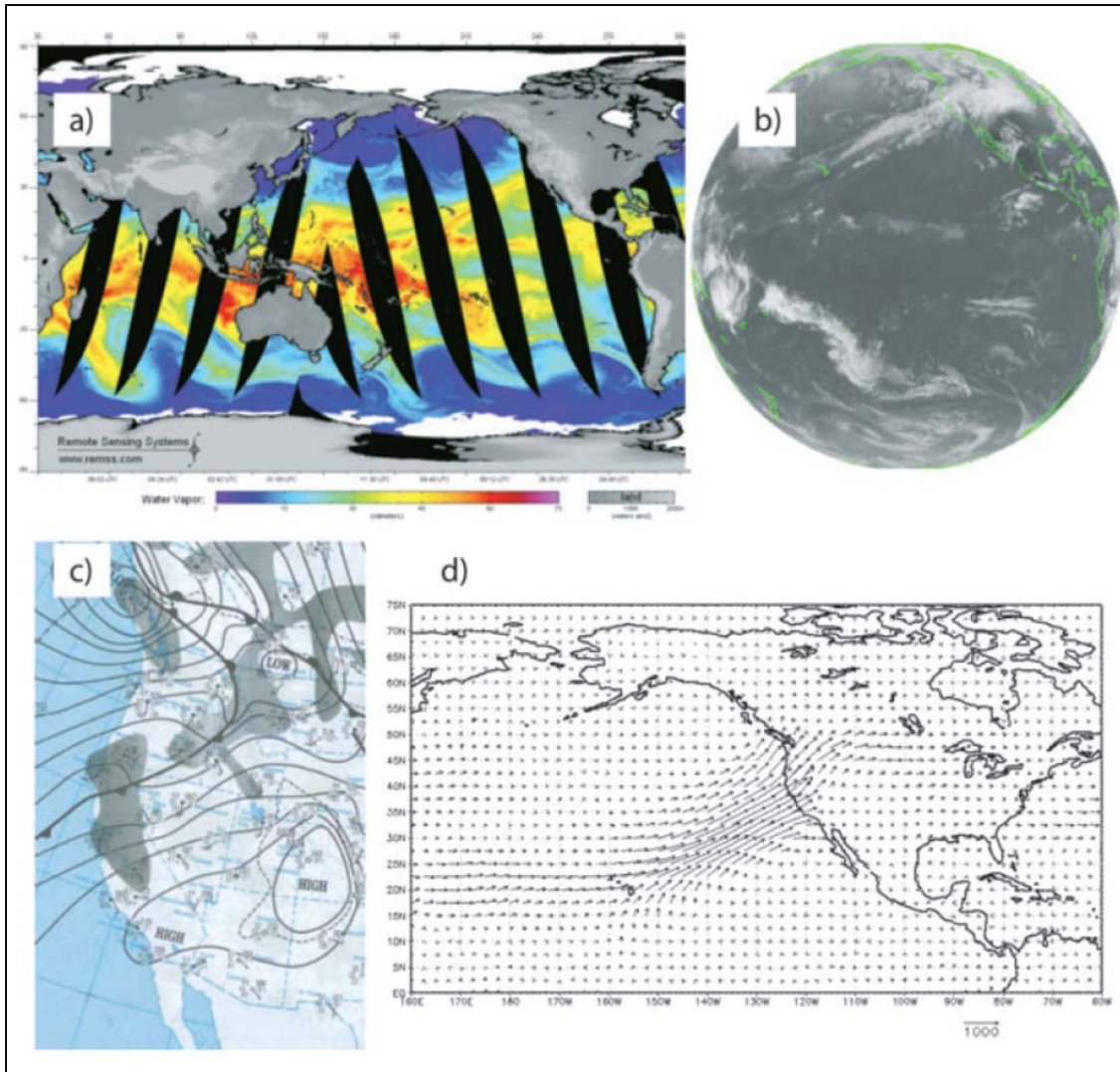
Figure 3-1. Various approaches to visualizing AR conditions. Sources include: (a) SSM/I integrated water vapor imagery; (b) infrared satellite imagery; (c) surface weather map; and (d) NCAR-NCEP reanalysis water vapor transport. [*Extracted from Dettinger, 2011 – Figure 1*].
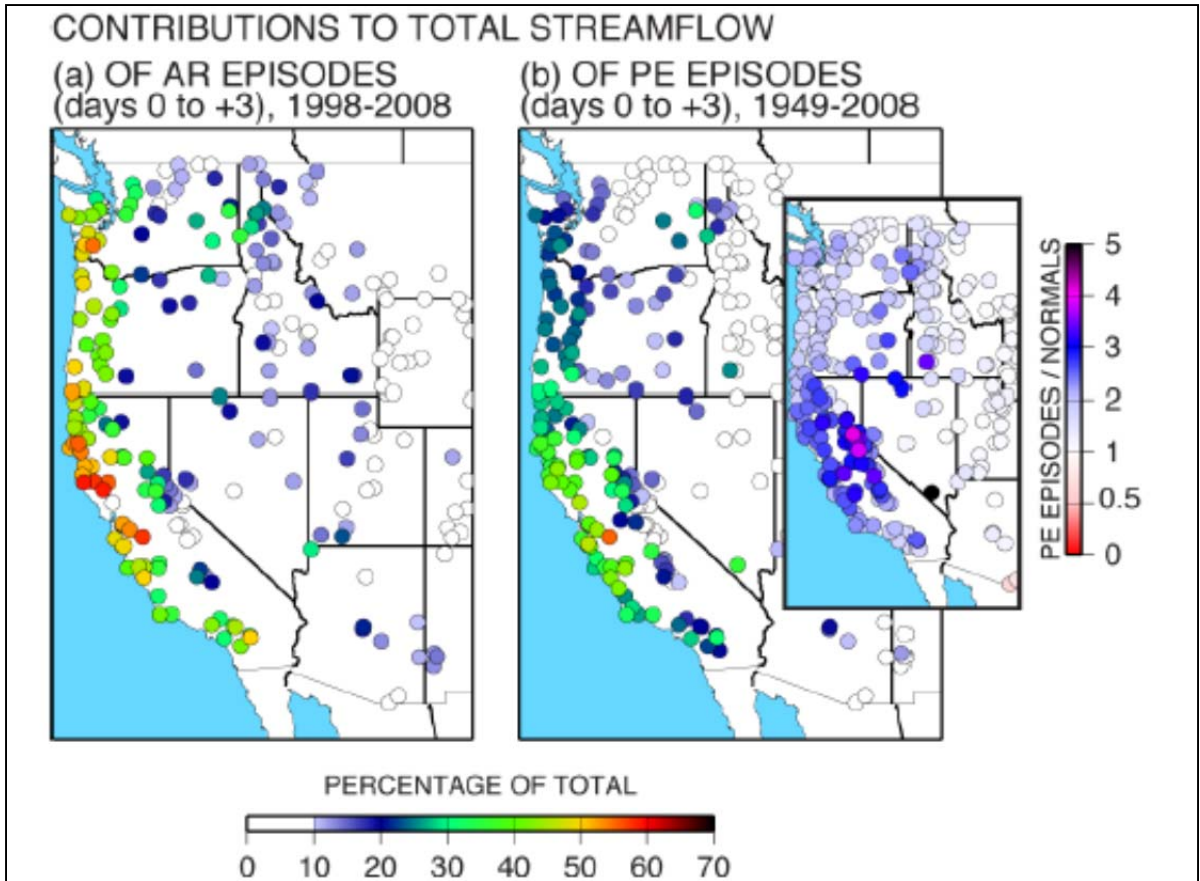
Figure 3-2. Contributions of streamflow during the cool season (November to April) by (a) ARs for 1998-2008 and (b) PEs for 1949-2008. Streamflow is the concurrent day and three following days. Total streamflow is the annual volume [*Extracted from Dettinger et al., 2011 – Figure 9*].
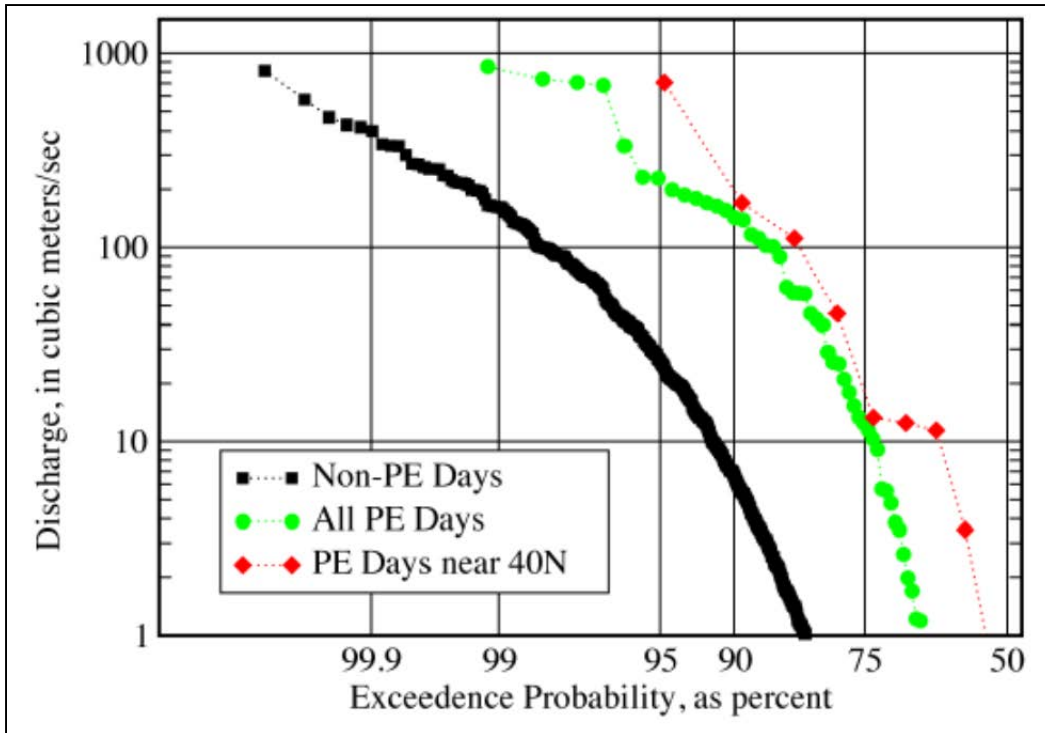
Figure 3-3. Exceedance probabilities for daily changes in river discharge for North Fork American River above North Fork Dam above Sacramento, CA for the period 1949-1999. [*Extracted from Dettinger et al., 2011 – Figure 5*].

3.1.1 Background

California is well-known for large precipitation events and associated floods. Leverson (2001) performed a detailed review of 23 storms affecting the California Coast Ranges as part of an extreme rainfall study for Los Banos Dam. Goodridge (1996) provided an extensive review of extreme rainfall events from the period 1862-1995 that describes the conditions associated with the 1000-year rainfall events. A total of 46 storms with reports of 1000 year or more rainfalls were analyzed at a total of 246 meteorological reporting stations (Figure 3-4). A comparison of the one day 1000-year rainfall to the mean annual precipitation across the state indicates large variability with the one day storm accounting for only 15-20 percent of the annual average precipitation in the northwest corner to over 150 percent of normal in the southeast (Goodridge, 1996). This dipole highlights the highly variable precipitation across the state.
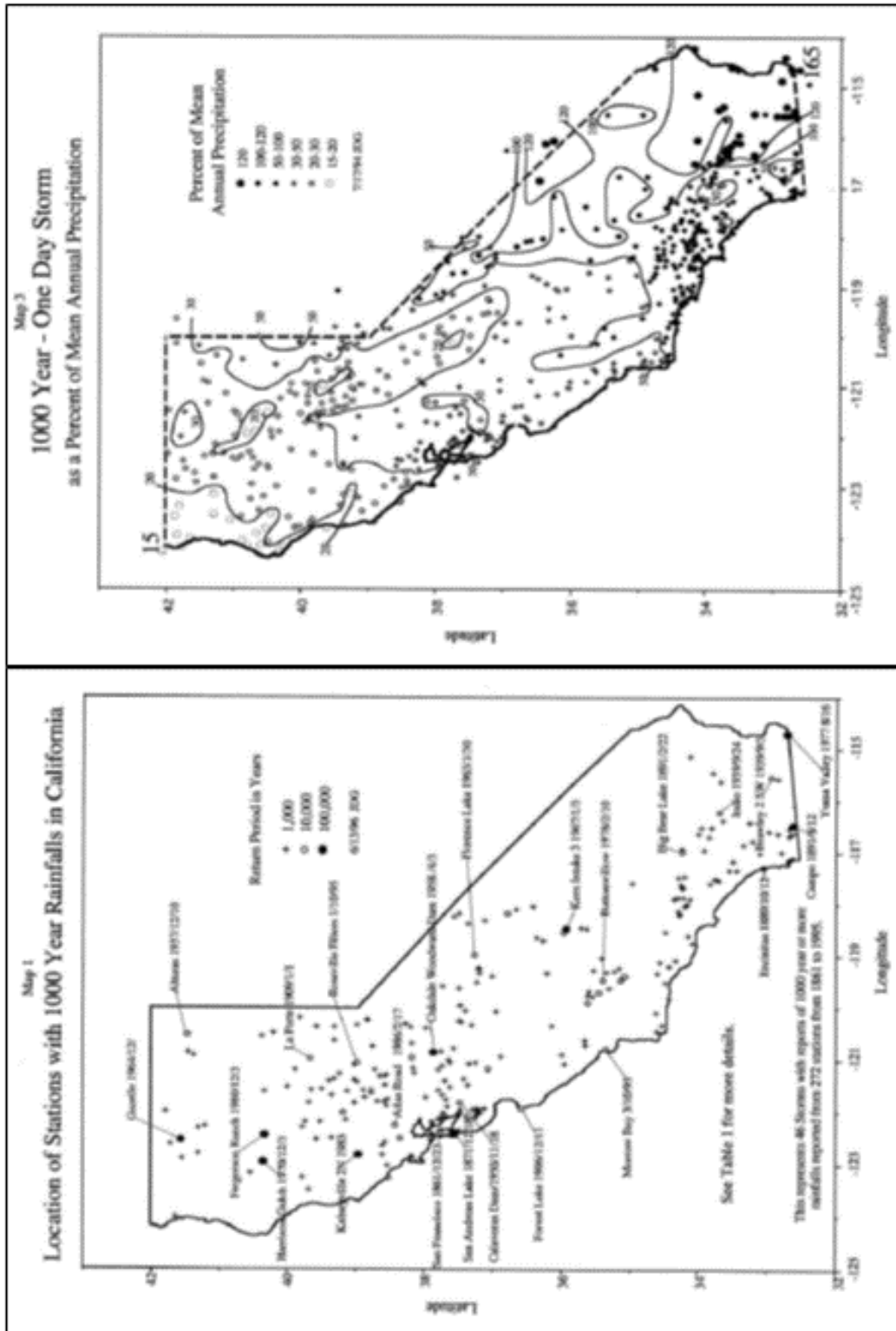
Figure 3-4. Locations of 1000-year rainfalls in California (bottom) and percent of annual mean precipitation (top). [*Extracted from Goodridge (1996) – Maps 1 and 3*].
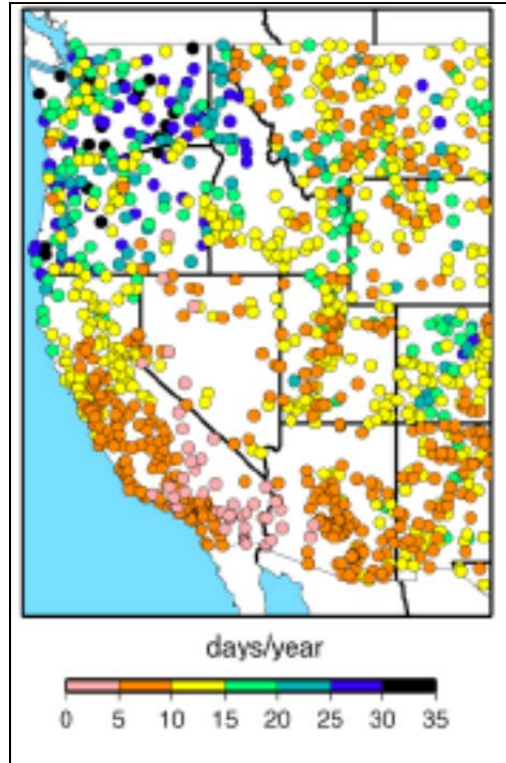
Figure 3-5. Average number of days per year to obtain half of total precipitation for water years 1951-2008. [*Extracted from Dettinger et al., 2011 – Figure 2c*].
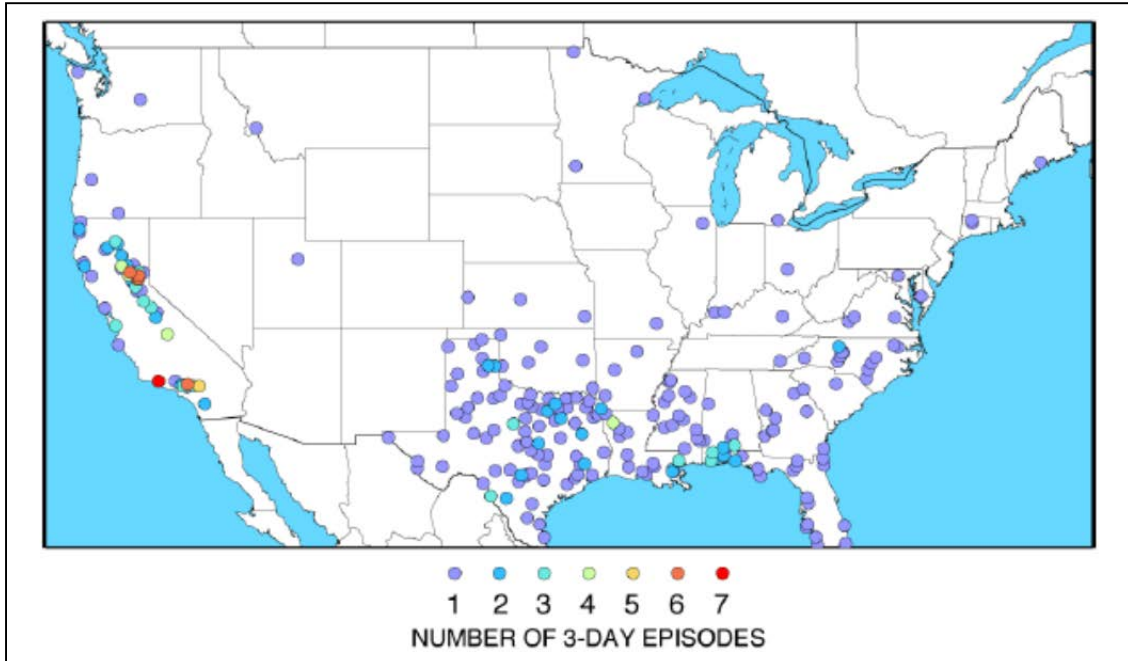
Figure 3-6. Number of reported 3-day precipitation totals at COOP weather stations that exceed 40 cm from 1950 to 2008. [*Extracted from Dettinger et al., 2011 – Figure 4*].

3.1.2 Atmospheric Rivers

3.1.2.1 *Frequency and Seasonality of ARs*

Using NCEP-NCAR reanalysis data (Kalnay et al., 1996), Dettinger (2004) developed a catalog of 206 daily PE events in a fifty-two year period that affected the West Coast, suggesting that these events are relatively frequent, on the order of four per year across the entire state. A study in Southern California by Haynes (2001) suggested a frequency of two per year during the period 1949-1997, with the heaviest events occurring once every three years. The occurrence of PE circulations has a distinct seasonality with a peak during the cool season (Figure 3-7). In addition, there is a migratory signal in the mean position of the jet stream that oscillates between 32N and 40N latitude with the most southward progression from January to March (Figure 3-7), indicating preferred times of year for different regions of California to receive the heaviest precipitation from PE storms. Haynes (2001) found that storms with more than three (3) inches of rainfall in 24 hours were clustered during the period of November to April across Southern California with a peak occurrence in January when the jet stream associated with ARs is in its southernmost position.
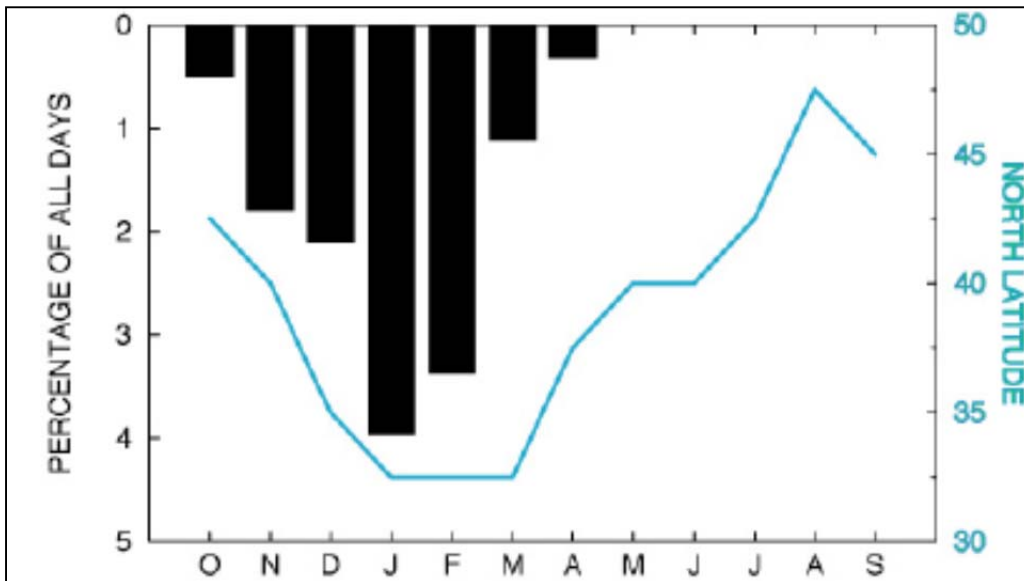
Figure 3-7. Seasonal cycle of PE circulations and mean latitude of the jet stream. [*Extracted from Dettinger, 2004 – Figure 4*].

3.1.2.2 *Synoptic Characteristics of ARs*

ARs can be easily understood by first considering the structure of a mid-latitude cyclone (Figure 3-8). Southwesterly winds in the warm sector ahead of a cold front transport substantial amounts of moisture and heat into the storm and, if focused and intense, can result in a AR-type storm along the west coast of the United States. The moisture is often conveyed from the tropics but can also be sourced from regions outside the tropics. To affect California, the general synoptic set-up is a closed upper-level low pressure off the Pacific Northwest or

British Columbia coast (Haynes, 2001) with sub-tropical influx of moisture within the warm sector of the associated surface low pressure system. Ralph et al. (2006) evaluated seven floods on the Russian River and determined the integrated water vapor observed was greater than 2 cm in each event with a distinct low level jet. The associated moisture flux from AR-type events are typically 3 or more standard deviations above normal (Leverson, 2001; Junker et al., 2008;Table 3-1). However, this moisture intrusion is not necessarily required if continental air is ingested into the storm at upper levels which aids in destabilization of the atmosphere and enhanced convective activity (Haynes, 2001). In addition, latent heat from condensation at the cloud level can also lower stability and allow cross-mountain flow to penetrate heavy rains farther inland (Galewsky and Sobel, 2004).
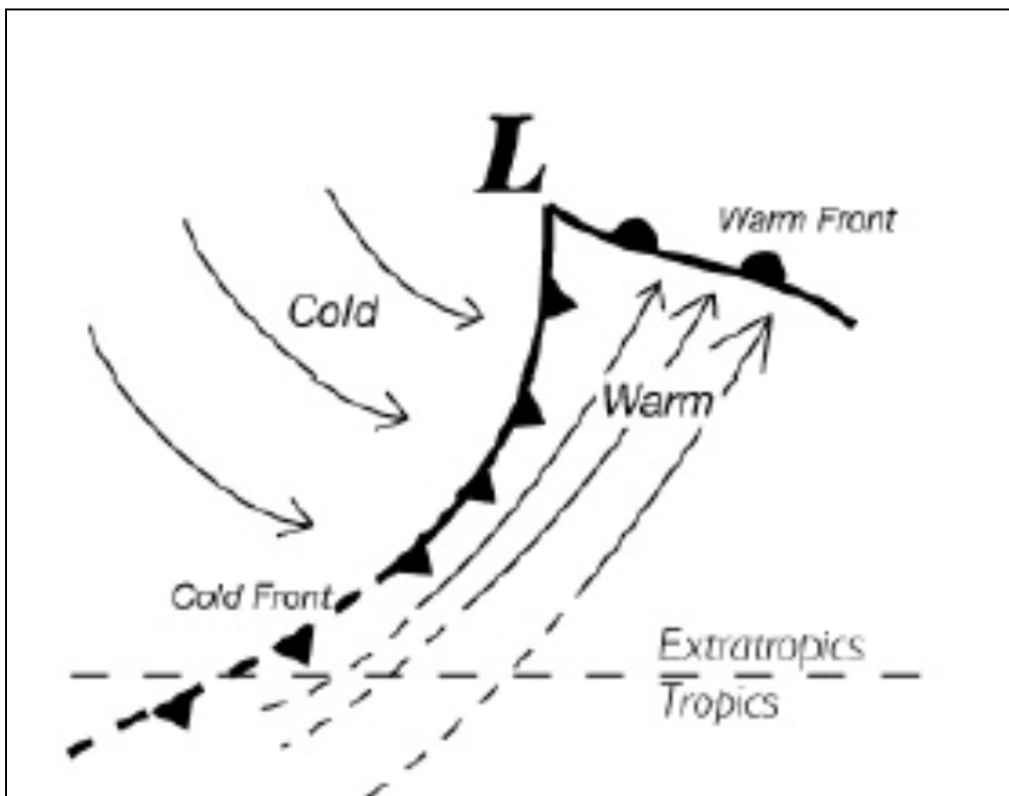
Figure 3-8. Idealized structure of a mid-latitude low-pressure system. [*Extracted from Dettinger, 2004 – Figure 3*].

Table 3-1. R-square values between different parameters and the maximum precipitation in the Sierra Nevada. In particular, the moisture flux (MF), precipitable water (PW), and u- and v-components of the wind at two points (P1 and P2) are correlated with the maximum precipitation. [*Extracted from Junker et al., 2008 – Table 1*].

Parameter	R square (P1)	R square (P2)
850-hPa MF	0.52	0.50
700-hPa MF	0.59	0.47
700-hPa component of MF perpendicular to the Sierra Range	0.51	0.40
850-hPa component of MF perpendicular to the Sierra range	0.54	0.43
PW	0.48	0.40
700-hPa u component	0.25	0.22
700-hPa v component	0.15	0.24
850-hPa u component	0.07	0.28
850-hPa v component	0.32	0.28

The trajectory of ARs can vary greatly, impinging on the mountainous terrain of California from a multitude of directions. The orientation of the moisture flux perpendicular to the terrain determines the location of maximum uplift and, hence, is generally associated with the region of heaviest precipitation. The heaviest precipitation typically occurs on the windward side of the mountains, especially along the coastal ranges. Though rare, PE storms can also generate leeside precipitation, such as in the Truckee River Basin in the central Sierra Nevada. These storms are typically warmer aloft, associated with a mid-level AR above the traditional low-level AR, and indicate a northward shift in the position of the upper-level trough over the Gulf of Alaska compared to traditional windward-focused precipitation events (Underwood et al., 2009; Kaplan et al., 2009). Figure 3-9 shows the typical set-up for an AR with adjustments made by Kaplan et al. (2009) for lee-side heavy precipitation/flooding events.
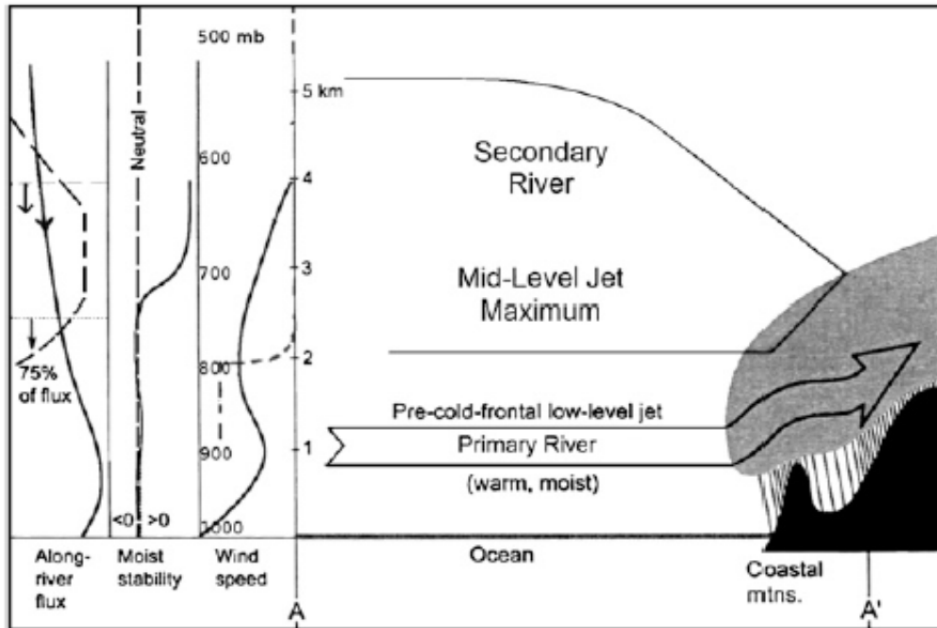
Figure 3-9. Conceptual model from Ralph et al. (2004) for low-level AR modified for addition of features and processes associated with lee-side flood events. [*Extracted from Kaplan et al., 2008 – Figure 2*].

As a result of the warm conveyor belt of moisture present during ARs, the resulting rain-snow line is usually high and results in more direct runoff than occurs in colder storms which generate large amounts of snowfall at lower elevations (Dettinger, 2011). Multiple early season storms can create large snow packs at higher elevations that quickly convert to runoff in AR events when the pack is ripe and rainfall occurs even at the highest elevations. In addition, quasi-stationary AR events with multiple embedded disturbances can cause phase changes of precipitation from snow-to-rain and rain-to-snow over a period of several days, leading to ripe snowpack and enhanced runoff potential.

3.1.2.3 Climate Signals and ARs

The term "teleconnection" refers to an atmospheric circulation pattern which is recurring and/or persisting over a particular geographic region. These teleconnections can be related to multiple spatial (i.e., from synoptic to planetary) and temporal (i.e., from several days to several years) scales.   The nature of a teleconnection pattern is to affect the preferred position of jet streams and associated pressure systems which thereby influences the temperature, rainfall, and storm tracks over large geographic regions. Due to the large areal impacts of teleconnection patterns, these signals offer the potential to be traced historically using coarse datasets, such as paleoreconstruction information (see Table 3-3). Several climate signals that result in teleconnections that have been shown to have impacts on California precipitation will be discussed in the current study, including: El Niño Southern Oscillation (ENSO); Pacific Decadal Oscillation (PDO); and, Madden-Julian Oscillation (MJO). These climate signals are related to convective activity in the Pacific Ocean. Convection in the Pacific has been

29

shown to be related to the development of meteorological conditions conducive for large rainfall events (Kaplan et al., 2009; Jones, 2000; Mo and Higgins, 1997; Higgins et al., 2000). We include a brief description of each climate pattern discussed in this literature review in the following sections; however, for a comprehensive list of and details regarding teleconnection patterns and related climate signals, please refer to the Climate Prediction Center (CPC) website at http://www.cpc.ncep.noaa.gov/.

3.1.3   El Niño /Southern Oscillation (ENSO)

Per the CPC, "[t]he ENSO cycle refers to the coherent and sometimes very strong year-to-year variations in sea surface temperatures, convective rainfall, surface air pressure, and atmospheric circulation patterns that occur across the equatorial Pacific Ocean. El Niño and La Niña represent opposite extremes in the ENSO cycle. El Niño refers to the above-average sea surface temperatures that periodically develop across the east-central Pacific. It represents the warm phase of the ENSO cycle… La Niña refers to the periodic cooling … [and] … represents the cold phase of the ENSO cycle." The reversal of sea surface temperature anomalies associated with different phases of ENSO is provided in Figure 3-10. There is also a neutral phase of ENSO [not shown] which occurs when the sea surface temperatures are near-normal in the equatorial region. The Southern Oscillation is directly related to the ENSO phenomenon and represents a reversal in sea level pressure as a result of the regional warming/cooling of the sea surface temperatures.
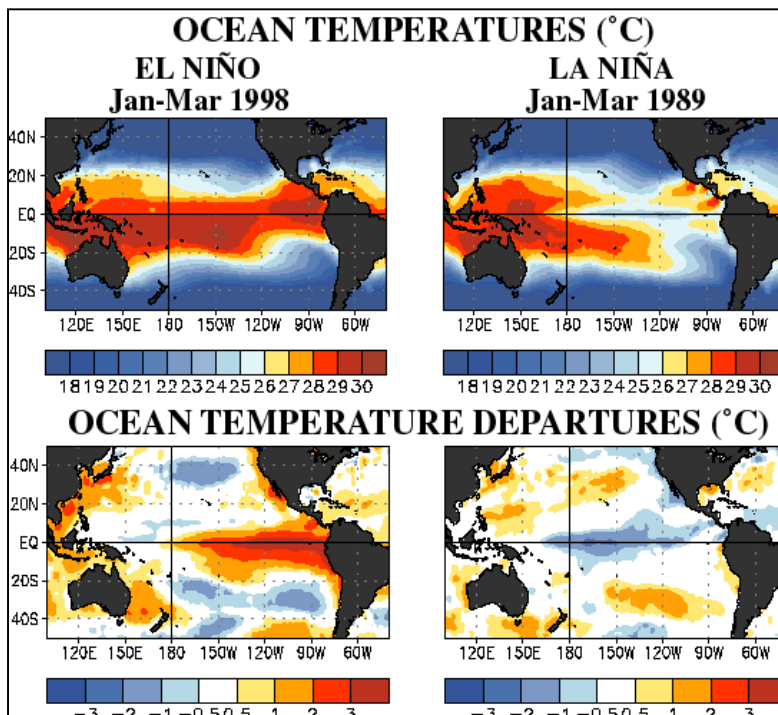
Figure 3-10. Sea surface temperature (i.e., ocean) patterns associated with different phases of ENSO. [*Extracted from the CPC website at http://www.cpc.ncep.noaa.gov/products/analysis_monitoring/ensocycle/ensocycle.shtml*].

Weather patterns during the winter season of El Niño are typically associated with wetter conditions across the Southwest United States; and, for La Niña , wetter conditions are typically more prevalent across the Pacific Northwest and northern California (Figure 3-11; Cayan et al., 1999). The preferred position of the jet stream (and, therefore, storm track) during the different phases of ENSO indicates the potential focus regions for the heaviest precipitation events, shown by the green/wet shaded areas in Figure 3-11.
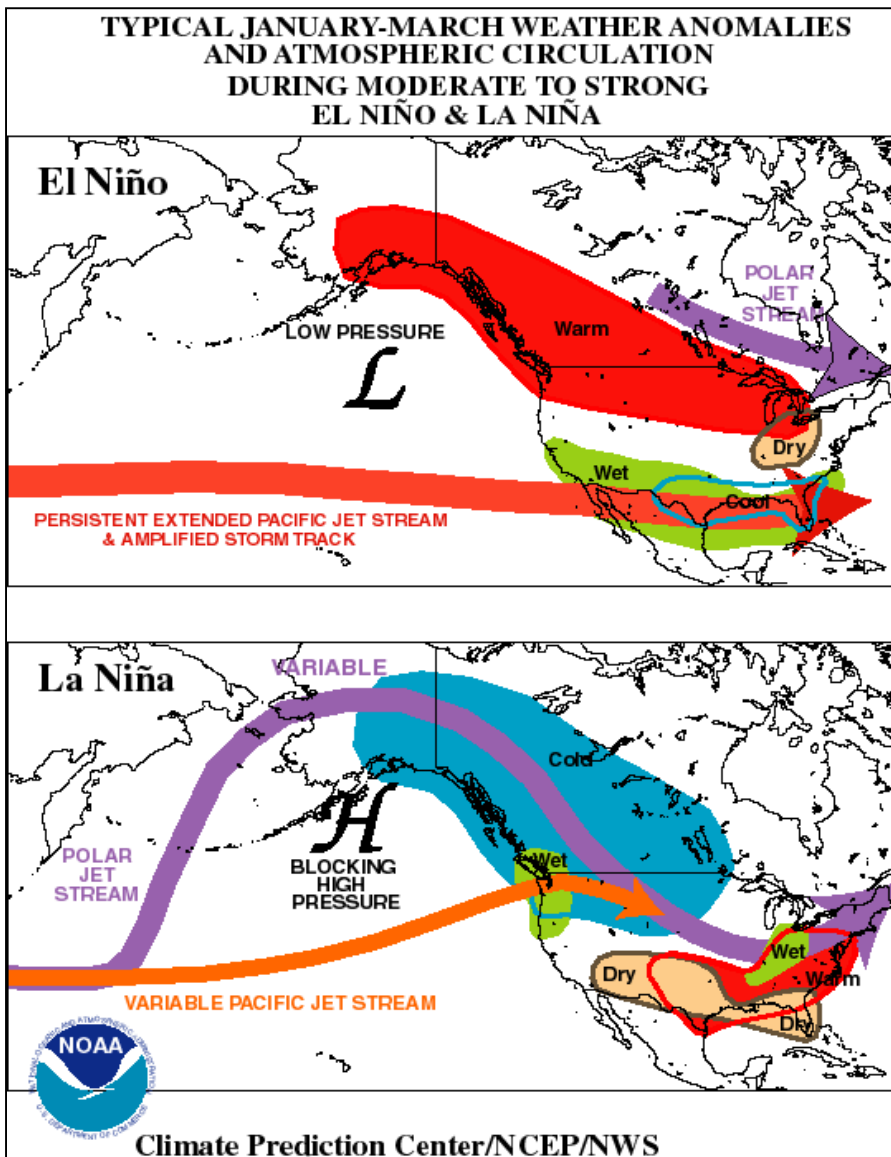
Figure 3-11. Typical winter season flow patterns and weather anomalies associated with ENSO. [*Extracted from the CPC website at http://www.cpc.ncep.noaa.gov/products/analysis_monitoring/ensocycle/nawinter.shtml*].

The implications of ENSO on AR events, however, are uncertain. Dettinger et al. (2011) found strong correlations between the contribution of AR precipitation to water year total precipitation, particularly across southern and south-central California during the warm phase of ENSO (i.e., El Niño; Figure 3-12). The shifts in ENSO phase are generally associated with changes in the persistence and duration of wet/dry episodes; therefore, correlations with longer duration (i.e., monthly to annual) precipitation amounts are typically stronger. In addition, this leads to even stronger correlations with streamflow since runoff efficiency is increased/decreased during wet/dry episodes (Figure 3-13; Cayan et al., 1999). The red (blue) regions in Figure 3-13 correspond to large precipitation and streamflow events that are highly correlated to El Niño (La Niña), which is clearly indicated across the Southwest and Pacific Northwest, respectively. In contrast to the relationships identified for southern California, central and northern California show no correlation with either phase ENSO (white regions in Figure 3-12 and Figure 3-13) as these portions of California are within a transition zone. Less correlation has been found with individual extreme precipitation events. Haynes (2001) and Dettinger (2004) found that El Niño events had at least one heavy precipitation event, but there was no correlation with the frequency of heavy precipitation events in a given year with the state of ENSO. Four of nine La Niña events had no storms occurring in California (Dettinger, 2004).
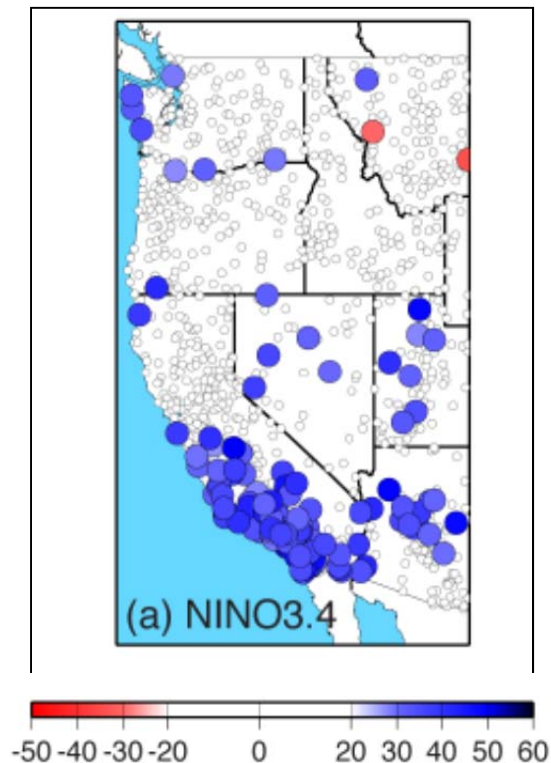
Figure 3-12. Correlations of AR contributions to water year precipitation totals with Nino3.4 sea surface temperatures. [*Extracted from Dettinger et al., 2011 – Figure 12a*].
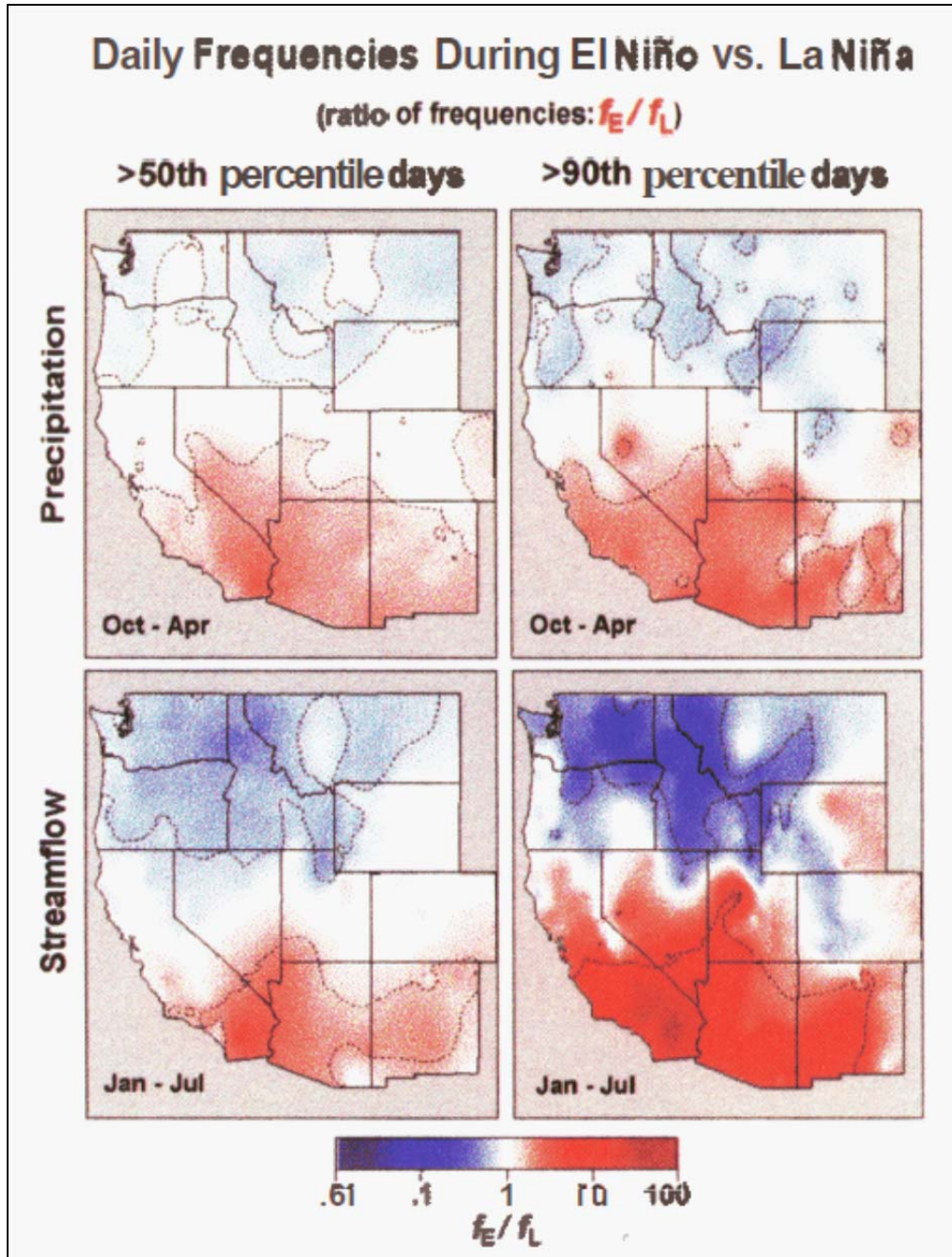
Figure 3-13. Ratio of frequencies (El Niño /La Niña) for days with (a) precipitation > 50th percentile; (b) precipitation > 90th percentile; (c) streamflow > 50th percentile; and (d) streamflow > 90th percentile. Red denotes ratios > 1.0 (El Niño more frequent cases than La Niña); blue indicates the opposite relationship for ratios < 1.0). [*Extracted from Cayan et al. (1999) – Figure 7*].

In contrast, Cayan et al. (1999) suggest that ENSO may impact low to median daily precipitation events across central California and high precipitation events in a small coastal region that extends inland 100 km (not including the Sierra Nevada). In comparing to neutral ENSO years, Cayan et al. (1999) also suggest

there is a +/- 30 percent likelihood of extreme events during active ENSO years across the western United States. Higgins et al. (2000) investigated the relationships between extreme precipitation events across the West Coast of the United States and transitions between different ENSO states. They found that the largest percentage of extreme events occurred during warm to neutral transitions, but that this relationship varied from north to south with notable differences across ENSO transition categories across the Pacific Northwest and southern California (Figure 3-14).
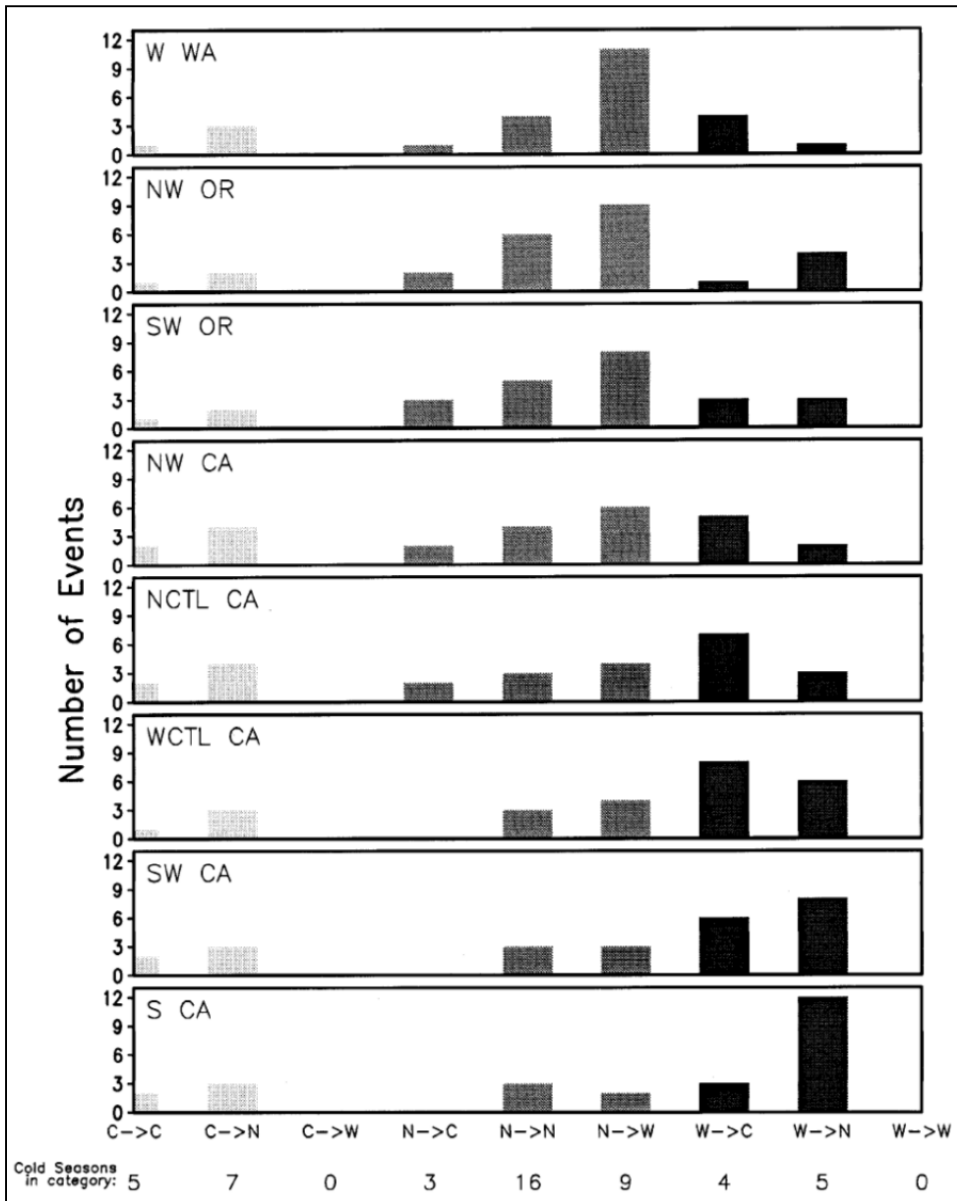
Figure 3-14. Distribution of the top 25 3-day precipitation events among categories of ENSO transitions for California and the Pacific Northwest. [*Extracted from Higgins et al. (2000) – Figure 3*].

Due to the impact of ENSO on precipitation patterns, this tropical connection can also affect the streamflow/flooding potential. As described earlier, Cayan et al. (1999) propose that the antecedent precipitation related to persistent wet/dry periods affect the runoff potential, making any precipitation event more likely to produce flooding. Similar patterns exist in the relationships with ENSO and flooding events with strongest correlation at low latitudes (32-35N, positive with El Niño) and higher latitudes (41-42N, negative with El Niño) (Figure 3-15; Andrews et al., 2004). Andrews et al. (2004) also indicate a relationship with the magnitude of floods, such that El Niño floods are generally larger than non-El Niño flood events. This deviation can be clearly seen in their example exceedance probability plot from San Juan Creek in Figure 3-16.
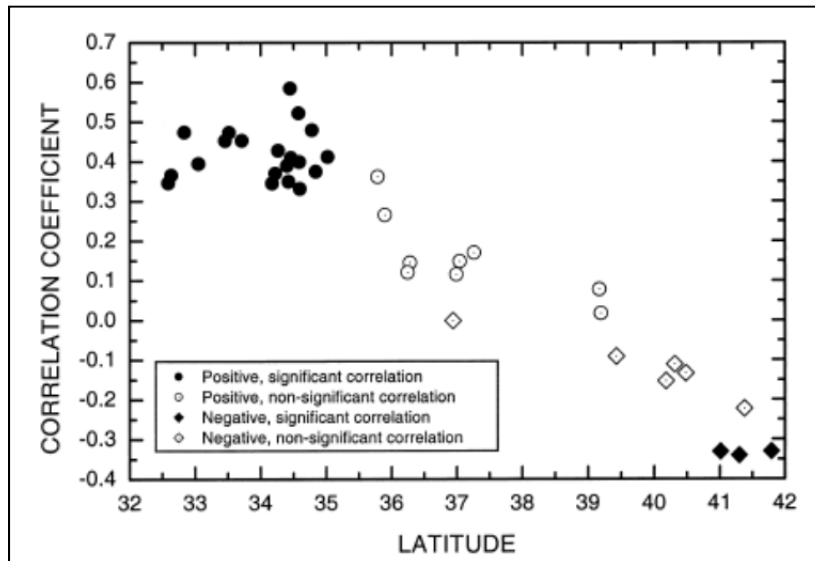
Figure 3-15. Correlation of log flood discharge on ENSO vs. gauge latitude. [*Extracted from Andrews et al. (2004) – Figure 2*]
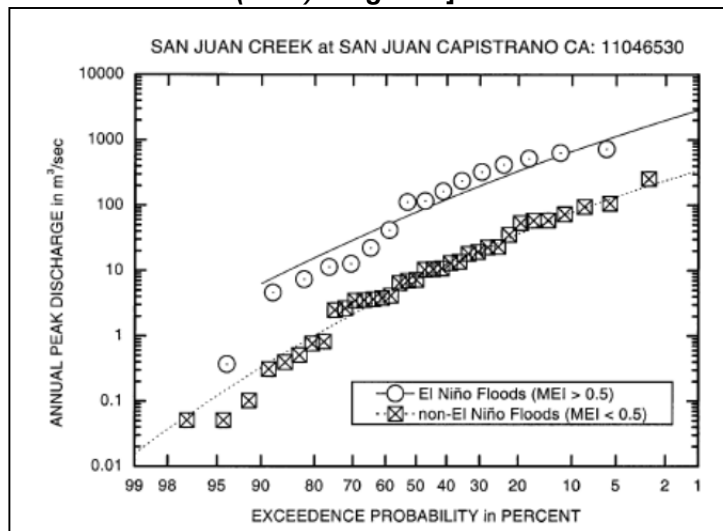
Figure 3-16. Comparison of El Niño vs. non-El Niño annual peak flood probability of exceedance graph for San Juan Creek. [*Extracted from Andrews et al. (2004) – Figure 5*].

3.1.4 Pacific Decadal Oscillation (PDO)

The PDO is a multi-decadal phase shift in the sea surface temperature anomalies north of 20N latitude. Both ENSO and PDO influence sea surface temperatures, sea level pressure, and surface winds. PDO is different from ENSO in the duration (several decades compared to several years) and the location of sea surface temperature anomalies. PDO is observed in the upper latitudes of the northern Pacific Ocean, with secondary effects at lower latitudes. A comparison of the sea surface temperature and wind patterns associated with PDO and ENSO is shown in Figure 3-17.
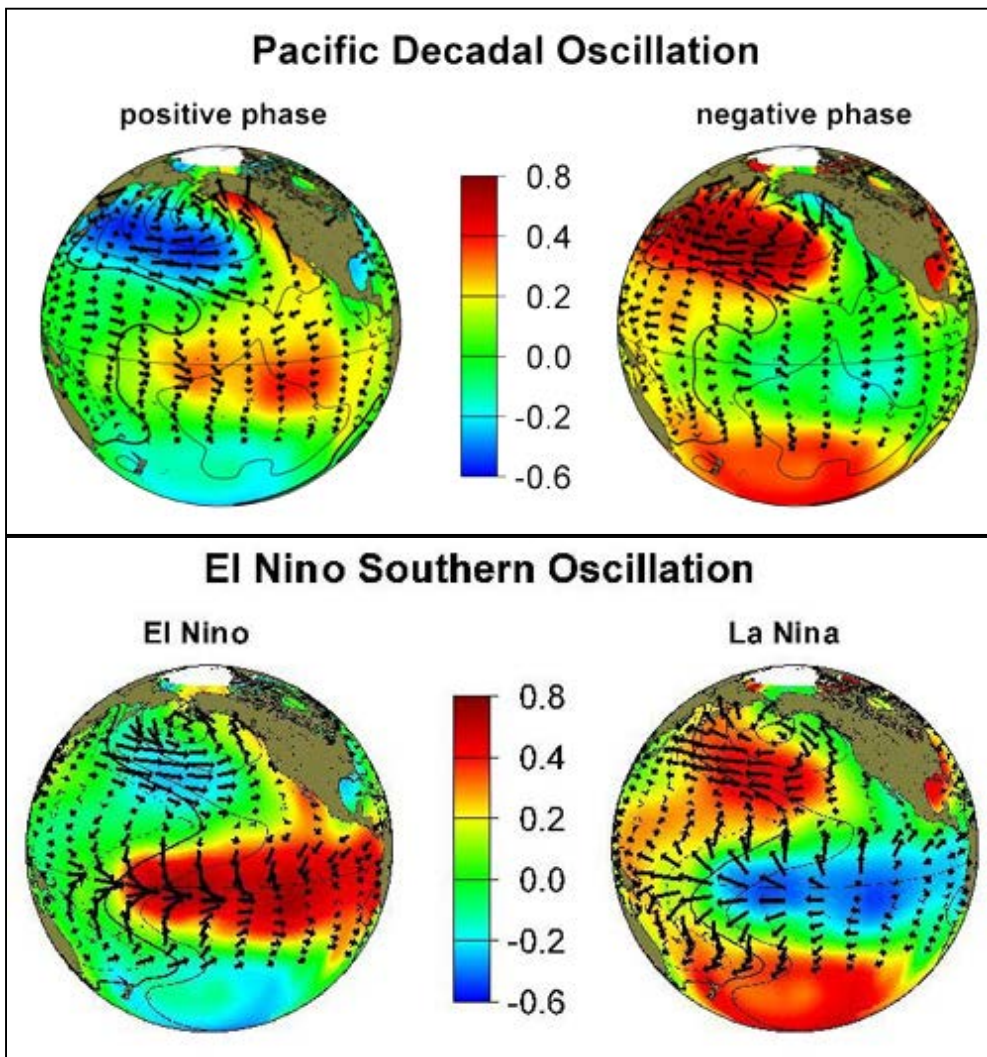
Figure 3-17. Comparison of sea surface temperature anomalies (shaded) and wind circulations (arrows) associated with the PDO (top) and ENSO (bottom). [*Extracted from Mantua (2000)*].

36

Similar impacts to sensible weather associated with ENSO occur across North America during the warm/positive or cool/negative state of the PDO (Table 3-2; Zhang et al., 1997; Mantua, 1999). For example, the warm phase of PDO would generally be associated with enhanced precipitation over the southwestern United States as with an El Niño pattern. In addition, Dettinger (2004) identified that winters with the most pronounced AR circulation patterns were related to the positive phase of PDO. Subsequently, Dettinger et al. (2011) found strong relationships with negative sea surface temperature anomalies in the far western Pacific Ocean and positive anomalies in the northern Pacific for central and northern California events, more typical of a slight southward deviation from the cool phase of the PDO, which normally focuses precipitation across the Pacific Northwest.

Table 3-2. Summary of North American climate anomalies associated with extreme phases of the PDO. First row of this table is most applicable to California [*Extracted and modified from Mantua (1999) – Table 1*].

Climate Anomalies	Warm Phase PDO	Cool Phase PDO
October-March southern US/Northern Mexico precipitation	Above average	Below average
October-March Northwestern North America and Great Lakes precipitation	Below average	Above average
Northwestern North American spring time snow pack and water year (October-September) stream flow	Below average	Above average
Winter and spring time flood risk in the Pacific Northwest	Below average	Above average

3.1.5 Madden-Julian Oscillation (MJO)

The MJO is an intraseasonal (30 to 90 days) variability in the tropical atmosphere that is related to a signal that migrates eastward, resulting in regions of enhanced and suppressed deep tropical convection. As the wave propagates eastward across the Pacific, warming/cooling sea surface temperatures occur immediately preceding/following it passage. A simplistic representation of MJO is provided in Figure 3-18.
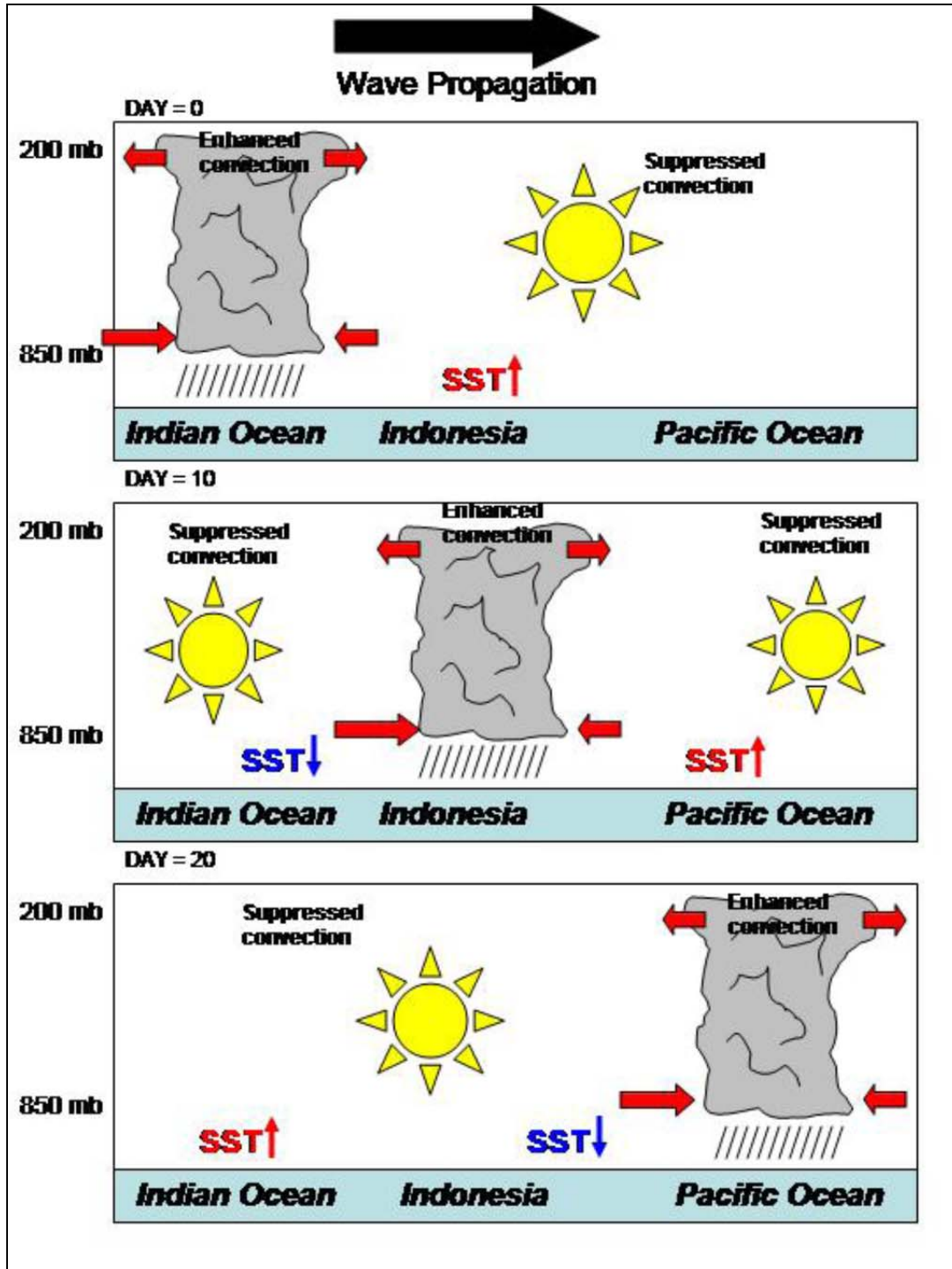
Figure 3-18. Equatorial vertical cross section of the MJO as it propagates eastward. Winds shown as red arrows. Sea surface temperature (SST) trends shown with labels and up/down arrows. [*Extracted from Gottschalek et al. (2012) – Figure 1*].

In a review of extreme precipitation events in California for the period 1958-1996, Jones (2000) observed that the frequency of extremes is higher when tropical activity is high in association with the MJO (Figure 3-19). Mo and

38

Higgins (1997) also found that intraseasonal oscillations (20-60 days) modulate California precipitation during ENSO events. An extreme event was defined as Type I, II, or III, with the threshold precipitation required to be at least 5, 10, or 15 percent of the annual mean precipitation, respectively. Jones (2000) found a slight preference for a higher number of events when the convection is focused in the Indian Ocean. The magnitude of the MJO event, however, was not correlated with the frequency of events (Jones, 2000). The Climate Prediction Center (2012) states that "winters with weak-to-moderate cold episodes, or ENSO-neutral conditions, are often characterized by enhanced 30-60 day MJO activity. A recent example is the winter of 1996/97, which featured heavy flooding in California and in the Pacific Northwest (estimated damage costs of $2.0-3.0 billion at the time of the event) and a very active MJO. Such winters are also characterized by relatively small sea surface temperature anomalies in the tropical Pacific compared to stronger warm and cold episodes. In winters like 1996/97, there is a stronger linkage between the MJO events and extreme west coast precipitation events. The MJO can affect the generation of AR circulation patterns and enhance precipitation impacts along the West Coast of the United States by providing a deep tropical connection and elongated jet stream (Figure 3-20).
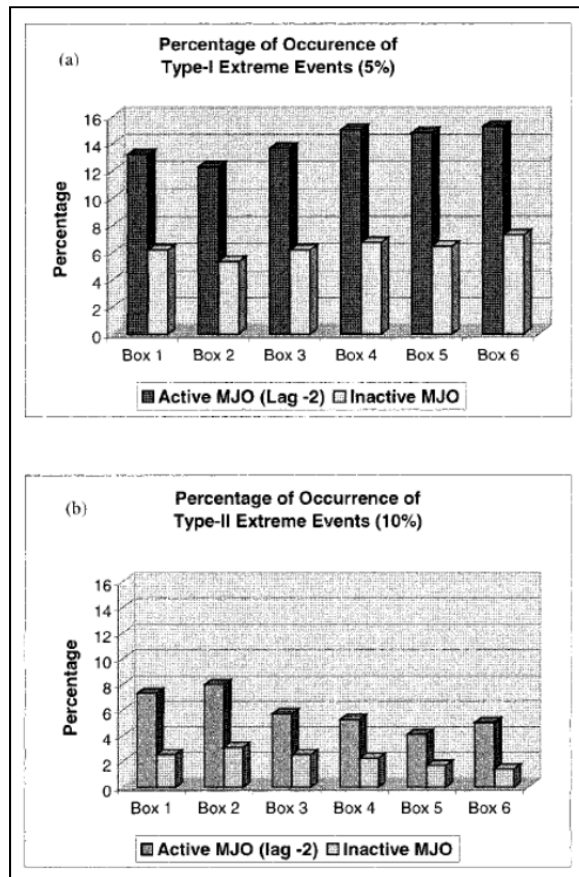
Figure 3-19. Percentage of (a) Type I extreme events and (b) Type II extreme events that occur during active and inactive MJO periods. [*Extracted from Jones (2000) – Figure 8*].
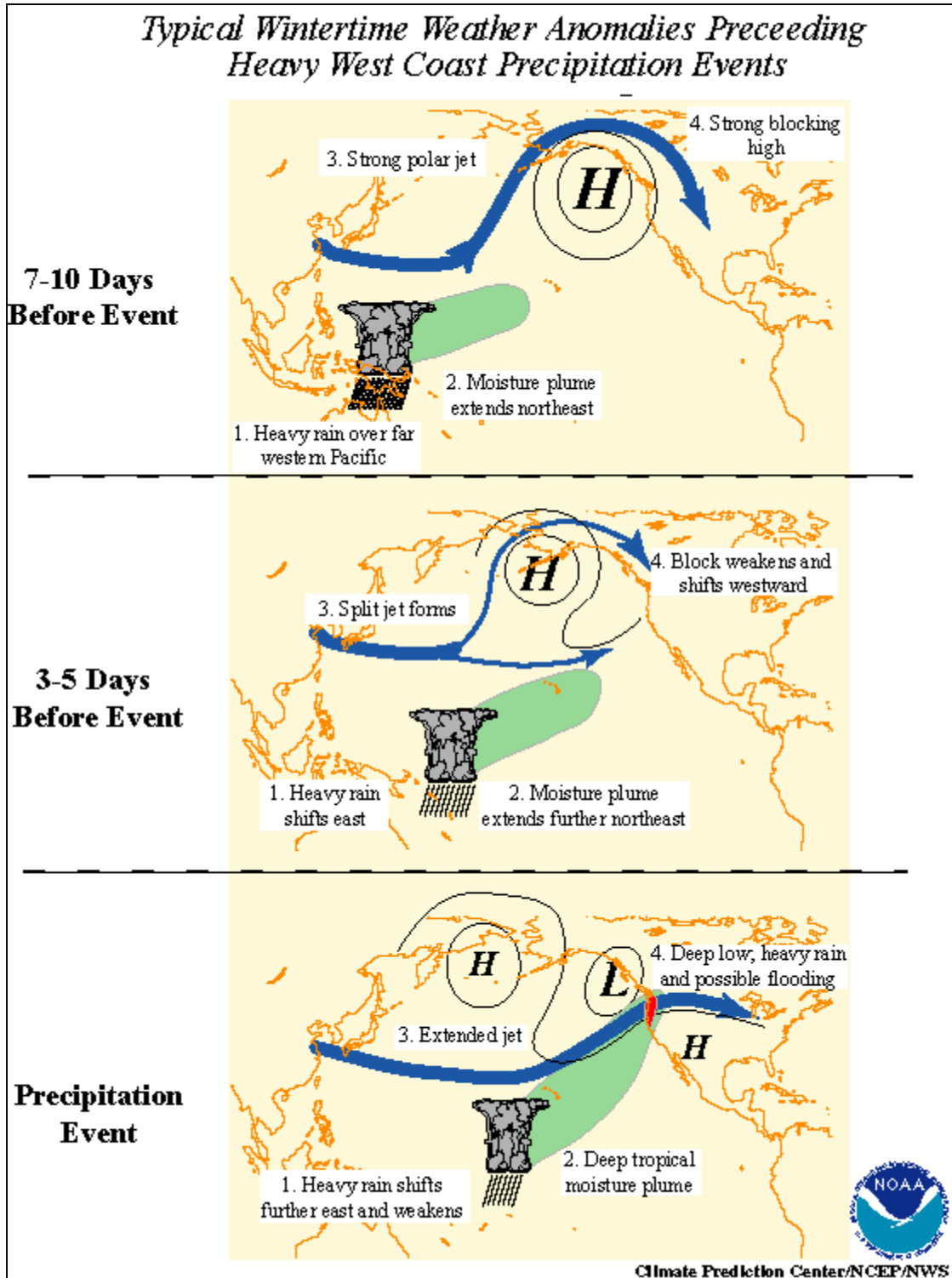
Figure 3-20. The effects of MJO in enhancing PE/AR precipitation events across the western United States. [*Extracted from CPC (2012) – Figure 1*].

3.1.6 Paleoreconstruction of Climate Signals

As described in the previous section, large scale climate signals (e.g., ENSO, PDO, MJO) often generate identifiable preferences in precipitation and temperature across substantial expanses of real estate. As such, the changes in meteorological conditions over long time periods (seasons to years) can leave physical markers on the landscape and in biological matter (i.e., tree rings, ice stratification, alluvial deposits, coral density, etc.). Records of these markers are available at time scales (hundreds to many thousands of years) that extend far beyond the observational records (at most 150 years). These paleorecords can be used to infer the occurrence of past cycles of climate by comparing recent observations of the physical markers with the occurrence of various climate signals. Although not performed in this study, much research has been devoted to the reconstruction of climate signals using paleorecords. Table 3-3 provides a snapshot of the available paleoreconstructions which might prove useful in identifying the atmospheric forcing mechanisms related to past extreme precipitation and flood events in California. Though not a climate signal directly, the reconstruction of sea surface temperatures may offer additional inferences on the state of PDO and/or ENSO for historical periods beyond 2,000 years before present.

Table 3-3. Potential sources of paleoclimatological information related to PDO, ENSO, and sea surface temperature (SST) in the eastern tropical Pacific Ocean. [*Extracted from the National Climatic Data Center's World Data Center for Paleoclimatology at http://www.ncdc.noaa.gov/paleo/recons.html*].

Climate Signal	Source	Years Reconstructed
PDO	Biondi et al. (2001)	330
	D'Arrigo and Wilson (2006)	420
	D'Arrigo et al. (2001)	300
	Felis et al. (2010)	120
	MacDonald and Case (2005)	1,000
	Shen et al. (2006)	530
ENSO	Cook et al. (2008)	700
	Wilson et al. (2010)	460
	Cook (unpublished)	575
	Mann et al. (2000)	330
	Braganza et al. (2009)	450
	Gergis and Fowler (2009)	470
	Li et al. (2011)	1,100
	Quinn and Neal (1983)	500
	Stahle et al. (1998)	270
	Yan et al. (2011)	2,000
	McGregor et al. (2010)	350
SST (Eastern Tropical Pacific)	Evans et al. (2002)	400
	Liu and Herbert (2004)	1,830,000
	Dubois et al. (2009)	30,000
	Dubois et al. (2011)	100,000
	Kienasi et al. (2006)	36,000
	Lawrence et al. (2006)	5,089,000
	Marchitto et al. (2010)	13,000
	Leduc et al. (2007)	90,000

3.1.7 Trends, Climate Change, and ARs

The extreme rainfall catalog from Goodridge (1996) evaluated trends in 1000-year storms and related forcing mechanisms (i.e., sea surface temperatures offshore and tropical cyclones). An increasing trend was indicated in sea surface temperatures, tropical cyclones, 1000 year storms, and variability of state average rainfall (e.g., Figure 3-21). It should be noted however that the availability of superior and additional observational data since the mid-20th century may be, at least partially, responsible for the apparent increasing trends in observations.

Figure 3-21. 1000-year storm frequency and rainfall variability [*Extracted from Goodridge (1996) – Figure 2*].

That said, recent climate change studies related to extreme rainfall events and flooding in California suggest increased risk related to flooding in future climates. Dettinger (2011) used the A2 greenhouse gas emissions scenarios from a seven member, global climate model (GCM) ensemble. They found that the number of years with higher numbers of AR events (Table 3-4), ARs with greater than historical water vapor transport (Table 3-5), and temperatures associated with the AR (Figure 3-22) show increases. In addition, the peak season for ARs lengthens.

The combination of all these factors could create conditions favorable for more frequent and more severe flooding in California (Dettinger, 2011).

Table 3-4. Trends in number of AR days/100 years from seven climate models. Bold indicates statistical significance. [*Extracted from Dettinger (2011) – Table 1*].

Climate Model	Change in # AR Days/100 Years	R^2 of Trend Fit (in %)
CCC	+7.2 days	30
CNRM	+2.4	4*
ECHAM	+4.5	10
GFDL	+0.4	0.2
GISS	+0.3	0
MIROC	+2.2	7
MRI	+3.6	15

Table 3-5. Trends in intensity (integrated water vapor x upslope wind speed) of AR days/100years from seven climate models. Bold indicates statistical significance. [*Extracted from Dettinger (2011) – Table 2*].

Climate Model	Change/100 Years	% Change/100 Years	R^2 (in %)
CCC	+5.7 cm H_2O m/s	+11%	12
CNRM	+4.0	+9%	8
ECHAM	+3.8	+7%	6
GFDL	+0.1	0	0
GISS	+1.6	+4	3
MIROC	−0.3	−1	0
MRI	+2.1	+5	3*
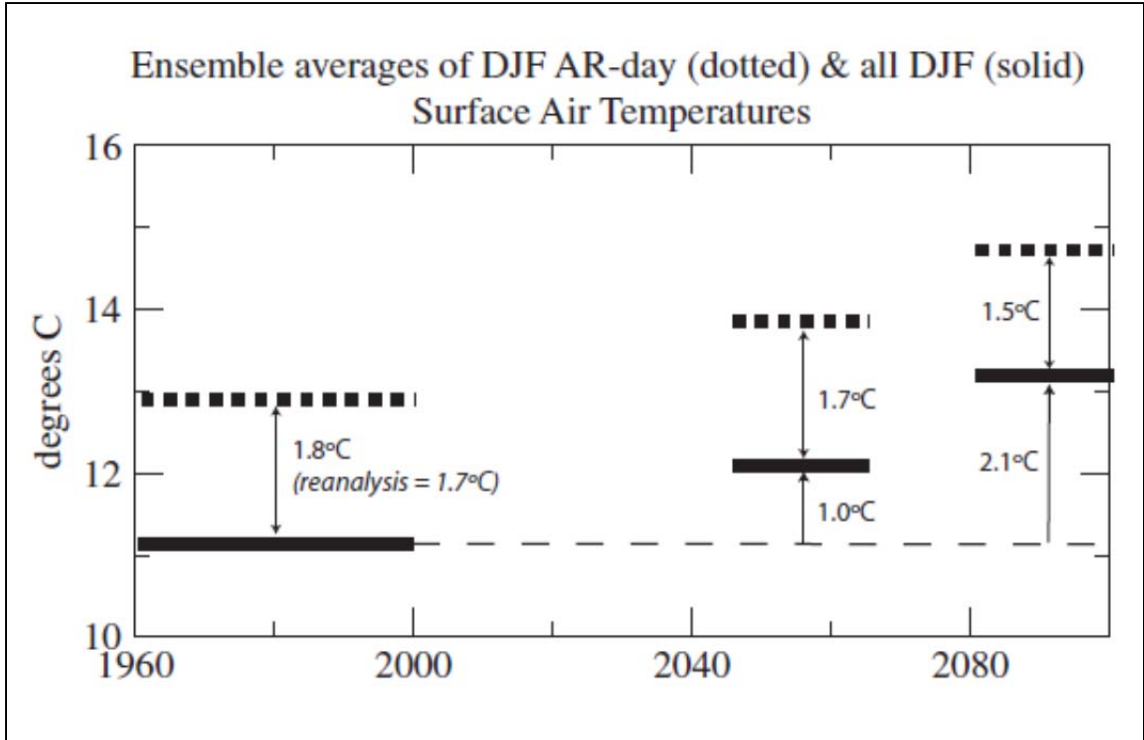
Figure 3-22. Ensemble average temperatures on December-February AR days (dotted) and all December-February days (solid) for historical and future climate scenarios. [*Extracted from Dettinger (2011) – Figure 8*].

Das et al. (2010), however, show conflicting results in their comparison of results from three coupled ocean-atmosphere GCMs in the Sierra Nevada. The GFDL CM2.1 model indicates neutral or drying compared to the other two models (CNRM CM3 and NCAR PCM1), which indicate increased frequency of floods and 3-day flood magnitude in the late 21st century. In general, however, the results agree with Dettinger (2011) in that the frequency of storms is expected to increase. Additionally, Das et al. (2011) show an increased number of days with precipitation in the form of rain rather than snow and, hence, the occurrence of a greater proportion of rainfall-induced versus snowmelt driven flood events under future conditions, particularly in the southern Sierra Nevada (Figure 3-23). This could be directly related to the increasing air temperatures in climate simulations shown in Dettinger (2011).
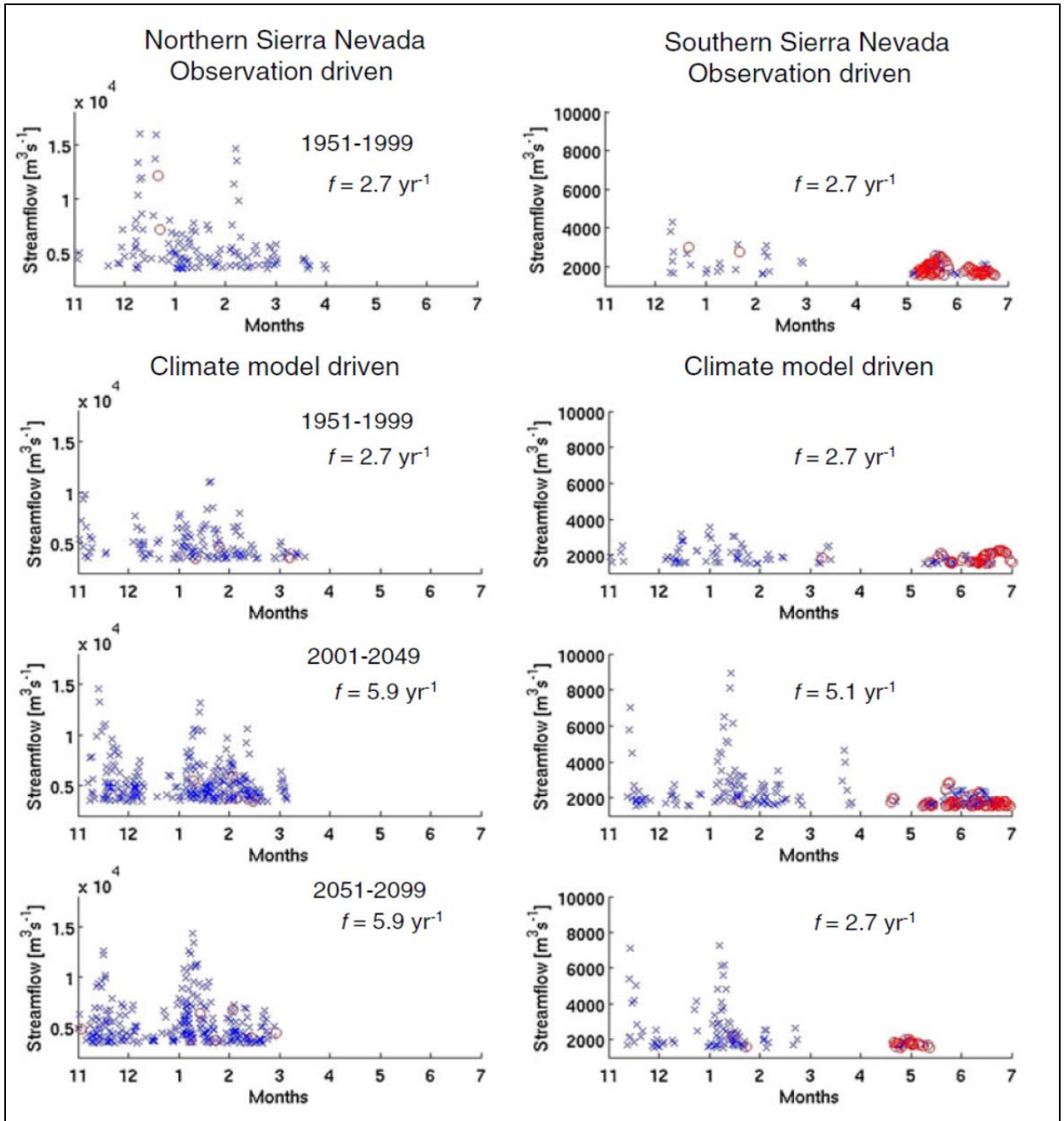
Figure 3-23. Floods in California northern Sierra Nevada (left) and southern Sierra Nevada (right). Panels on first row show observed meteorology driven VIC simulated streamflows. Second through fourth rows show floods using downscaled CNRM CM3 driven VIC simulated streamflows for 1951-1999, 2001-2049, and 2051-2099, respectively. Frequency of floods per year (f) is provided. Blue "X" symbols indicate rainfall-driven floods; red circles are snowmelt-driven floods. [*Extracted from Das et al. (2011) – Figure 5*].

3.1.8 Summary of Findings

Rainfall in California is highly variable with a limited number of days contributing to a majority of the annual precipitation. In California, the dominant driver of extreme rainfall events is ARs, sometimes also referred to as the "Pineapple Express". ARs generally account for 20 to 60 percent of the total cool season streamflow across California, corresponding to the large precipitation contribution provided by these events. ARs are associated with strong southwesterly moisture advection and upslope flow along the orographic regions in California, which serve to focus the heaviest precipitation amounts. Secondary mid-level AR circulations are also observed and directly impact the occurrence of heavy rainfall and flooding in leeside regions.

 ENSO forcing is apparent across northern and southern California in seasonal and annual precipitation totals, but less so in central California (i.e., Sierra Nevada), which is located in the transition region between two preferred jet stream positions. Individual event correlations with ENSO are less clear or non-existent; however, flooding events may be correlated due to the predecessor wet conditions associated with persistent rainy periods associated with ENSO phases (i.e., La Niña in Pacific Northwest; El Niño in Southwest). A transition of warm-to-neutral ENSO conditions has been related to a higher frequency of extreme precipitation events in general along the West Coast. Though central California events are poorly correlated with ENSO, there is a strong correlation with a southward shift in the PDO. Intraseasonal variations in the tropical pacific (e.g., MJO) often modulate the ENSO signal and have the capability of amplifying the enhanced precipitation teleconnection over the Pacific Northwest during La Niña events.

Trend analyses and climate change models of future conditions indicate a general increased frequency of AR events, extreme precipitation, and flooding from the historical observations and in a majority of GCMs, respectively. It is important to note that future projections from GCMs are highly variable in future predictions of precipitation due, in part, to the lack of sufficient resolution to adequately model convective precipitation.

Future research could make broad judgments on the occurrence of floods based on reconstructions of ENSO and MJO; however, the focus should be constrained to regions of southern and extreme northern California; and, the Pacific Northwest based on this literature review. Reconstructions of PDO might be useful for assessment of floods in the Sierra Nevada of central California from a paleohydrology perspective.

3.2 Hydrology of the Sierra Nevada region

The study area is subdivided based on hydrologic units developed by the U.S. Geological Survey (Seaber et.al., 1994). Hydrologic units are divided into regions based on major geographic areas and further divided into subregions based on river systems. California falls into Region 18, defined as the "California Region **--** (a) the drainage within the United States that ultimately discharges into the Pacific Ocean within the state of California; and (b) those parts of the Great Basin (or other closed basins) that discharge into the state of California. Includes parts of California, Nevada, and Oregon."

The subregions considered as part of this study (Figure 3-24) are as follows:
- **Subregion 1802 --** Sacramento: The Sacramento River Basin and drainage into Goose Lake. California, Oregon. Area = 27,600 mi^2.
- **Subregion 1803 –** Tulare - Buena Vista Lakes: The drainage into the Tulare and Buena Vista Lake closed basins. California. Area = 16,200 mi^2.
- **Subregion 1804** -- San Joaquin: The San Joaquin River Basin. California. Area = 15,600 mi^2.

There are 810 USGS streamflow stations located in the study area (Figure 3-25). These gages are well distributed across the Sierra Nevada drainages.

Figure 3-24. Subregions used in hydrologic study.
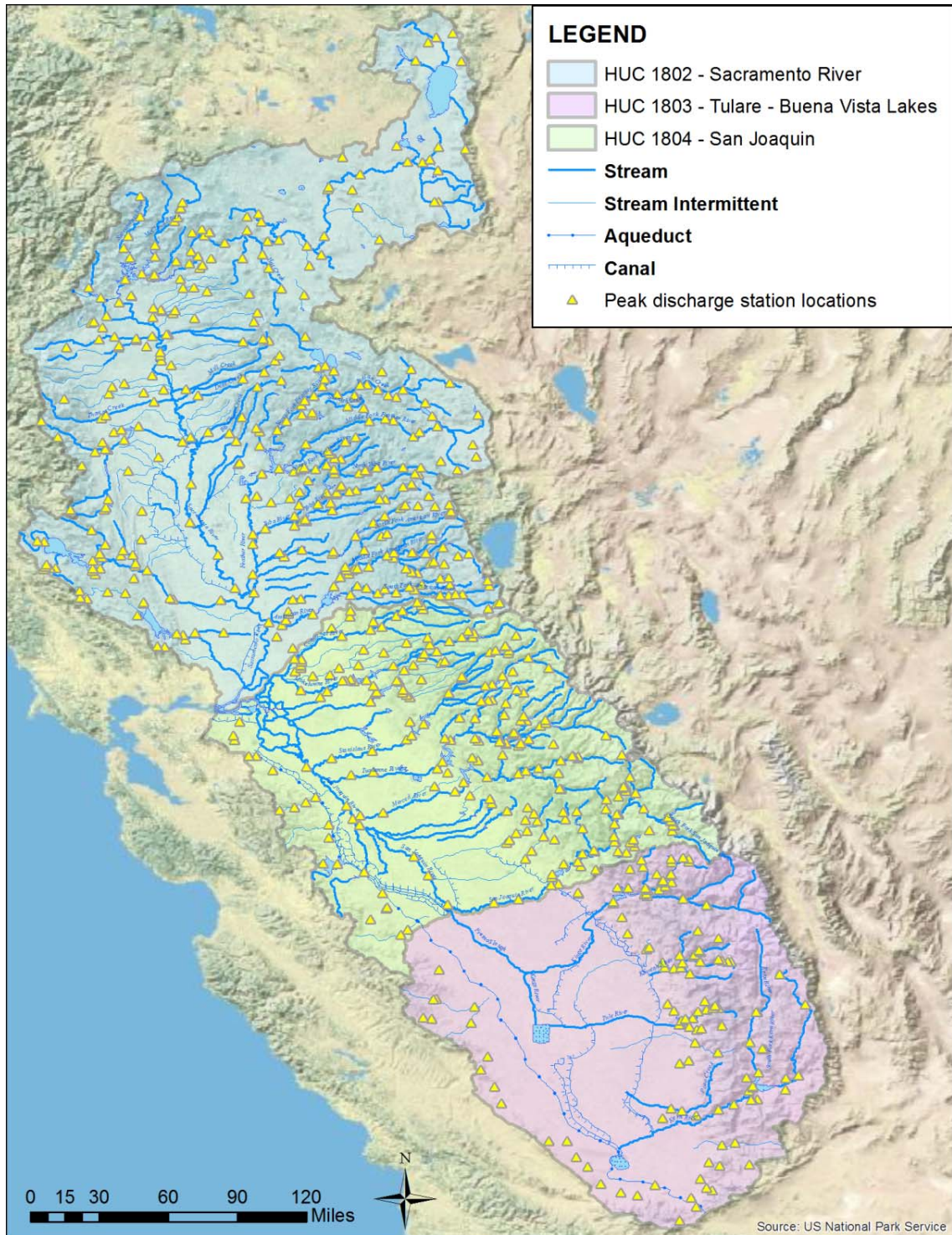
Figure 3-25. Peak discharge streamflow gage station locations.

3.2.1 Envelope curve data

A regional peak discharge envelope curve is used to determine the regional historical flood potential for a certain drainage area size. The curve is developed by plotting the maximum peak flows versus drainage areas for a selected region, then drawing a curve that encompasses the highest values. The regional flood potential for a specific drainage basin size can be determined by intersecting its drainage area with the envelope curve. In this study it is useful to compare the peak discharge data for the three hydrologic subregions of interest (1802, 1803, and 1804). Only basins with at least 0.1 mi^2 of contributing area were included in this chart. The envelope curve is shown in **Figure 3-26** and a map of the locations of the gage stations defining the curve (designated with letters and shown in a table on the chart) is provided in Figure 3-27. Note that points N and O are due to a dam failure on the Middle Fork of the American River on 12/23/1964 and are plotted on the chart, but are not included in the envelope curve development. Paleohydrologic bounds are also plotted on the envelope curve and are derived from paleoflood studies in the American River Basin (Klinger and England, 2002) and San Joaquin River Basin (Godaire and Bauer, 2012). The following paragraphs summarize these paleoflood investigations.

Paleoflood and non-exceedance data were collected on the San Joaquin River near Friant Dam to address the Dam Safety 2003-SOD-C Recommendation to evaluate hydrologic risks associated with the overtopping of Friant Dam. Three study reaches were used to develop paleoflood and non-exceedance data. The Coyote reach and Skaggs Bridge reach are located approximately 26 and 32 miles downstream of Friant Dam, respectively. The Horseshoe Bend reach is located approximately 19 miles upstream of the high pool of Millerton Reservoir. These reaches were used to develop the data because they preserve stratigraphy that is conducive to developing paleoflood and non-exceedance information and they encompass most or all of the drainage area for Friant Dam.

In Coyote and Skaggs Bridge reaches, degree of soil formation and lack of evidence for recent flooding at sites SR1 and SR3 indicate terrace stability and form the basis for a non-exceedance bound. Radiocarbon dating and hydraulic modeling indicate that a flood with a discharge of 105,000-140,000 ft^3/s, has not been exceeded in the last 980 to 2,340 Cal yr BP (1,040-2,400 years) (Table 3-6). Site SR4 consists of flood deposits over a buried surface and is used to develop paleoflood information. Based on hydraulic modeling and historical flood peak discharge estimates, at least 6 floods have inundated this surface over a span of 290 to 490 Cal yr BP. Thus, a maximum return interval for each of these floods ranges from about 60-90 years. The peak discharge estimate of 44,000 ft^3/s for the paleoflood information is derived from the hydraulic modeling at site SR4 and the upper estimate of 110,000 ft^3/s from the largest historical flood at old Millerton near Friant Dam (1867, McGlashan and Briggs, 1939; England and Levish, 1998).

In Horseshoe Bend reach, slackwater deposits preserve a record of floods that can be used to develop paleoflood information. A soil auger from site SR6 below the

50

stage of the 1997 flood indicates that flood deposits overlie a buried soil that was formed within the last 300 Cal yr BP. It was difficult to determine from the soil auger whether flood deposits other than the 1997 flood are preserved in the stratigraphy at this site. Peak discharge estimates for the 1997 flood stage in this reach using the slackwater deposits indicate that the 1997 flood had a peak discharge of 70,000-72,000 ft^3/s, while the nearby USGS gage reports the 1997 peak discharge as 99,200 ft^3/s. A soil auger from SR5 reveals flood deposits that are above the stage of the 1997 flood and are about 830 to 980 Cal yr BP (890-1,040 years) old based on radiocarbon dating. Peak discharges required to inundate this surface are slightly larger than the 1997 flood stage and are estimated at 72,000-74,000 ft^3/s. To encompass the uncertainty between the HEC-RAS model and USGS peak discharge estimates, the peak discharge for the paleoflood deposits at site SR5 ranges from the modeled discharge of 73,000 ft^3/s to the peak discharge of 110,000 ft^3/s for the largest historical peak discharge estimate (Table 3-6).

Table 3-6. Summary of paleoflood and non-exceedance data for the San Joaquin River near Friant Dam (DA = 1680 mi^2).

Type of Estimate	Peak Discharge (ft^3/s)	Age Estimate (Cal yr BP)	Number of floods
Paleoflood (downstream reaches)	44,000-110,000	290-490	≥6
Paleoflood (upstream reach)	73,000-110,000	860-980	≥1
Non-exceedance	105,000-140,000	980-2,340	0

A detailed study for Folsom Dam was conducted on several rivers that drain the central Sierra Nevada and include the American River, Cosumnes River, Stanislaus River, and Mokelumne River (Klinger and England, 2002). Based on this regional study, several paleoflood estimates and a non-exceedance bound were developed using four specific sites: 1) North Fork American River at Ponderosa Bridge; 2) South Fork American River near Kyburz; 3) South Fork American River near Lotus; and 4) lower American River near Fair Oaks (Table 3-7). Many other sites were used for stratigraphic information to corroborate the paleoflood and non-exceedance estimates through archeology, radiocarbon data and obsidian hydration age estimates. Paleoflood estimates indicate that between 2 and 5 floods larger in magnitude than historical floods have occurred within the past 150 to 650 years. At least one flood larger than historical floods was documented and occurred between about 1400-1600 years ago. Evidence for an additional paleoflood between 650 and 1125 years ago was also documented at the Kyburz site and appeared to be similar in magnitude to the paleoflood with a 1400-1600 year age estimate. To summarize, at least four paleofloods with magnitudes of 1.3 to 2 times larger than the largest historical floods have occurred within the past 1600 years. Peak discharge estimates for the paleofloods varied based on the study site.

A non-exceedance bound was developed on the North Fork American River at Ponderosa Bridge based on soil development on remnants of gravelly Pleistocene terraces between Ponderosa Bridge and Codfish Creek (Table 3-7). The well-developed soil, highly weathered clasts and surface morphology of the terrace was correlated to late Pleistocene deposits in the western Sierra and assigned an age of 10,000 years. Peak discharge estimates for the non-exceedance bound range from 240,000-360,000 ft^3/s.

Table 3-7. Paleoflood and non-exceedance estimates in the American River Basin.

Site	River name	Drainage area (mi^2)	Type of estimate	Peak discharge (ft^3/s)	Age estimate (yrs)
Sand Flat	South Fork American River near Kyburz	193	paleoflood (2 to 5) paleoflood (≥ 1) paleoflood (≥ 1)	32,000-49,000 67,000-81,000 67,000-81,000	<650 years 650-1,125 years 1,380-1,650 years
Old Rock Bridge	South Fork American River near Lotus	695	paleoflood (≥ 1)	170,000-254,000	1,000-1,600 years
Fair Oaks	Lower American River	1888	paleoflood (≥3) paleoflood (≥1)	400,000-550,000 600,000-850,000	152-700 years 700-2,000
Ponderosa Bridge	North Fork American River	330	non-exceedance	240,000-360,000	10,000 years

The envelope curve is primarily defined by gages in the Sacramento River Basin, however a curve enveloping only the Tulare – Buena Vista Basin or San Joaquin River Basin points would not be dramatically lower for the basin areas up to 100 mi^2. The peak discharges recorded at larger contributing areas are lower in the southern basins than in the Sacramento River Basin. Paleoflood data from the Sacramento River basin mostly plot above the envelope curve and indicate that floods of larger magnitude than historical peak discharges have occurred during the past 1,000 to 2,000 years. Paleoflood data from the San Joaquin River Basin plot below the envelope curve and suggest that the envelope curve could be a suitable upper limit for floods in this basin. Relationships between paleoflood data between the two regions are similar to the historical peak discharge relationships in which peak flows are generally higher in the Sacramento River Basin than in the San Joaquin River Basin. Results from the Kern River study (Klinger et al., in press) will shed light on the Tulare-Buena Vista Lakes Basin in the southern Sierra Nevada.
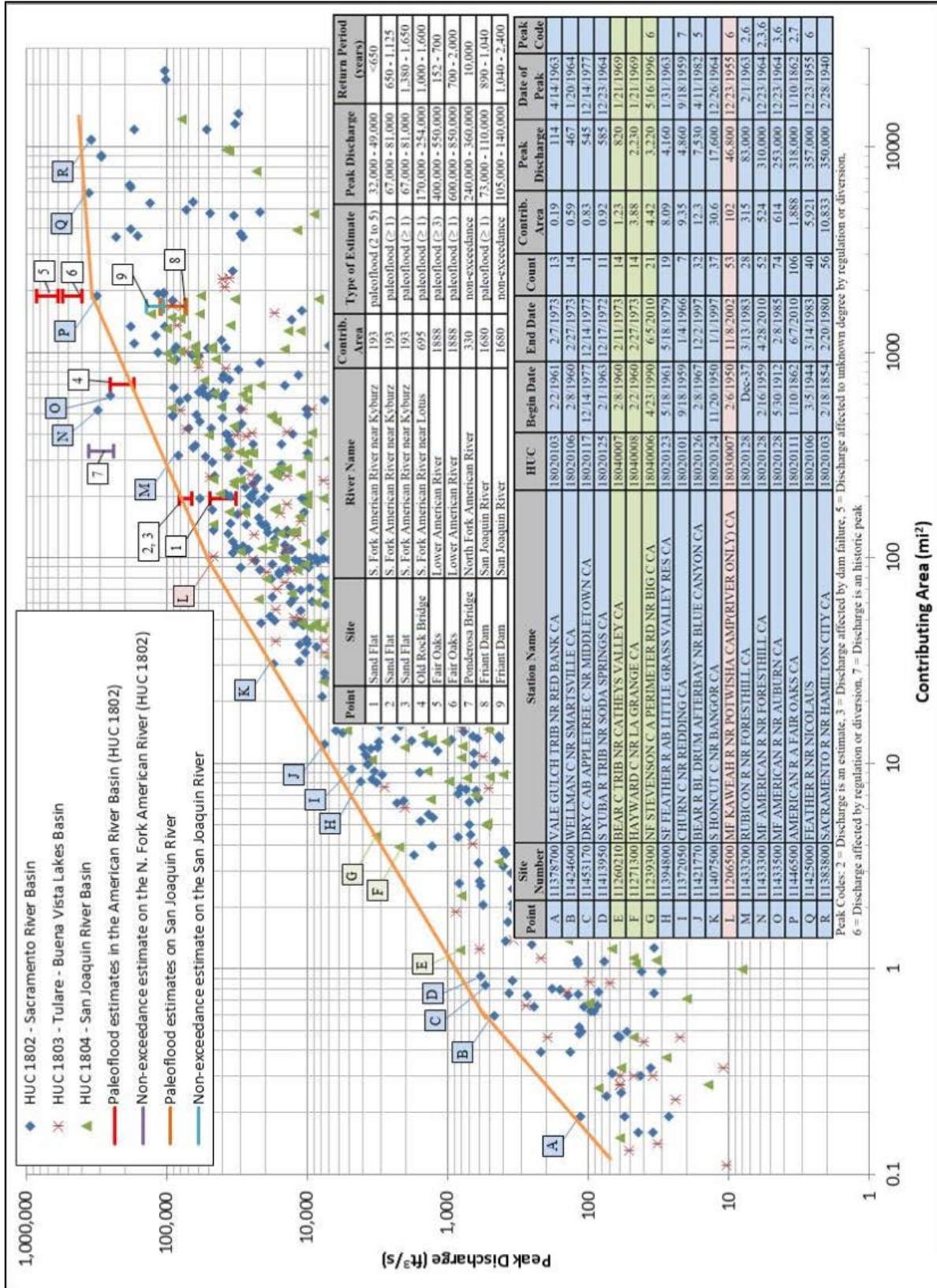
Figure 3-26. Envelope curve of maximum annual peak discharges for the Sierra Nevada region.
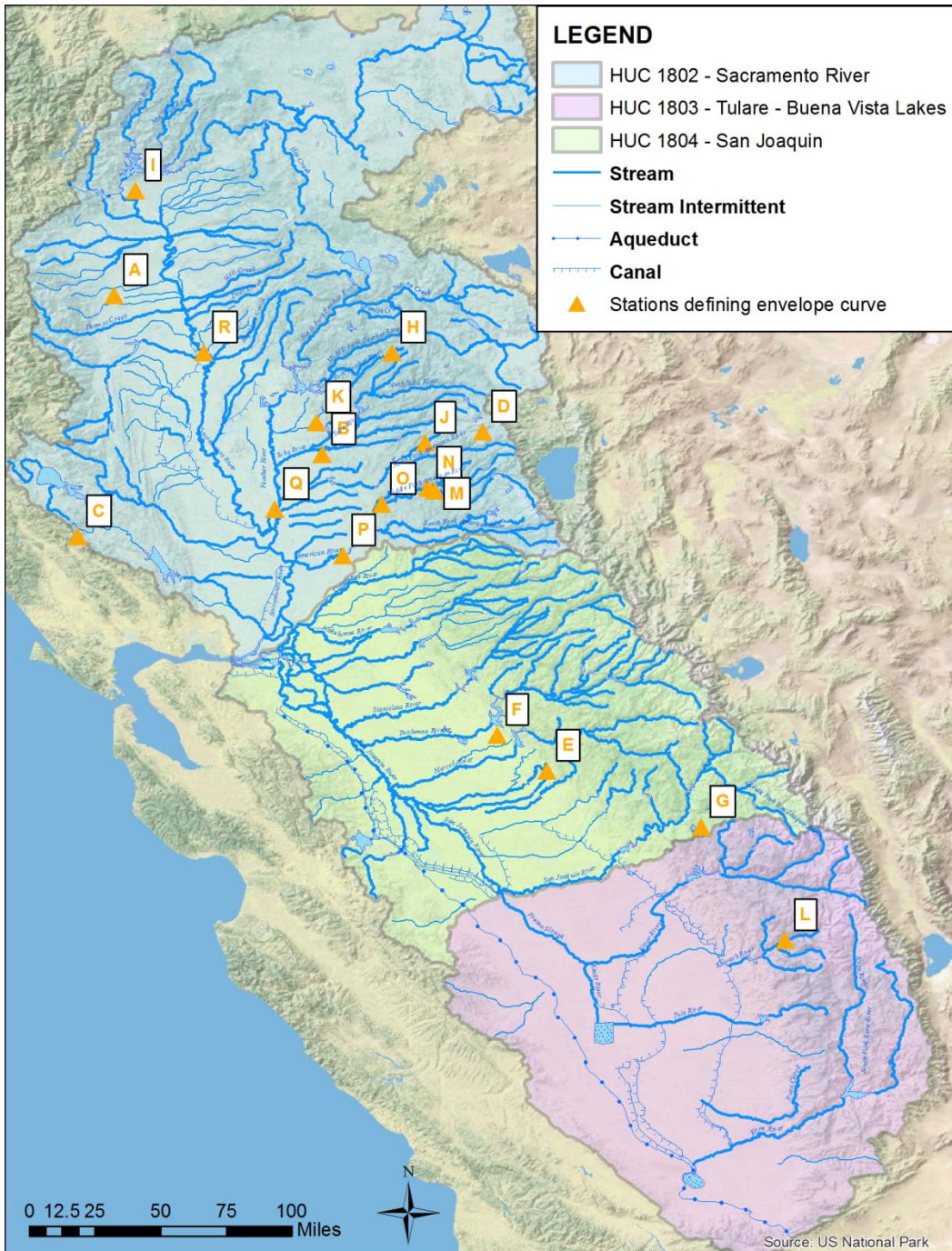
Figure 3-27. Streamflow gage stations defining the envelope curve. Stations are listed in table on Figure 3-26.

3.2.2 Regional flood frequency analysis

3.2.2.1 Data

Flood frequency analyses were performed on representative drainages in each of the subregions of interest. Stream flow stations chosen for the study were ideally unregulated and had long periods of record. However, stations that were regulated were assigned a higher uncertainty in the flow record. For example, unregulated stream flow stations were assigned a discharge uncertainty of 10% and 30% for large magnitude floods while regulated streams were assigned a discharge uncertainty of 25% and 50% for large magnitude floods.

Hydro-climatic data network (HCDN) stream flow stations were considered when choosing stations to include in the flood frequency analysis. The HCDN is a set of stream flow records that are relatively free of confounding anthropogenic influences. This dataset has been developed for the purpose of studying the variation in surface-water conditions throughout the United States (Slack and Landwehr, 1992).

The HCDN stations as well as the stations used in the flood frequency analysis for this study are shown in Figure 3-28. Seventeen stations were chosen for the flood frequency analysis (Table 3-8).
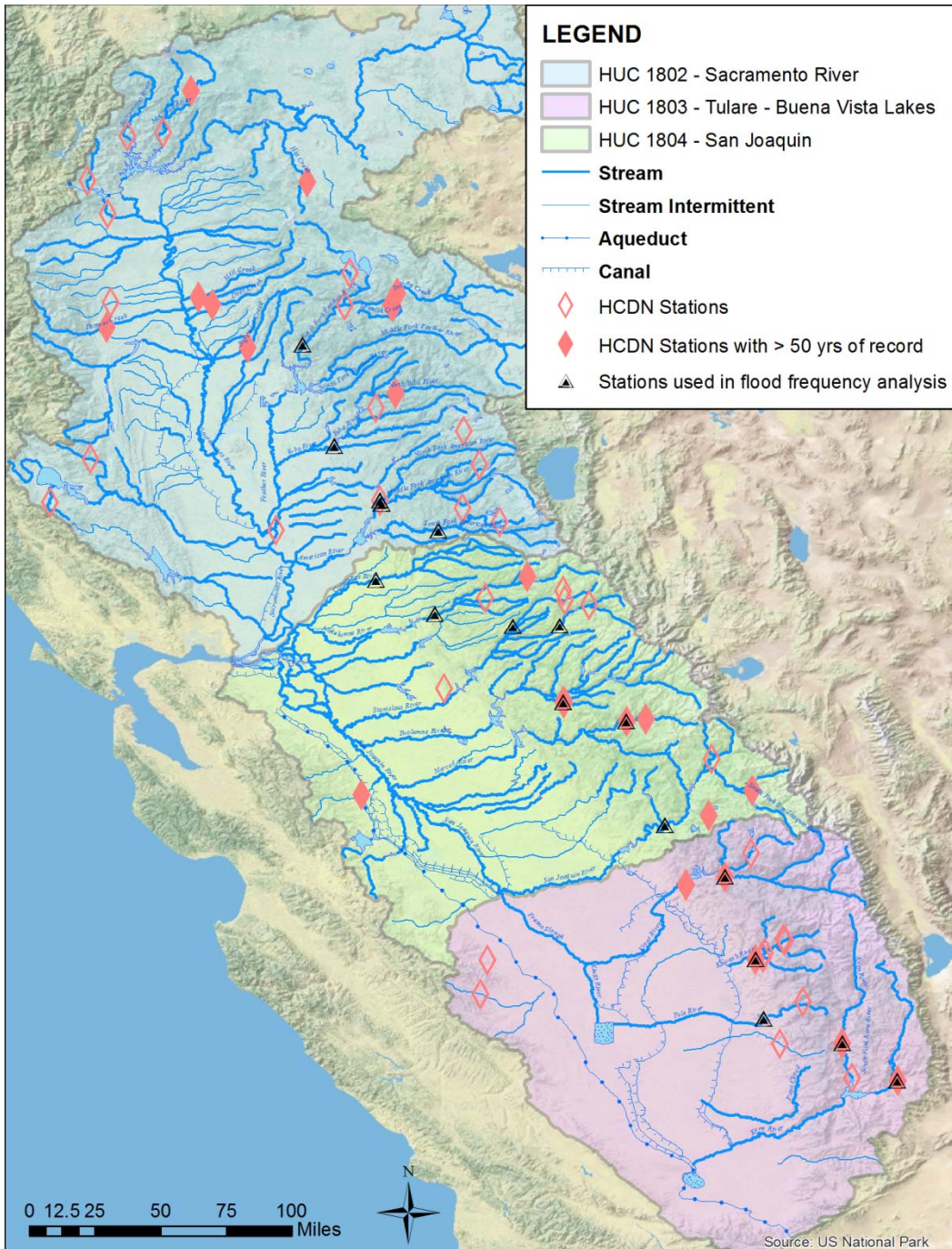
Figure 3-28. Locations of HCDN stations and stream flow gage stations used in flood frequency analysis.

Table 3-8. Stream flow stations used in flood frequency analysis.

Site Number	Station Name	Elev (ft)	Record Begin	Record End	Count	Contrib. Area (mi^2)	Peak Discharge (ft^3/s)	Date of Peak
Tulare-Buena Vista Lakes (HUC 1803)							
11186000	KERN R NR KERNVILLE (RIVER ONLY) CA	3620	6/4/1912	6/6/2010	99	846	60,000	12/6/1966
11189500	SF KERN R NR ONYX CA	2900	5/19/1912	4/28/2010	90	530	28,700	12/6/1966
11203500	TULE R NR PORTERVILLE CA	580	4/7/1902	2/2/1960	59	253	25,500	11/19/1950
11210500	KAWEAH R NR THREE RIVERS CA	611	3/23/1904	12/2/1960	58	519	80,700	12/23/1955
11213500	KINGS R AB NF NR TRIMMER CA	1001	5/17/1927	9/26/1982	53	952	59,100	12/23/1955
San Joaquin (HUC 1804)							
11242000	SAN JOAQUIN R AB WILLOW C NR AUBERRY CA	1175	11/18/1950	6/9/2010	60	1295	99,200	1/2/1997
11266500	MERCED R A POHONO BRIDGE NR YOSEMITE CA	3862	6/10/1917	6/7/2010	94	321	24,600	1/3/1997
11281000	SF TUOLUMNE R NR OAKLAND RECREATION CAMP CA	2800	4/6/1923	12/2/2001	80	87	11,900	12/23/1955
11292700	MF STANISLAUS R A HELLS HALF ACRE BRIDGE CA	3411	12/23/1955	6/7/2010	55	287	26,600	12/23/1955
11294500	NF STANISLAUS R NR AVERY CA	3388	5/11/1915	6/29/2011	91	166	36,000	1/31/1963
11319500	MOKELUMNE R NR MOKELUMNE HILL CA	585	2/19/1901	6/6/2010	86	544	41,300	1/2/1997
11335000	COSUMNES R A MICHIGAN BAR CA	168	3/19/1907	2/27/2010	104	536	93,000	1/2/1997
Sacramento River (HUC 1802)							
11404500	NF FEATHER R A PULGA CA	1305	1/26/1912	3/16/2011	100	1953	105,400	1/1/1997
11418000	YUBA R BL ENGLEBRIGHT DAM NR SMARTSVILLE CA	1108	2/6/1942	6/5/2010	68	1108	171,000	12/22/1964
11427000	NF AMERICAN R A NORTH FORK DAM CA	715	1/27/1942	4/28/2010	69	342	65,400	12/23/1964
11433500	MF AMERICAN R NR AUBURN CA	552	5/30/1912	2/8/1985	74	614	253,000	12/23/1964
11443500	SF AMERICAN R NR CAMINO CA	1620	4/6/1923	12/19/2010	89	493	62,300	1/2/1997

3.2.2.2 Flood Frequency Analysis

Flood frequency curves for seventeen drainages were developed for this study by combining annual instantaneous peak flow and paleoflood data using a Bayesian, Maximum Likelihood Estimator (MLE) approach. The flood frequency program FLDFRQ3 (O'Connell, 1999) was utilized because it readily incorporates peak discharge and discharge measurement uncertainties. The maximum likelihood frequency model was run using the log base 10 Pearson Type III (LP3) distribution, with parameters μ, σ, and γ (mean, standard deviation, and skew).

This program uses a Bayesian approach to include measurement uncertainty in the parameter estimation procedure. A measurement error source in this study is peak

discharge measurement errors from the gaged record. Bayesian methods and likelihood functions are used to incorporate data and parameter uncertainties (O'Connell, 1999). Regional skew is not incorporated in FLDFRQ3. Peak-flow frequency median (50%), 5% and 95% confidence limit peak discharge estimates were developed. Paleoflood data and paleohydrologic bounds were not used in the flood frequency analyses due to the lack of data on most rivers in the study area.

The results of the flood-frequency analyses for all seventeen rivers are shown in Table 3-9. To calculate the unit discharge, or normalized discharge, the magnitude of each flood at selected recurrence intervals was divided by the drainage area at the location of the gaging stating where the data was collected (Figure 3-29).

Table 3-9. Flood Frequency Analysis Results.

Discharge magnitudes and associated 95% confidence intervals for select recurrence intervals						
NF Feather River; drainage area 1953 mi^2						
Data type	10 yr	25 yr	50 yr	100 yr	200 yr	500 yr
Magnitude	49,093	61,831	69,336	75,207	79,928	84,674
Normalized	25	32	36	39	41	43
Upper limit	58,745	77,100	90,567	103,489	115,207	130,285
Lower limit	41,823	52,929	58,541	62,270	64,766	66,778
Yuba River; drainage area 1108 mi^2						
Data type	10 yr	25 yr	50 yr	100 yr	200 yr	500 yr
Magnitude	72,732	101,497	122,084	141,559	159,581	181,251
Normalized	66	92	110	128	144	164
Upper limit	105,486	178,997	255,522	353,896	477,494	689,998
Lower limit	55,770	74,544	84,189	90,673	95,085	98,826
NF American River; drainage area 342 mi^2						
Data type	10 yr	25 yr	50 yr	100 yr	200 yr	500 yr
Magnitude	36,280	49,709	59,785	69,642	79,398	91,881
Normalized	106	145	175	204	232	269
Upper limit	49,255	77,714	105,756	140,137	181,981	250,852
Lower limit	28,725	38,552	44,565	49,212	52,734	56,141
MF American River; drainage area 614 mi^2						
Data type	10 yr	25 yr	50 yr	100 yr	200 yr	500 yr
Magnitude	40,850	58,403	72,861	88,385	105,057	128,646
Normalized	67	95	119	144	171	210
Upper limit	56,944	93,286	130,787	179,151	240,969	348,855
Lower limit	31,930	43,846	52,204	59,732	66,437	74,149
SF American River; drainage area 493 mi^2						
Data type	10 yr	25 yr	50 yr	100 yr	200 yr	500 yr
Magnitude	25,762	35,749	41,678	46,388	50,161	53,772
Normalized	52	73	85	94	102	109
Upper limit	33,527	49,345	61,676	74,449	86,488	101,550
Lower limit	20,121	28,769	33,407	36,477	38,317	39,795

Cosumnes River; drainage area 536 mi^2						
Data type	**10 yr**	**25 yr**	**50 yr**	**100 yr**	**200 yr**	**500 yr**
Magnitude	30,875	43,011	51,829	60,353	68,467	78,474
Normalized	58	80	97	113	128	146
Upper limit	39,234	59,184	76,973	97,158	119,799	152,806
Lower limit	25,342	34,601	40,474	45,315	49,147	53,078

Mokelumne River; drainage area 544 mi^2						
Data type	**10 yr**	**25 yr**	**50 yr**	**100 yr**	**200 yr**	**500 yr**
Magnitude	17,970	26,361	33,614	41,686	50,559	63,684
Normalized	33	48	62	77	93	117
Upper limit	25,962	48,915	76,973	119,045	181,289	310,081
Lower limit	14,179	19,336	22,463	24,981	27,034	29,181

NF Stanislaus River; drainage area 166 mi^2						
Data type	**10 yr**	**25 yr**	**50 yr**	**100 yr**	**200 yr**	**500 yr**
Magnitude	15,576	28,499	43,239	64,229	93,368	150,738
Normalized	94	172	260	387	562	908
Upper limit	24,059	52,728	93,096	161,626	276,864	553,129
Lower limit	11,373	18,775	25,941	34,611	45,011	61,917

MF Stanislaus River; drainage area 287 mi^2						
Data type	**10 yr**	**25 yr**	**50 yr**	**100 yr**	**200 yr**	**500 yr**
Magnitude	8,704	11,228	12,761	13,975	14,972	15,922
Normalized	30	39	44	49	52	55
Upper limit	13,033	20,974	28,449	37,352	47,608	63,379
Lower limit	6,827	8,532	9,094	9,364	9,500	9,586

SF Tuolumne River; drainage area 87 mi^2						
Data type	**10 yr**	**25 yr**	**50 yr**	**100 yr**	**200 yr**	**500 yr**
Magnitude	5,281	8,354	11,158	14,432	18,195	23,986
Normalized	61	96	128	166	209	276
Upper limit	7,815	15,284	24,495	38,328	58,762	101,105
Lower limit	3,996	5,982	7,447	8,811	10,058	11,532

Merced River; drainage area 321 mi^2						
Data type	**10 yr**	**25 yr**	**50 yr**	**100 yr**	**200 yr**	**500 yr**
Magnitude	10,304	14,358	17,972	22,165	27,025	34,594
Normalized	32	45	56	69	84	108
Upper limit	13,035	20,098	27,382	36,854	49,177	71,124
Lower limit	8,643	11,447	13,679	16,018	18,493	21,963

San Joaquin River; drainage area 1295 mi^2						
Data type	**10 yr**	**25 yr**	**50 yr**	**100 yr**	**200 yr**	**500 yr**
Magnitude	26,182	35,180	39,656	42,754	44,775	46,601
Normalized	20	27	31	33	35	36
Upper limit	40,832	67,044	88,878	111,022	132,172	158,445
Lower limit	19,532	26,409	28,659	29,710	30,159	30,477

Kings River; drainage area 952 mi^2						
Data type	**10 yr**	**25 yr**	**50 yr**	**100 yr**	**200 yr**	**500 yr**
Magnitude	23,969	36,248	48,145	63,023	81,384	112,550
Normalized	25	38	51	66	85	118

Data type	10 yr	25 yr	50 yr	100 yr	200 yr	500 yr
Upper limit	35,843	64,695	98,977	149,881	224,266	379,396
Lower limit	18,305	25,467	31,531	38,136	45,296	55,841
Kaweah River; drainage area 519 mi^2						
Data type	**10 yr**	**25 yr**	**50 yr**	**100 yr**	**200 yr**	**500 yr**
Magnitude	18,163	32,302	48,130	70,482	101,364	161,073
Normalized	35	62	93	136	195	310
Upper limit	31,357	72,420	133,694	243,594	44,034	945,415
Lower limit	12,703	19,982	26,748	34,709	440,484	58,563
Tule River; drainage area 253 mi^2						
Data type	**10 yr**	**25 yr**	**50 yr**	**100 yr**	**200 yr**	**500 yr**
Magnitude	4,001	7,301	10,802	15,422	21,419	32,006
Normalized	16	29	43	61	85	127
Upper limit	6,036	14,840	28,307	52,614	95,833	206,313
Lower limit	2,841	4,730	6,273	7,825	9,345	11,267
Kern River; drainage area 846 mi^2						
Data type	**10 yr**	**25 yr**	**50 yr**	**100 yr**	**200 yr**	**500 yr**
Magnitude	9,882	15,895	21,735	28,937	37,729	52,333
Normalized	12	19	26	34	45	62
Upper limit	7,625	25,756	39,570	59,474	87,876	144,158
Lower limit	13,931	11,351	14,455	17,781	21,324	26,334
SF Kern River; drainage area 530 mi^2						
Data type	**10 yr**	**25 yr**	**50 yr**	**100 yr**	**200 yr**	**500 yr**
Magnitude	3,257	6,797	11,329	18,385	29,259	52,660
Normalized	6	13	21	35	55	99
Upper limit	5,555	14,925	30,591	8,489	121,774	295,061
Lower limit	2,229	4,069	5,997	61,550	11,673	17,125
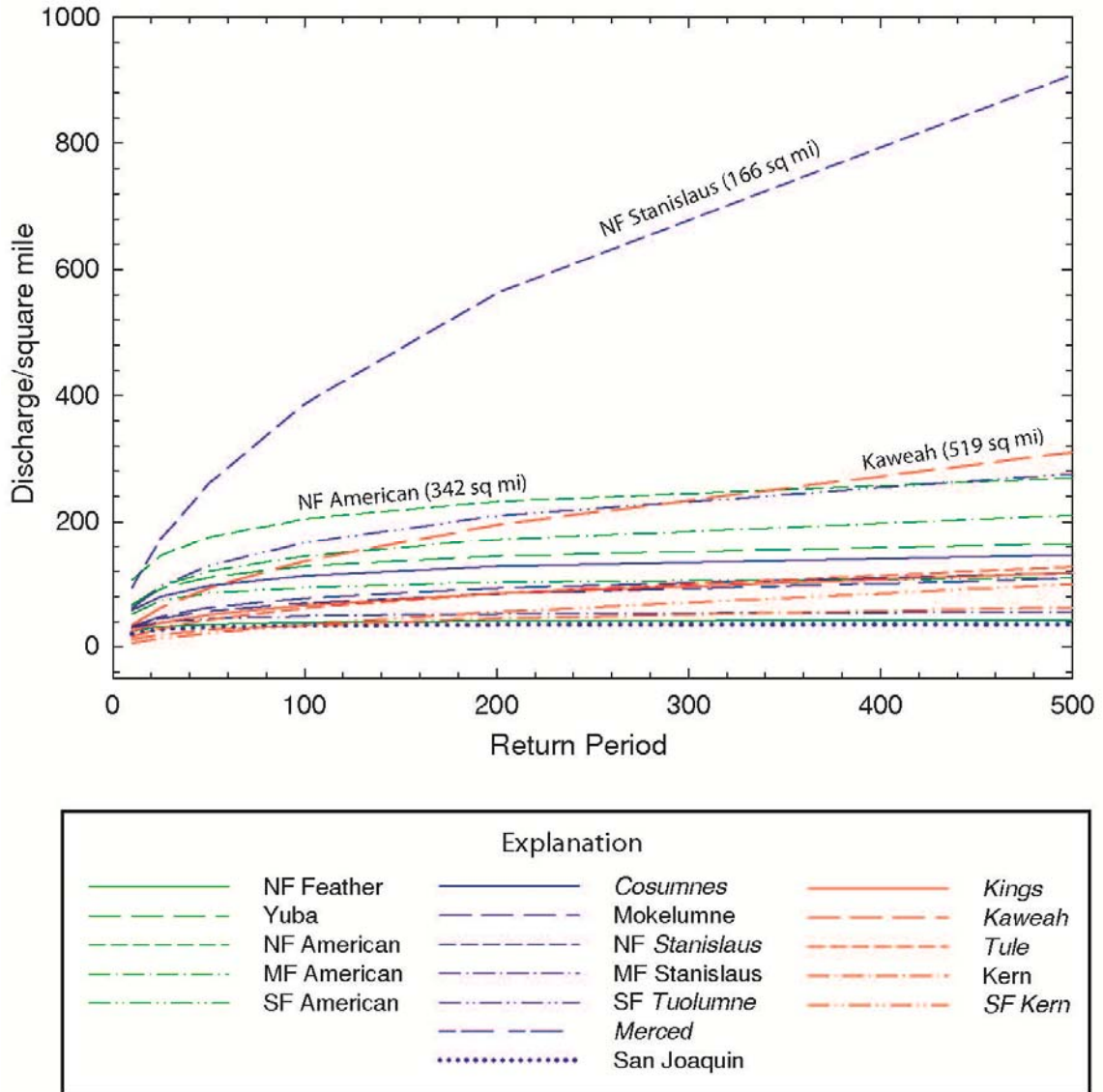
Figure 3-29. Unit discharge flood frequency analysis results (Stations in subregion 1802 shown in blue, stations in subregion 1803 shown in red, stations in subregion 1804 shown in green. Italicized stations are unregulated for all or most of the record.)

With few exceptions, the drainages in the Sacramento River subregion (HUC 1802) have the highest unit discharges overall. Of the five drainages in the Sacramento River subregion (Feather, Yuba, and the NF, MF, and SF of the American River), the North Fork of the American River has the highest unit discharge at all recurrence intervals but the smallest drainage area at 342 mi^2. This is related to its geographic position, where ARs are able to penetrate inland through the gap in the Coast Range at San Francisco Bay to deliver copious amounts of moisture to the American River Basin. The orientation of the mountain front perpendicular to the storm track as well as basin shape are also likely to play a significant role in extreme flood generation. The second highest unit discharge comes from the Middle Fork of the American River followed by

61

the Yuba, South Fork of the American and North Fork of the Feather River. The North Fork of the Feather River has the largest drainage area at 1953 mi^2 but the second smallest unit discharge in the whole study area. Elevation may also play a key role in flood generation at these sites. The unit discharge flood frequency curves generally follow a pattern where the lowest elevation sites (NF American River and MF American River) have the largest unit discharges and the highest elevation sites (SF American River and NF Feather River) have the smallest unit discharges for a given recurrence interval. Since the largest floods occur during the winter, the lower elevation sites will likely receive a greater proportion of the precipitation as rain during storms whereas the higher elevation sites may receive a greater proportion as snow. Thus, the lower elevation sites are likely to experience greater runoff during the winter events. When comparing overall discharge magnitudes, the Yuba River experiences the largest floods followed by the Middle Fork of the American, North Fork of the Feather, North Fork of the American and South Fork of the American. This order loosely follows the order of drainage area with the larger basins having greater magnitude floods than the smaller basins, but smaller unit discharges, which is common (Figure 3-30).
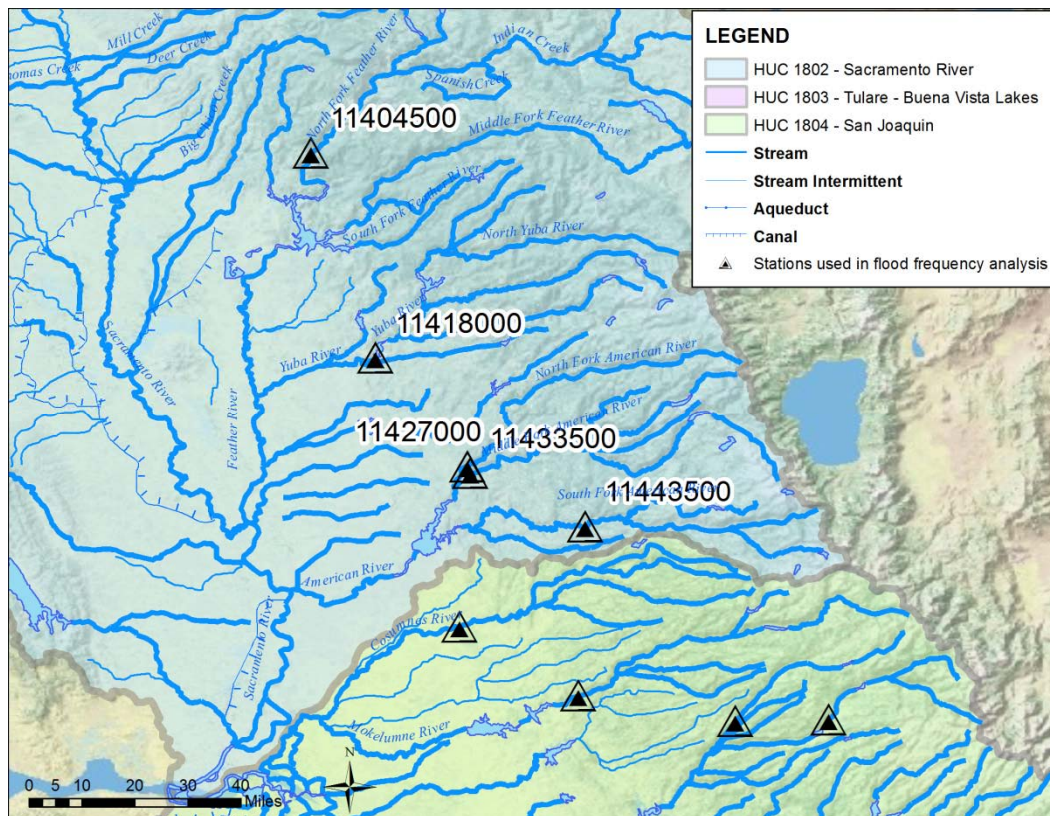
Figure 3-30. Stream flow station locations in HUC 1802 – Sacramento River.

The seven rivers in the San Joaquin subregion (North and Middle Forks of the Stanislaus, Cosumnes, Mokelumne, South Fork of the Tuolumne, Merced and San Joaquin Rivers) have both the highest unit discharge (North Fork of the Stanislaus) and the lowest unit discharge (San Joaquin) of the whole study area (Table 3-9; Figure 3-31). The other five rivers are almost evenly spaced

62

throughout the unit discharge graph (Figure 3-29). The North Fork of the Stanislaus has a unit discharge that is more than three times larger (for the 500-yr flood) than the next highest unit discharge (North Fork American River). Moreover, its discharge magnitude for the higher recurrence intervals is the third largest out of all the seventeen rivers yet the drainage area is the second smallest. The North Fork of the Stanislaus is discussed further in the Flood Frequency Analysis section. The South Fork Tuolomne follows a similar pattern, with high unit discharges and a small drainage area. The San Joaquin River has the smallest unit discharge and the second largest drainage area. Generally, with the exception of the Tuolumne and San Joaquin Rivers, the rivers with the largest unit discharges also have the largest magnitude floods regardless of drainage area size, a contrast from the Sacramento River subregion. Relationships between elevation of the gage site and unit peak discharges are not readily apparent in this subbasin.
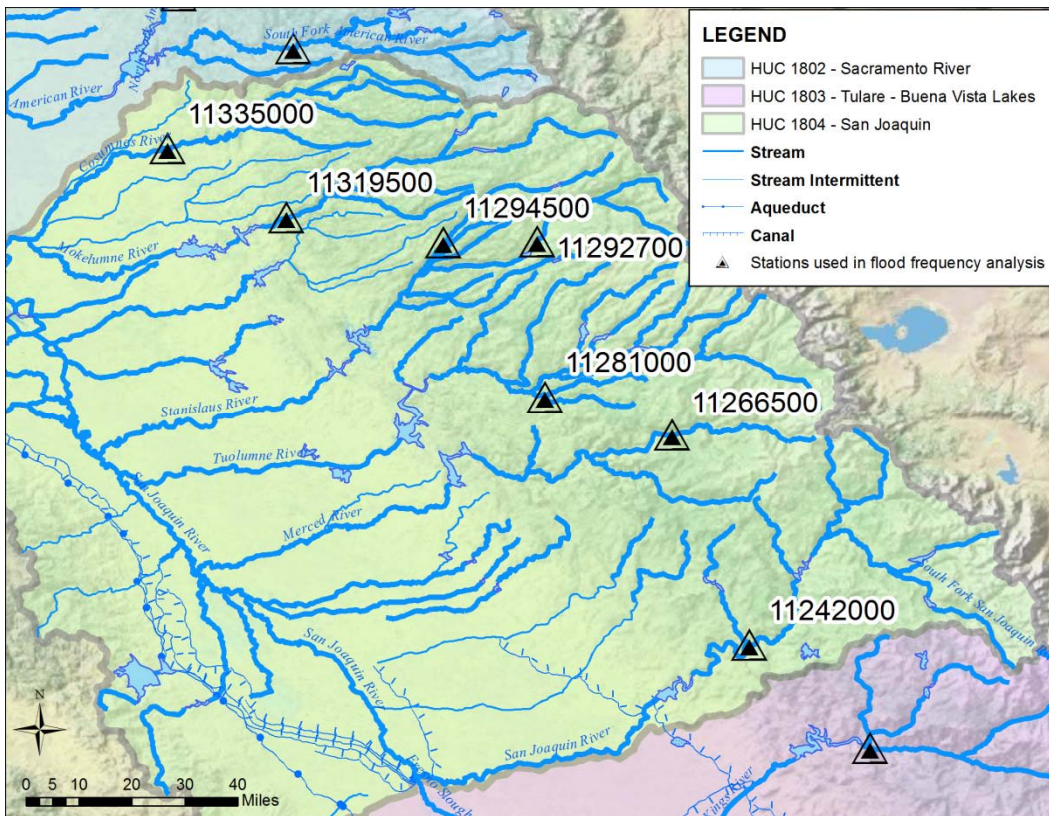
Figure 3-31. Stream flow station locations in HUC 1804 – San Joaquin River.

Overall, the five rivers (Kings, Kaweah, Tule, Kern, and South Fork Kern River) in the Tulare – Buena Vista Lakes subregion (HUC 1803) have the lowest unit discharge magnitudes and some of the lowest total discharge magnitudes for each recurrence interval even though they have relatively large drainage areas (Figure 3-29; Figure 3-32). The Kaweah River has the highest unit discharge in the southern basin and the second largest at higher return periods compared to the whole study area. However, at more frequent return periods, the unit discharge is significantly less when compared to other rivers. This is discussed in detail in the section on the Kaweah River. The Kaweah also experiences the highest

63

magnitude floods, similar in size to the North Fork Stanislaus but over 2.5 times the basin area. The Tule River and the Kings River have very similar unit discharge values followed by the South Fork Kern and Kern Rivers. Unlike the other basins, drainage area for the main river in the Tulare-Buena Vista basin does not seem to play as large or a roll role in flood magnitude. For example, at return periods greater than 50 years the Kings River experiences the second largest floods and has the third largest unit discharge but has the greatest drainage area. The Kern River has the second largest drainage area but experiences the second smallest flood magnitudes and has the smallest unit discharge. It is likely that elevation plays a key role in generating larger floods on the Kaweah River since its elevation is much lower than the other gage sites investigated in the subbasin and would allow for a greater proportion of precipitation to occur as rainfall. The equidimensional shape of the Kaweah River basin also allows for similar time of concentration for floods from the tributary arms, such that the peaks from the upper subbasins will coalesce on the main stem with similar timing to produce a large peak flow. Other basin characteristics such as topography and latitude may also play a large role in determining flood magnitude and may help to explain why a site such as the Tule River does not have as high a unit discharge when compared to the Kaweah River.
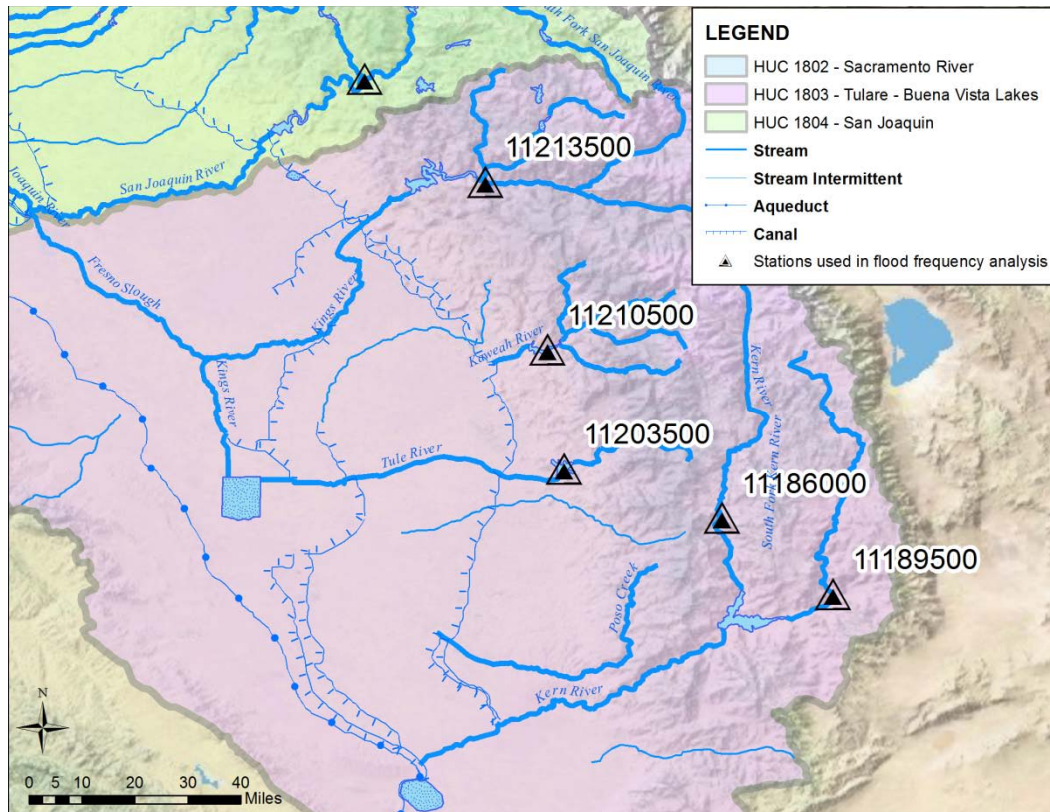
Figure 3-32. Stream flow station locations for HUC 1803 – Tulare – Buena Vista Lakes.

3.2.2.3 Gage Record Discussion

All of the peaks of record at the gage stations for the seventeen rivers examined in the study area occurred from November through February and all occurred in one of six years, 1950 (1), 1955 (4), 1963 (1) 1964 (3), 1967 (2), and 1997 (6). Every one of these years has been associated with PE/AR circulation patterns (Dettinger, 2005). In fact, almost all major historical storms in rivers in California have been associated with PE/ARs (Dettinger, 2011) with the largest events occurring from November to February. Smaller flood events that most of the annual peaks in the gaged records are attributed to are caused by a very different phenomenon and mostly occur from March to May. These floods are caused by later season snowmelt and although smaller and less flashy than the November to February floods, can yield a higher volume (Booth et al., 2006).

3.2.2.4 Flood Frequency Analysis

Frequency curves for all rivers included in the study are in Attachment A. When examining individual unit discharge magnitudes for the recurrence intervals shown in Figure 3-29, two rivers stand out: the North Fork of the Stanislaus River and the Kaweah River. The North Fork of the Stanislaus River has a significantly higher unit discharge for floods at every return period except for those less than about the 25-yr flood. Possible reasons for this are; 1) there might be systematic errors in the gaged record due to the logarithmic extension of the rating curve, 2) the shape of the curve might be affected by a mixed-population of flood events and need censoring at the smaller snowmelt-driven floods, 3) the location of the gage might be ideal for measuring streamflow at smaller discharges, but channel geometry might be a problem at higher discharges, and 4) the physiography of the basin might be such that it enhances streamflow. A more detailed study of the peak discharge estimates and gage site could provide justification to remove outliers or to adjust values from the gage (i.e., Meyer, 1993). The peak of record for the North Fork of the Stanislaus River was estimated based on a stage height of 15.0 ft from high water marks. The discharge estimate was then estimated from a rating curve extended above 14,000 ft^3/s on the basis of a slope-area measurement at gage height 13.8 ft. Therefore, any discharge above 14,000 ft^3/s is estimated based on the extended rating curve (Figure 3-33). These types of estimation have much more associated error than a direct measurement and can lead to artificially high extreme flows in the gaged record. However, most if not all of the extreme flows in the seventeen rivers were estimated using a similar method which alone does not explain why the North Fork of the Stanislaus is a high outlier in the unit discharge graph.
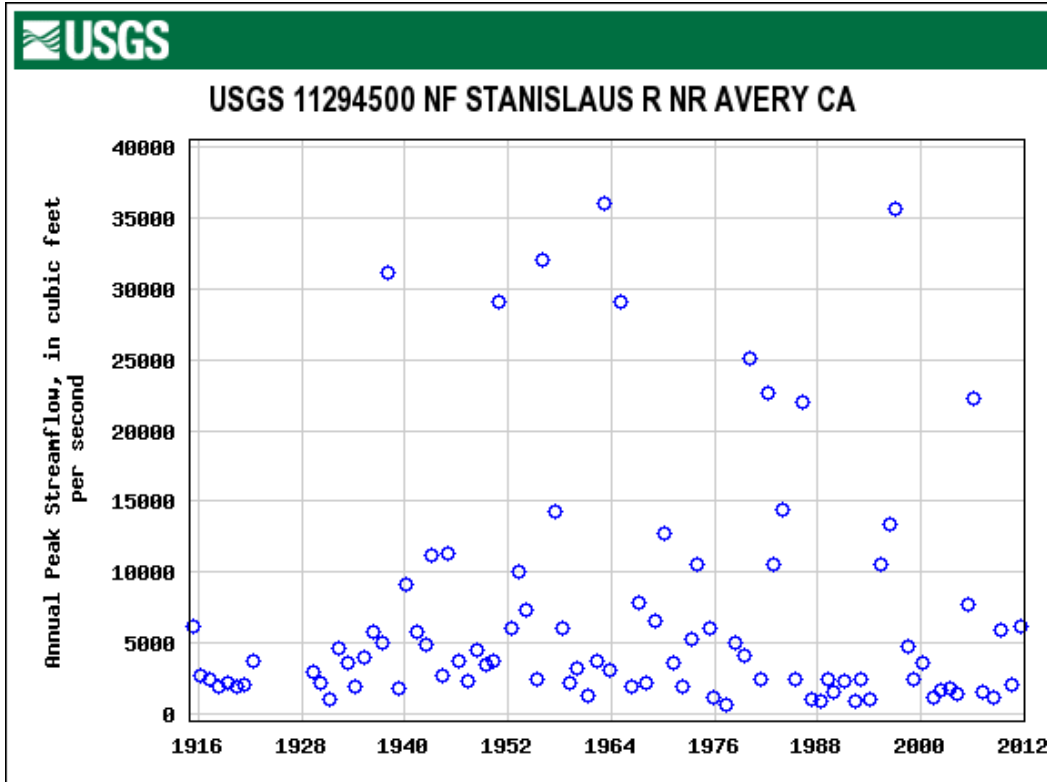
Figure 3-33. Annual peak stream flow data at station number 11294500 NF Stanislaus River near Avery, CA.

A graph of the annual peak flows at the USGS station no. 11294500 for the NF of the Stanislaus River (Figure 3-33) shows a break from about 15,000 ft^3/s to about 22,500 ft^3/s. With few exceptions, this break is the difference between the March-May snowmelt floods and the larger November –February AR floods. This distinct division along with the fact that there are several large floods above 22,500 ft^3/s likely influences the right-hand tail of the flood-frequency curve more than the smaller floods in the left-hand tail which would direct the frequency curve to higher discharge magnitudes at larger recurrence intervals (Figure 3-34). Other records in the basin do not have as large of a gap (relative to discharge magnitudes) as seen on the NF Stanislaus. This might explain why the discharge values are so high at the larger return periods.
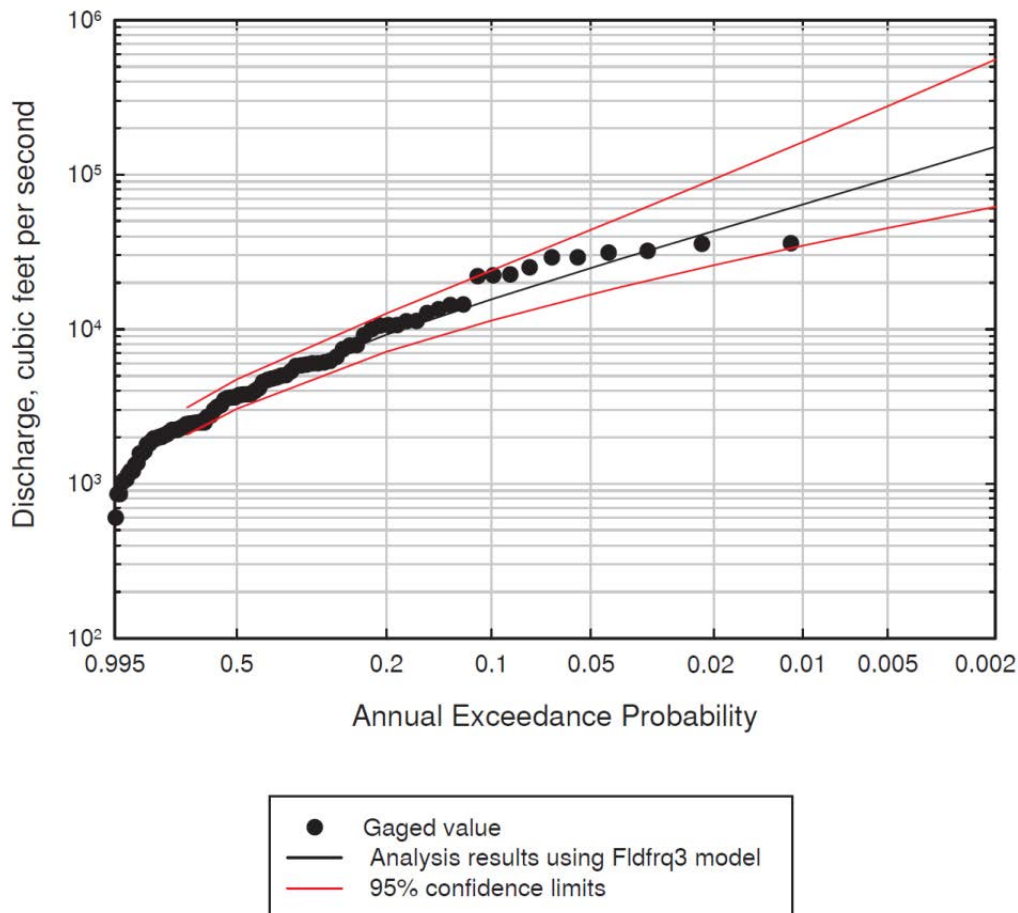
Figure 3-34. Flood frequency analysis for station 11294500 NF Stanislaus River. The gage record includes 91 annual peaks from 1915-1922 and 1929-2011.

Other factors that could possibly lead to significantly higher unit discharge values for basins in the same region include basin characteristics such as size, shape, orientation, elevation, geology, and slope. While there is no evidence to indicate a difference in most characteristics between the NF Stanislaus and the other basins nearby, the size is considerably smaller than most in the study area. The smaller size of the basin could lead to large flood magnitudes by allowing for less flood water attenuation. Additionally, smaller basins tend to have lower drainage densities and shorter channel lengths which could lead to increased flooding by reducing the time of concentration.

3.2.2.4.1 Kaweah River

The unit discharge curve for the Kaweah River (Figure 3-29) shows a relatively steep curve that starts with moderate flows for the lower recurrence intervals but sharply increases as the recurrence intervals increase. This is likely due to the occurrence of high outliers in a relatively short gaged record. The gaged record at the site of the flood-frequency analysis is 58 years and the largest peak flow is

80,700 ft^3/s. The second largest peak in the record is 52,000 ft^3/s. In Figure 3-35 clearly these flows are exceptionally large compared to the rest of the gaged record. These large flows skew the curve towards higher magnitude floods at larger recurrence intervals (Figure 3-36). For comparison of a similar sized unregulated basin, the Cosumnes Rivers has almost twice the record length (104 years) with a peak discharge magnitude of 90,000 ft^3/s and the next largest peak of record of 71,000 ft^3/s. These two flood events are significantly greater than any other in the gaged record (Figure 3-37), however, they do not have as much influence on the right-hand tail of the frequency curve (Figure 3-38). Unit discharge magnitudes are not as high as for those on the Kaweah River (Figure 3-29; Table 3-9) likely because the record is twice as long giving the smaller flows more influence over the frequency curve.
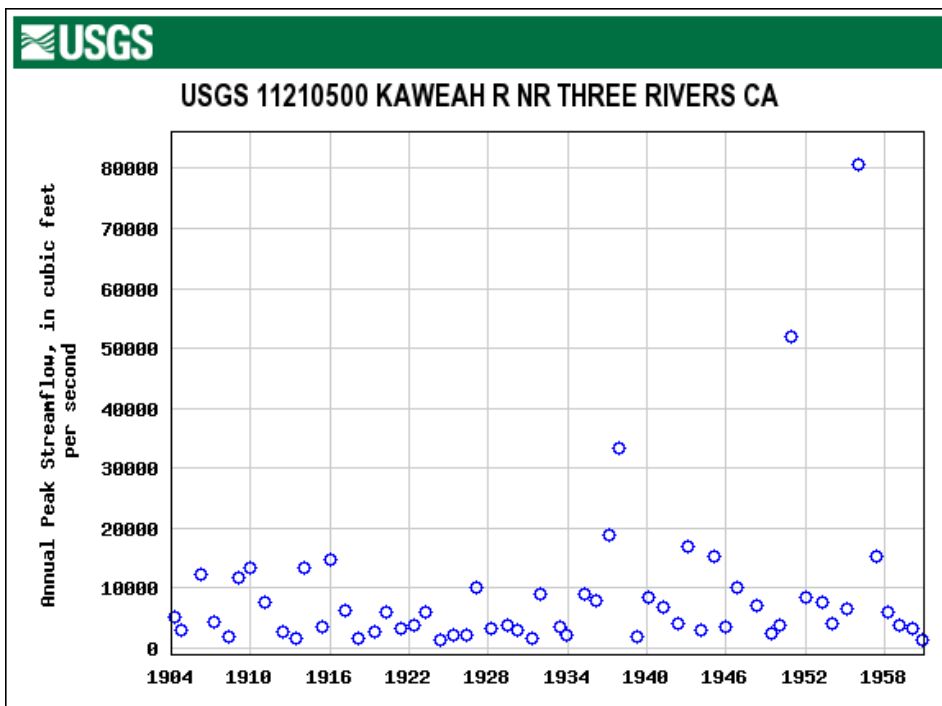
Figure 3-35. Annual peak stream flow data at station number 11210500 Kaweah River near Three Rivers, CA.

Kaweah River at USGS gage no. 11210500
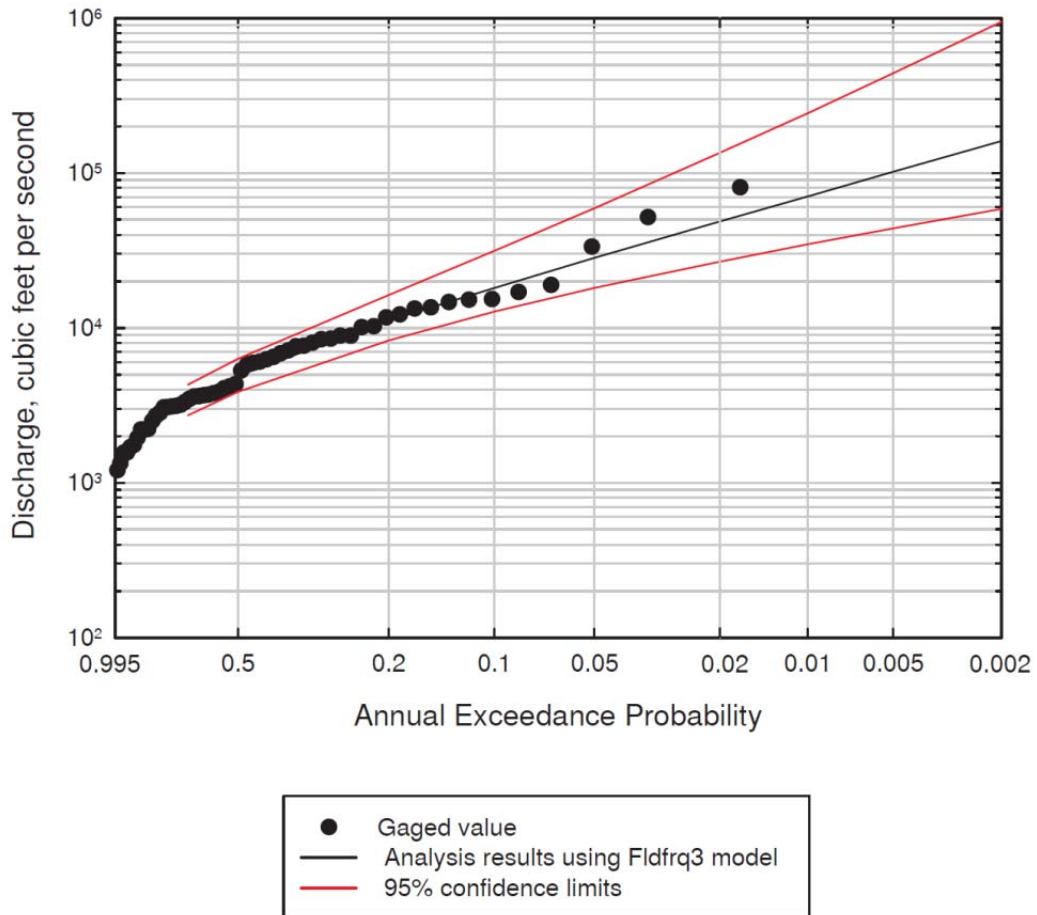
Figure 3-36. Flood frequency analysis for station number 11210500 Kaweah River. The gage record includes 58 annual peaks from 1904-1961.
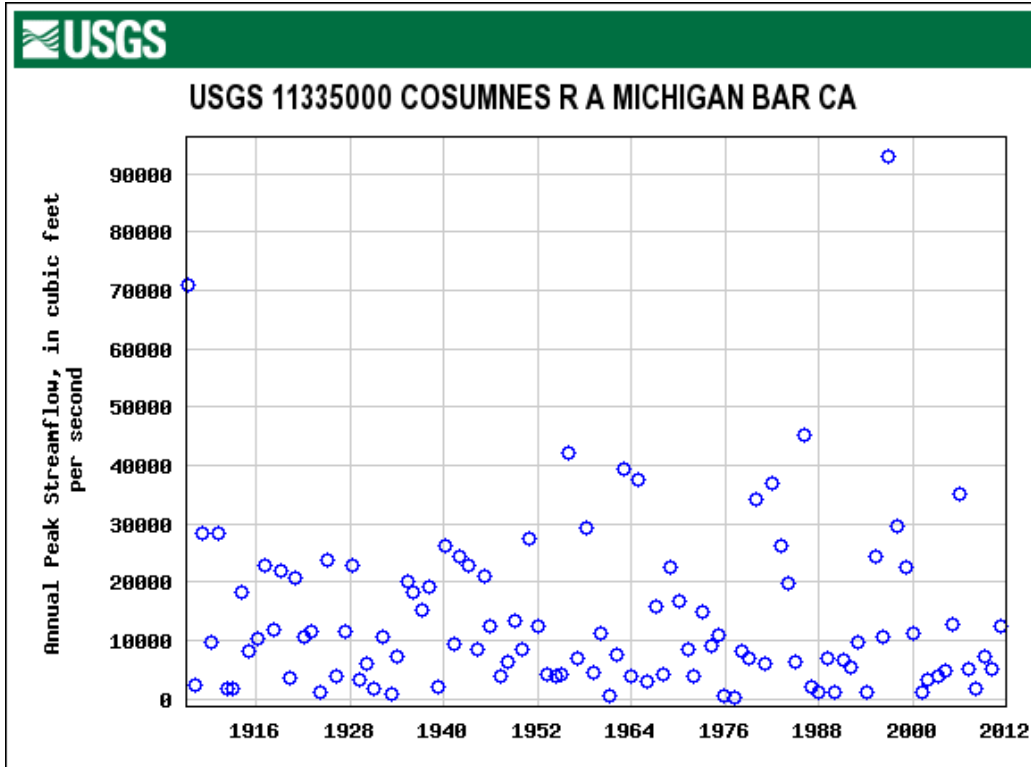
Figure 3-37. Annual peak stream flow data at station number 11335000 Cosumnes River above Michigan Bar, CA.
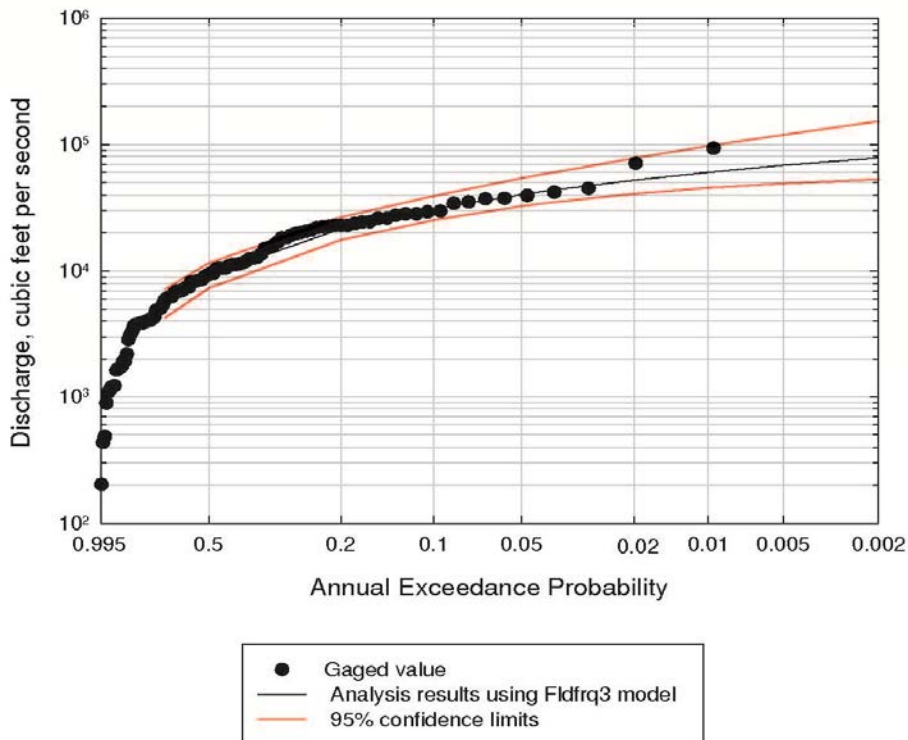
Figure 3-38. Flood frequency analysis for station number 11335000 Cosumnes River. The gage record includes 105 annual peaks from 1907-2011.

3.3 California regional radiocarbon data compilation and analysis

For the purposes of this study, approximately 150 radiocarbon ages were organized into regions with similar hydroclimatology (Table 3-10;Figure 3-39). These regions include: 1) Southern California; 2) Sierra Nevada; 3) west side San Joaquin Valley; and 4) Northern California. Radiocarbon ages collected for paleoflood studies were used to either estimate the age of paleofloods along a particular river or to estimate the onset of soil formation and stabilization of fluvial deposits comprising a stream terrace. A detailed table of radiocarbon ages can be found in Attachment C. The majority of radiocarbon ages are from soils and flood deposits in the Sierra Nevada region. These radiocarbon ages were collected as part of flood hazard studies for Folsom Dam and Friant Dam in the American River Basin and San Joaquin River Basin, respectively. A paleoflood study in the southern Sierra Nevada is currently underway for the Kern and Tule rivers (Klinger et al. in press)

Table 3-10. List of Regions in California used for this study and summary of radiocarbon ages from each region (See Attachments B and C for individual radiocarbon sample data).

Region	Relevant Dam/Project	River Name	Number of radiocarbon ages
Southern California	Bradbury	Santa Ynez	17
Sierra Nevada	Friant	San Joaquin	10
	Folsom	American Cosumnes Mokelumne Rubicon Stanislaus	60
	Isabella	Kern Tule	study in progress
West side San Joaquin Valley	Los Banos	Los Banos	5
	Cantua Creek	Los Gatos Cantua Creek Salt Creek	22
	Little Panoche	Little Panoche Creek	3
Northern California	East Park	Little Stony Creek	7
	Whiskeytown	East Clear Creek	9
	Trinity	Trinity River	16
	Shasta/Keswick	Sacramento River	2

To analyze for patterns in the timing of extreme floods or for patterns of increased or decreased fluvial deposition, radiocarbon ages from the alluvial deposits were calibrated using Oxcal V.4.1.7 (Bronk Ramsey et al. 2010) and their cumulative probabilities were plotted with 2σ uncertainty (95.4% confidence) (Attachment B). Time intervals with more ages have a higher probability density, while time intervals with fewer ages have a lower probability density. The ages were first analyzed by combining ages from both paleoflood deposits and stream terraces and then were separated and plotted for ages specific to paleoflood deposits or stream terraces. This exercise was performed to determine if differences between the ages and depositional settings were apparent. In most regions, ages from paleoflood deposits were few and were typically young, so separating the ages did not make a significant difference for the analysis. The number of radiocarbon ages from flood deposits in the Sierra Nevada were sufficient to analyze separately.

Radiocarbon data from alluvial deposits along the Santa Ynez River in the Coast Range in the Southern California region mostly fall within the last 500 Cal yr BP, with limited data from 500 to about 3200 Cal yr BP (Figure 3-40). Distinct breaks in the radiocarbon data occur between 2800 and 2000 Cal yr BP. However, this gap is based on limited radiocarbon ages and therefore should be regarded with caution. Other time periods with low probabilities are centered around 600 Cal yr BP and between 1300 and 900 Cal yr BP. On the Westside San Joaquin Valley, most of the radiocarbon ages fall within the last 1200 Cal yr BP (Figure 3-40). Time periods with lower probability densities are centered around 600 Cal yr BP, and range from 1800 to 1200 Cal yr BP and from about 3400 to 2880 Cal yr BP. Separating the radiocarbon ages between the two types of depositional environments does not appear to make a difference when examining for changes cumulative probabilities.

In northern California, radiocarbon ages have their greatest cumulative probabilities between 1290 and 0 Cal yr BP and between 3770 and 2120 Cal yr BP; gaps in the data range from 2120 to 1290 Cal yr BP and from 4420 to 3770 Cal yr BP (Figure 3-41). It should be noted that the older gap is only constrained by one radiocarbon age, so this interval is tentative at best.
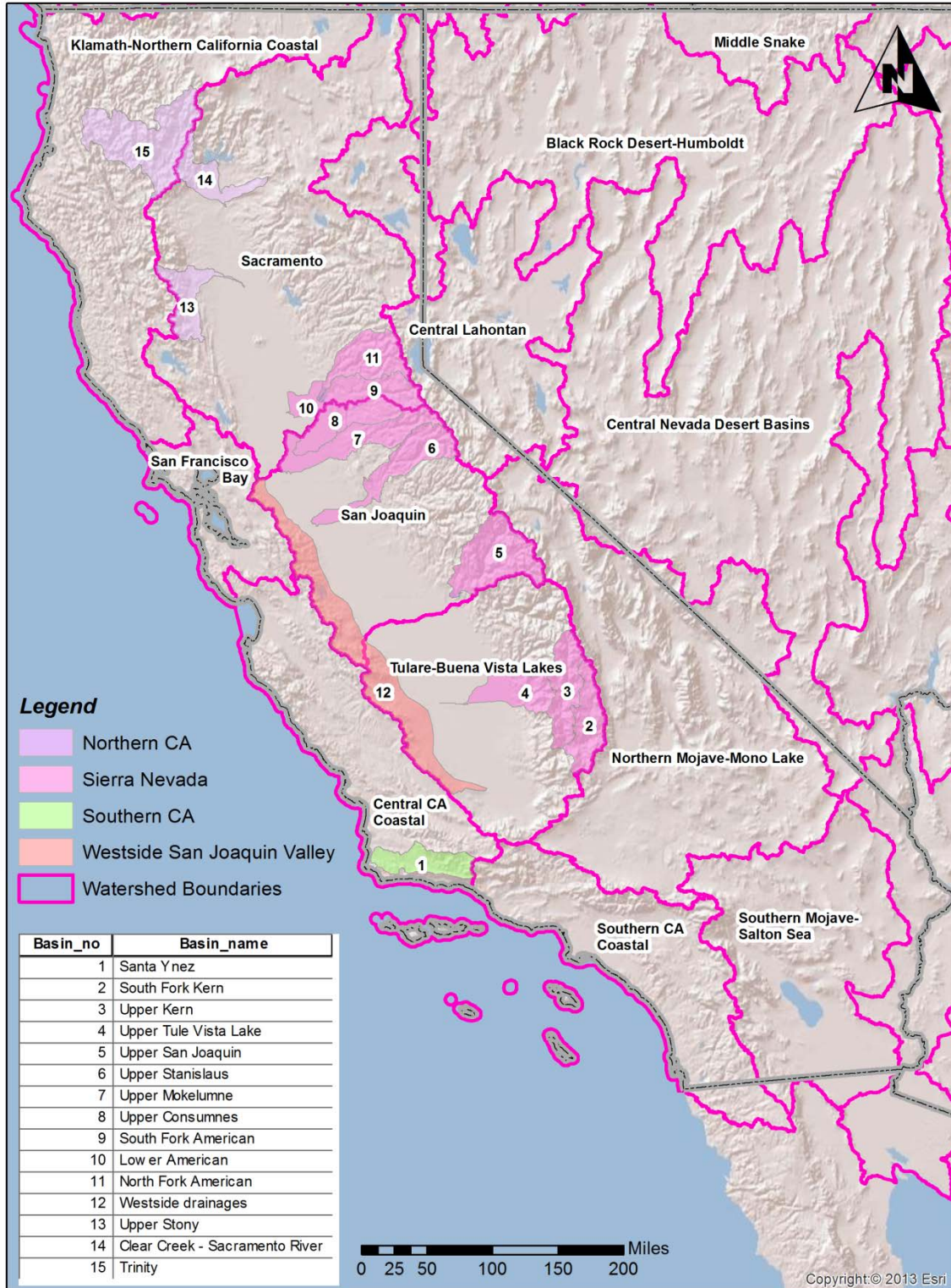
Figure 3-39. Regions of study during this research investigation. Basins with radiocarbon data used in the study are grouped into regions in the legend. A paleoflood study for basins 2, 3 and 4 is currently underway (Klinger et al. in press).
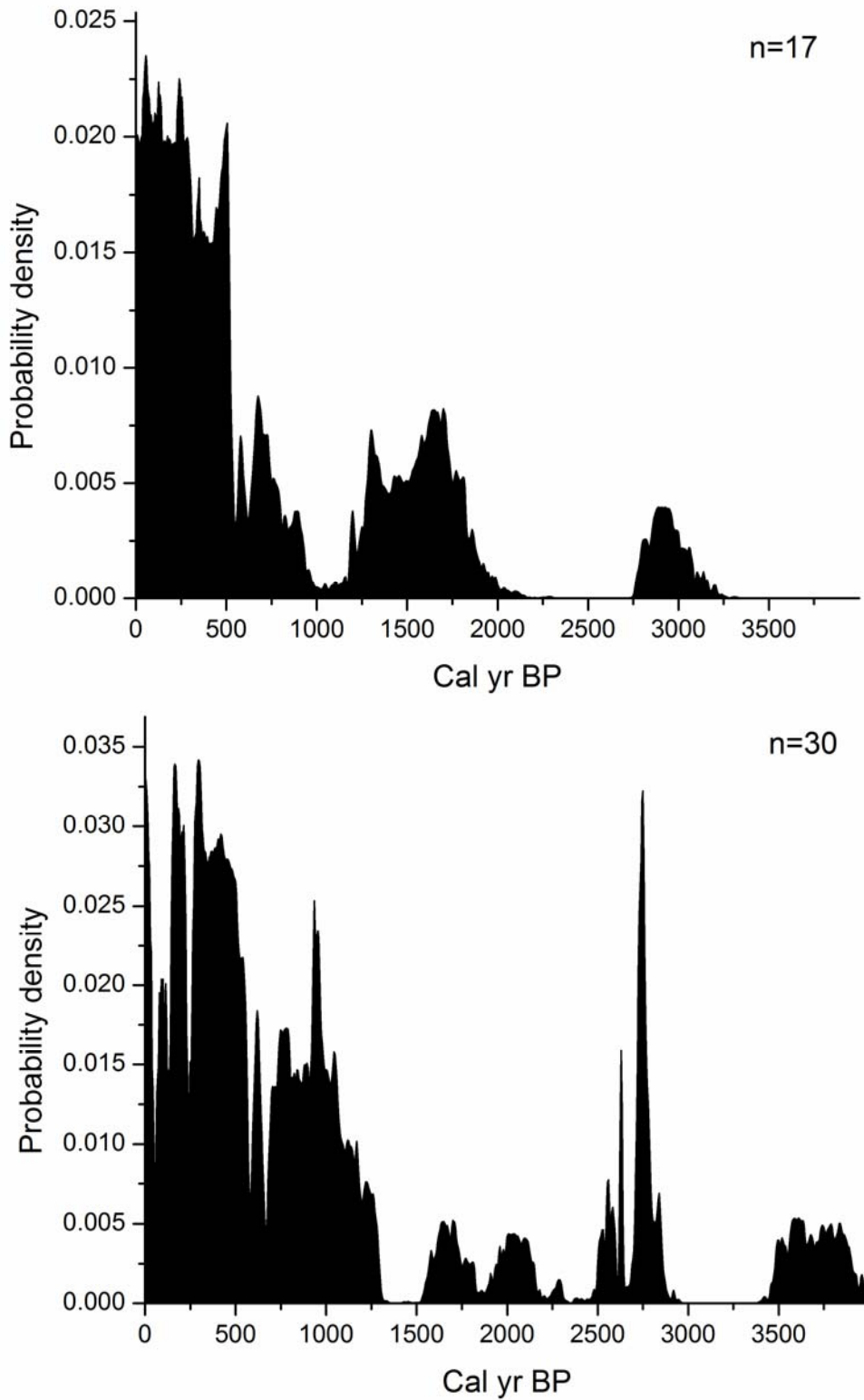
Figure 3-40. Cumulative probability plot of radiocarbon ages from Southern California, Coast Range region (Santa Ynez River)(top) and from western drainages, San Joaquin Valley (bottom).
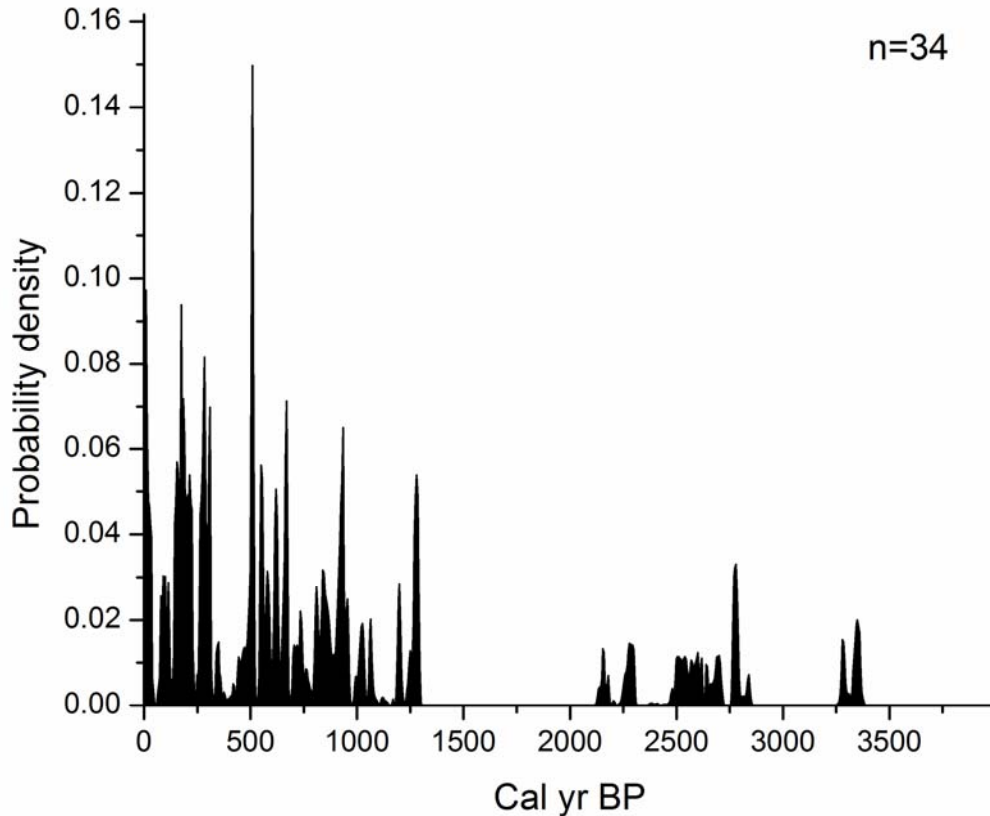
Figure 3-41. Cumulative probability plot of radiocarbon ages from the Northern California region.

Data from the Sierra Nevada region are separated into radiocarbon ages from paleoflood deposits and soils developed on stream terraces since there are enough of both types of deposits to compare the two. Radiocarbon ages from paleoflood deposits on rivers that drain the west side of the Sierra Nevada have the highest cumulative probabilities between 600 and 0 Cal yr BP, then have much smaller probabilities between about 1000 and 600 Cal yr BP (Figure 3-42). When examining the cumulative probability curve beyond 1000 Cal yr BP, the cumulative probabilities are low in general and it is difficult to determine whether any patterns in the data are meaningful. Radiocarbon ages older than 4000 Cal yr BP are sparse and therefore no conclusions are made regarding the data beyond 4,000 years. When examining radiocarbon data from soils developed on stream terraces, the highest cumulative probabilities are between 300 and 0 Cal yr BP. The probability plot drops to near 0 during the time interval between 900 and 600 Cal yr BP. There seems to also be a low point between 1700 and 1500 Cal yr BP and between 2900 and 2600 Cal yr BP. Comparing the two plots, high cumulative probabilities occur in both plots at <500 Cal yr BP, around 1,000 Cal yr BP and around 3,000 Cal yr BP. Low cumulative probabilities occur in both plots between 900 and 600 Cal yr BP.

75

Radiocarbon ages from flood deposits

Radiocarbon ages from soils
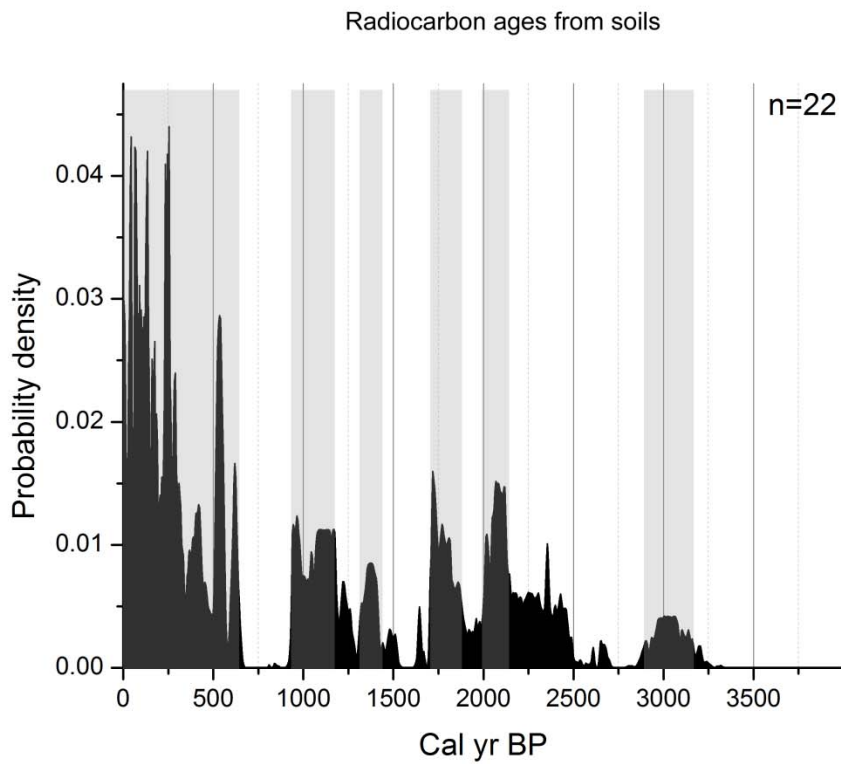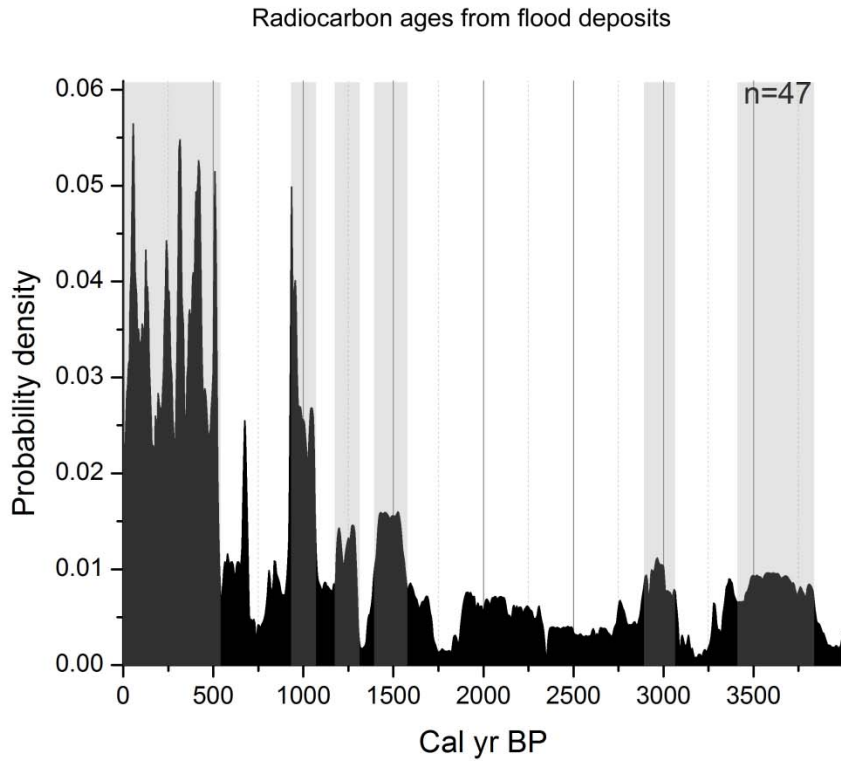
Figure 3-42. Cumulative probability plots of radiocarbon ages from flood deposits (top) and stream terraces (bottom) in the Sierra Nevada Region. Gray bands highlight the highest cumulative probabilities in each plot.

For each region, cumulative probabilities of the calibrated ages with 2σ uncertainty are plotted in order to analyze whether general patterns exist in the ages of the deposits among regions (Figure 3-43). Data are plotted for the last 4,000 Cal yr BP because the number of older radiocarbon ages decrease significantly and the dataset is probably too small to make any meaningful conclusions. All data, including ages from stream terraces and slackwater deposits, are plotted together in the single graph. Several time periods have a distinct change in the probability density of radiocarbon ages that are similar in different regions. This would suggest that there are periods of decreased fluvial deposition (inferred decrease in streamflow) and periods of increased fluvial deposition (inferred increase in streamflow). These changes do not appear to be simply related to the age of the deposits which could be viewed as a bias in preservation of the deposits, but rather they fluctuate over the last 4,000 Cal yr BP. While the cumulative probability varies with the number of radiocarbon samples collected along rivers in each region, similar patterns in the probability density can be detected. However, in the Coast Range region, the pattern may be somewhat similar but the cumulative probabilities are much lower and make comparison difficult. This is due to the smaller number of samples available for this region. For the last 1,000 Cal yr BP, a high probability density of radiocarbon ages exists for about the past 500 Cal yr BP. The most distinct decrease is from about 900-600 Cal yr BP. A significant decrease in the probability density of calibrated ages can be seen in the graph between about 1300 and 1100 Cal yr BP for all of the data sets except the Coast Range. Following this transition, there is much variation in the cumulative probabilities from region to region. Another increase in cumulative probability occurs for the Northern California and West San Joaquin Valley regions from about 2800-2500 Cal yr BP.
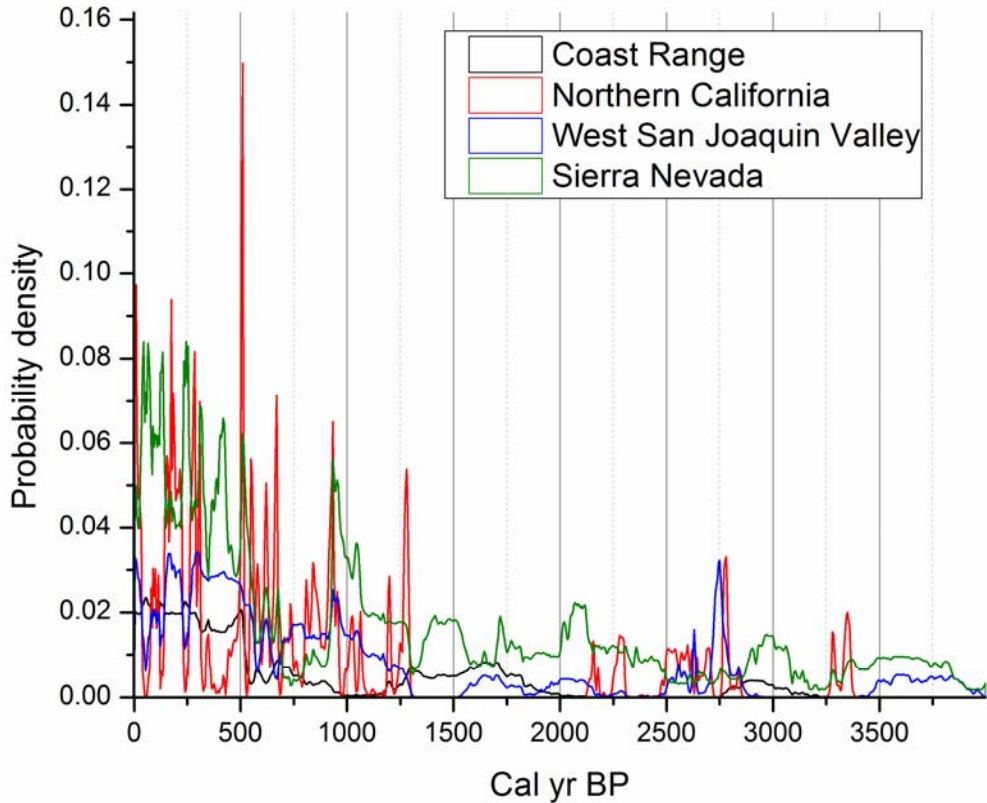
Figure 3-43. Cumulative probability curves for the 4 regions of California used in this study.

When comparing only the West side San Joaquin Valley and Sierra Nevada, some patterns in radiocarbon ages appear to be similar while others are not (Figure 3-44). These two regions are compared specifically because they are near to each other geographically, but have very different orographic factors that likely exert a large control over floods and the alluvial history within each region. Both datasets show a high probability density in radiocarbon ages for the past ~500 Cal yr BP and show a similar decrease in probability density between about 900 and 600 Cal yr BP. Both datasets also show an increase in cumulative probability at 1,000 Cal yr BP and also show a general decrease near about 1300 Cal yr BP. Patterns prior to 1300 Cal yr BP appear to be either opposite or slightly offset by varying amounts of time. Given the number of rivers sampled in each region, there appear to be enough interesting results to make this exercise worthwhile. Paleofloods documented on the San Joaquin River (Godaire and Bauer, 2012), the American River (Klinger and England, 2002), and Los Banos Creek (Klinger and Bauer, 2004) are shown on the graph and do not appear to necessarily fall within areas of the curve where the probability densities are high or low, but plot in both areas of the curve.
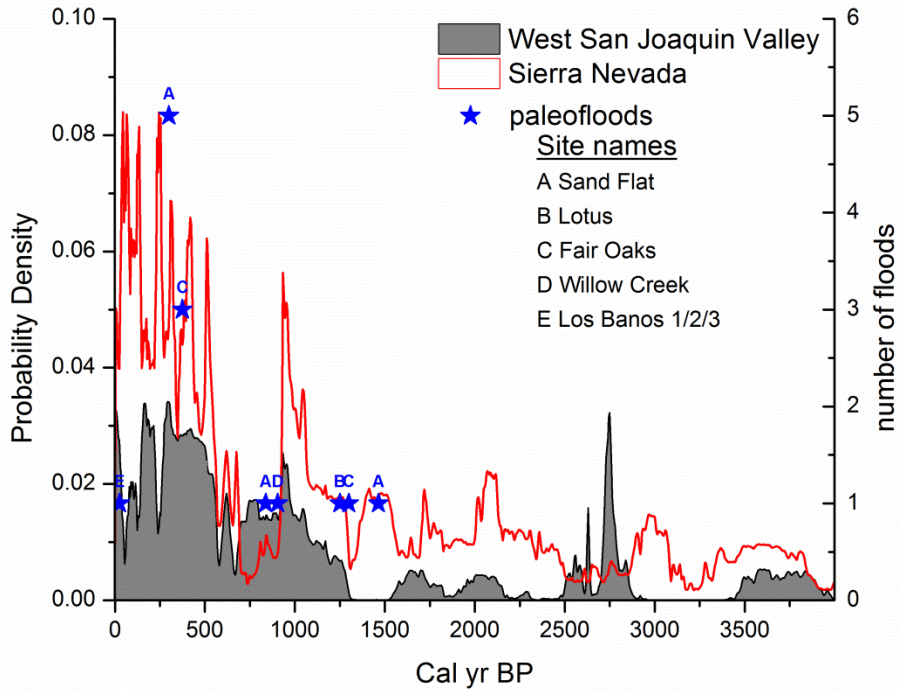
Figure 3-44. Cumulative probability curves for the Sierra Nevada and Westside San Joaquin Valley regions. Midpoints for paleoflood ages are plotted as blue stars. The number of paleofloods associated with each blue star is shown on the right vertical axis.

3.4 Paleoclimate data comparisons with radiocarbon ages in the Sierra Nevada region and other selected regions

Paleoclimate data are available for various areas in California from previous research using proxies such as tree rings, lake levels, changes in salinity, and pollen to infer climate conditions during the Holocene (<10 ka). Malamud-Roam et al. (2006) compile many of these studies for California and provide a summary of paleoclimate conditions during the Holocene for four regions: Coastal California, San Francisco Bay Estuary, Sierra Nevada and the White Mountains (Great Basin) (Figure 3-45). In addition, they provide detailed data regarding climate interpretations of changes based on salinity in the San Francisco Bay Estuary and flood history from various studies for the last 2000 years, including the USBR's (Klinger and England, 2002) study of paleofloods in the American River Basin. When considered as a whole, the paleoclimate records show generally consistent trends across the regions. From the early to mid-Holocene, the climate warmed with increasing temperatures and dry conditions. This trend peaked around 6000 to 5000 Cal yr BP. From 4000 to 2000 Cal yr BP, wet conditions dominated relative to the previous period with records of the wettest conditions between 3700 and 3000 Cal yr BP. During the most recent period from 2000 Cal yr BP to modern times, cooler and drier conditions have predominated. This period exhibits greater variability, with periods of prolonged droughts that

abruptly transition into brief, cool, wet periods as well as significant cool, wet periods. Some of this high variability may be due to the resolution of data within the last 2,000 years and is mostly summarized for the San Francisco Delta-Bay watershed, which includes the Sacramento and San Joaquin River basins. Significant droughts from studies at Mono Lake (Stine, 1990; 1994) include periods from A.D. 900-1150, corresponding to the Medieval Climatic Anomaly (A.D. 950-1250, 1000-700 Cal yr BP) and from A.D. 1200-1350 (750-600 Cal yr BP). Significant wet periods include the Little Ice Age (A.D. 1400-1700, 550-250 Cal yr BP). Malamud-Roam et al. (2006) also note that the modern period (A.D. 1850 to 1950) has been one of relative stability with fewer fluctuations in the extremes. While Malamud-Roam's summary of paleoclimate is helpful as far as an overall perspective, the resolution in Figure 3-45 is not great enough during some of the time periods to compare directly to the record of radiocarbon ages developed in this study.
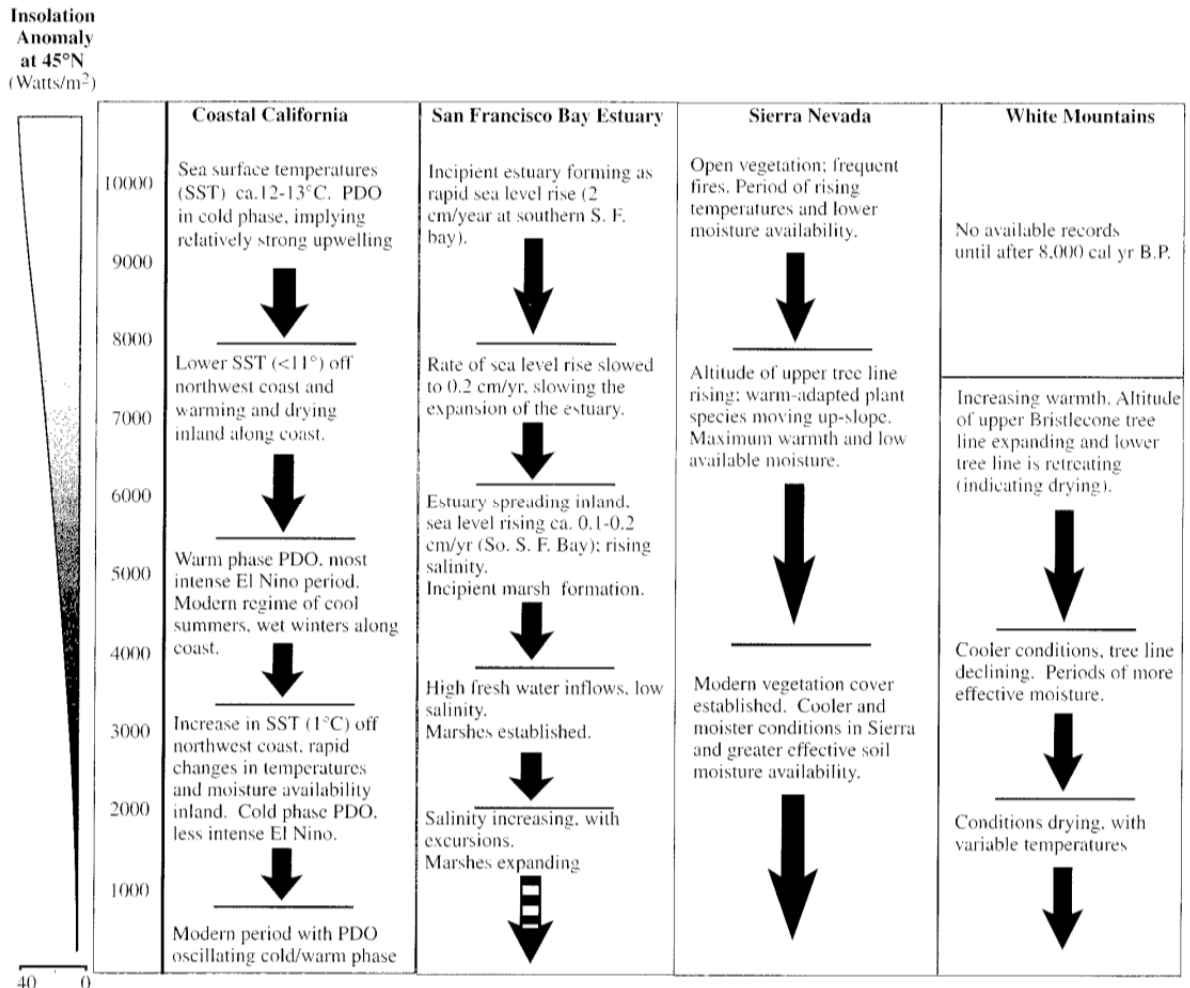
Figure 3-45. Summary of paleoclimate from multiple proxies in areas of California . Time in thousands of years is plotted on the vertical axis (From Malamud-Roam et al 2006).

For the late Holocene (<2ka), high resolution data that reconstructs relative streamflow can be obtained from work by Malamud Roam et al (2006, 2007) and from Meko et al. (2002) for the San Francisco Delta-Bay Watershed. Malamud-Roam et al. (2006; 2007) examined changes in the relative dominance of salt-tolerant plants versus tidal marsh vegetation in sediment cores in the San Francisco Bay Estuary to infer changes in fresh water inflow from the watershed. Reconstructed river flows are plotted in a relative sense according to the relative salt tolerance of vegetation in the sediment cores. Meko et al. (2002) utilized tree ring chronologies in the upper watersheds of the Sacramento and San Joaquin River basins. By calibrating the tree ring width with historical streamflow records, he was able to reconstruct river flows for both basins for the last ~1200 years. If the period of decreased probability of radiocarbon ages for the Sierra Nevada region is plotted on Figure 3-46, it appears to correspond with a period of decreased stream flow on the Sacramento and San Joaquin Rivers from tree ring based reconstructions and overlaps a portion of decreased streamflow from vegetation reconstructions of Malamud-Roam et al. (2006). This would suggest that periods of landform stability along these rivers correspond to periods of lower streamflow. However, this is only one comparison and even the streamflow reconstructions show quite a bit of variation.
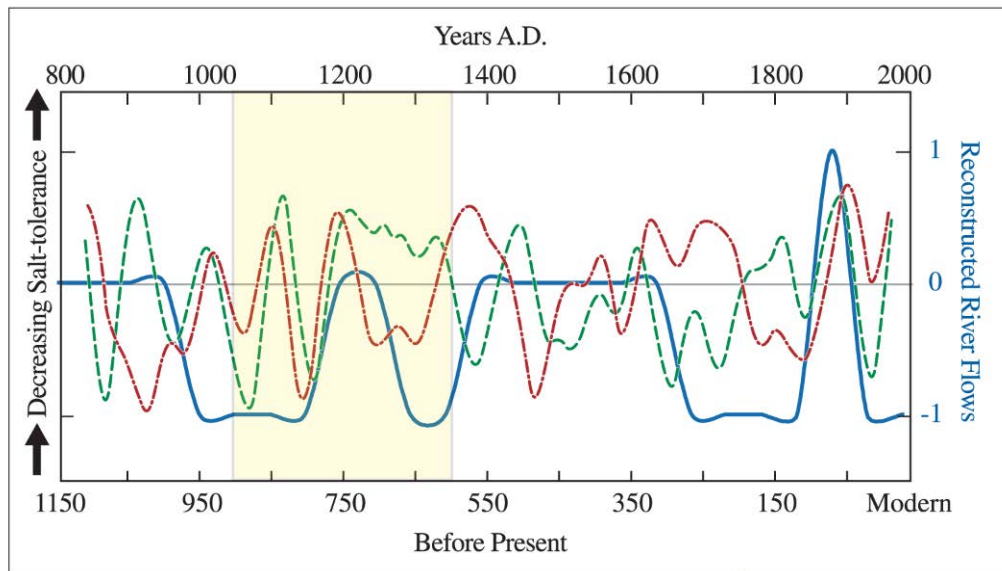
Figure 3-46. Time periods of few radiocarbon ages (shown as yellow band) are compared to reconstructed river flows (blue) based on changes in the dominance of salt-tolerant plants, which is correlated to river inflow (Malamud-Roam, 2002; Malamud and Ingram, 2004). Red and green lines are smoothed tree ring-based streamflow reconstructions of the San Joaquin and Sacramento Rivers, respectively (Meko et al. 2002). Figure is modified from Malamud-Roam et al. (2007).

Malamud-Roam et al. (2006; 2007) also plot their data along with droughts documented from buried tree stumps at Mono Lake (Stine, 1990; 1994) and from bristlecone pine chronologies in the White Mountains (LaMarche, 1974; Hughes and Graumlich, 1996; Hughes and Funkhouser, 1998) (Figure 3-47). Extreme

floods documented in this paper are derived from Schimmelmann et al (2003) in the Santa Barbara Basin, from Klinger and England (2002) in the American River Basin, and from Goman and Wells (2000) in the San Francisco Bay, among others. From the authors' perspective, these floods provide evidence for very wet episodes during the late Holocene. However, these floods appear to fall both within both dry and wet periods, and do not really appear to be occurring distinctly in either wet or dry intervals. The authors conclude that their inferred dry periods based on changes in vegetation in the San Francisco Bay estuary generally correspond to inferred droughts from Mono Lake by Stine (1990; 1994), although one earlier drought is documented from 1650 to 1300 Cal yr BP.

Cumulative probabilities of radiocarbon ages from this study again show low probability densities from about 900 to 600 Cal yr BP, which would correspond to one of the droughts identified in Figure 3-47 and would be contained within periods of extended drought between 1150 and 650 Cal yr BP that are documented by Cook et al. (1999, 2004) and Swetnam et al. (2009). Other regions of California show low probabilities of radiocarbon ages that extend to about 600 Cal yr BP, which would encompass the later drought as well. The Sierra Nevada region does not show evidence of decreased probability density specifically during the earlier drought between 1650 and 1300 Cal yr BP. The higher probability density of ages within the last 500 Cal yr BP corresponds to wetter conditions in the Sacramento and San Joaquin watersheds. This period has been documented as cooler and wetter from several different proxies including tree ring evidence (LaMarche, 1973, 1974; Hughes and Funkhouser, 1998; Hughes and Graumlich, 1996), ancient shorelines of Mono Lake (Stine 1990, 1994), floodplain sediments (Sullivan, 1982), estuary and tidal marsh cores (Malamud-Roam et al. 2006) and ocean cores (Jones and Kennett, 1999), indicating cooler coastal waters. The Little Ice Age also falls within this period and is documented as a time of wetter and cooler conditions (Bradley, 2003).
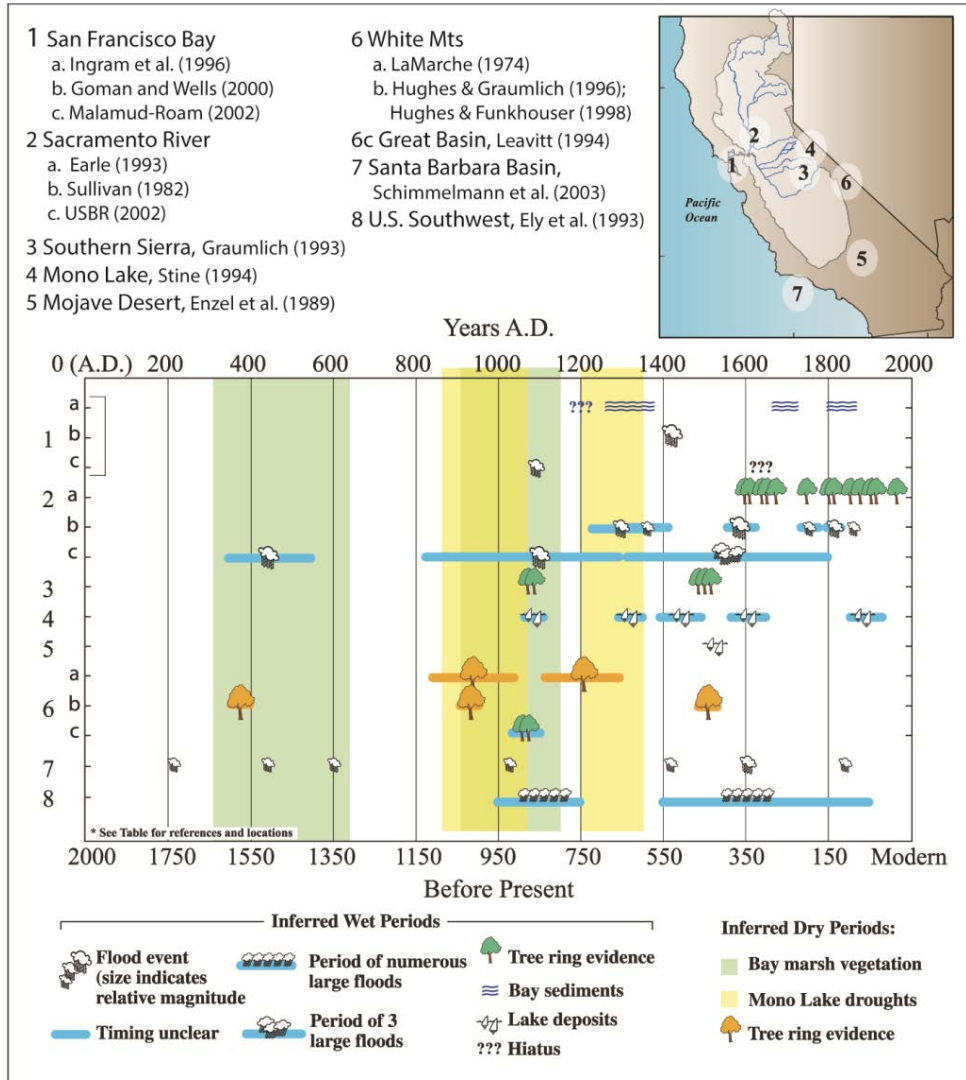
Figure 3-47. Evidence of inferred wet and dry periods during the late Holocene within the San Joaquin and Sacramento River watersheds. Data from southern California and the desert southwest are also included. Colored vertical bands indicate extended droughts (modified from Malamud-Roam et al. 2007). Time intervals with low probability densities of radiocarbon ages from this study would span the Mono Lake droughts in yellow (interval from this study =900-600 Cal yr BP for all regions).

Negrini et al. (2006) conducted research on lake levels at Tulare Lake, located in the Tulare-Buena Vista Basin (HUC 1803). Tulare Lake is fed by the Kern River and Kings River and therefore would be representative of climatic conditions in the southern Sierra Nevada. Negrini's research shows generally higher lake levels during the early Holocene and latest Pleistocene (>6ka) followed by lower lake levels with low amplitude fluctuations between about 5500 and 1000 Cal yr BP (Figure 3-48). After ~1000 Cal yr BP, the lake level began to rise, with a high stand centered between about 750 and 150 Cal yr BP. These results generally agree with results from this study, in which more radiocarbon ages (i.e., wetter conditions) are recorded during about the last 500 years, preceded by drier

conditions starting at about 700 Cal yr BP. The smaller fluctuations in the level of Lake Tulare are harder to compare to the cumulative probability plots of radiocarbon ages in this study. However, a paleoflood study of the Kern River Basin is currently underway at Reclamation and would be useful for comparing radiocarbon ages from this study.
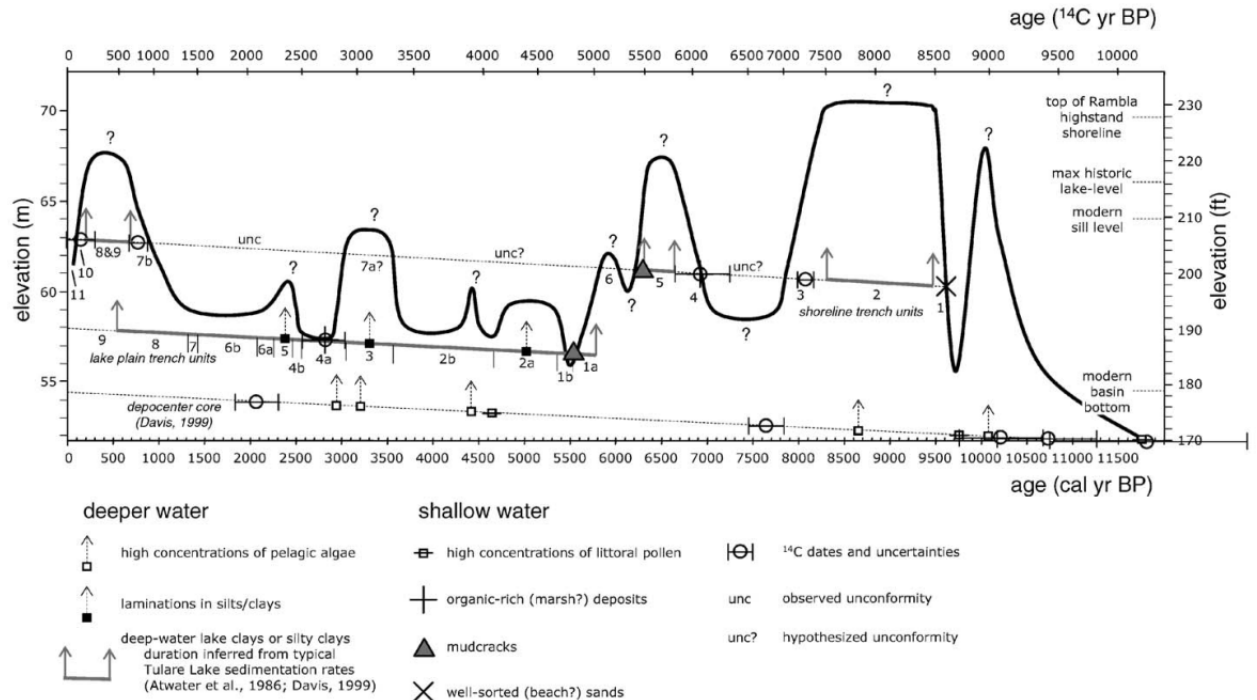
Figure 3-48. Reconstructed lake levels of Tulare Lake with supporting data from the study (taken from Negrini et al. 2006).

Paleoclimate reconstructions of large scale climate signals can be used to compare directly to the cumulative probability curve of radiocarbon ages in the Sierra Nevada region in order to determine whether any patterns exist between large scale climate signals and the paleorecord of fluvial deposition. Most of the reconstructions listed in Table 3-3 are probably too short to be compared to the data in this analysis. However, a few studies are worthy of mention.

Yan et al. (2011) produced a reconstruction of the Southern Oscillation Index (ENSO) for the past 2,000 years on a multi-decadal scale from precipitation proxies in the Galapagos and Indonesia. The Galapagos rainfall reconstruction is based on lake level history from grain size data in the Lago El Junco sediment core developed by Conroy et al. (2008). The Indonesia rainfall was based on a salinity reconstruction using planktonic foraminifera d18O and the Mg/Ca ratio (Oppo et al. 2009). The authors propose this index as a precipitation-based Southern Oscillation Index (SOIpr) because there is a correlation between precipitation and the SOI such that precipitation is positively correlated with SOI over the Indo-Pacific warm pool (Indonesia dataset) and negatively correlated over the eastern and mid-tropical Pacific (Galapagos dataset). Results of this study found that the index is negative during the Medieval Warm Period (or

84

Medieval Climatic Anomaly, AD 950-1250; 1000-700 Cal yr BP), indicating more El Niño dominated conditions. The index is positive during the Little Ice Age (AD 1400-1850; 550-100 Cal yr BP) in which La Niña conditions are more dominant. Plotting Yan et al. (2011) data with the cumulative probability curve of radiocarbon data for the past ~2,000 years shows that the curves have similar trends for about the past 1,000 years in which greater probabilities are evident during about the last 500 Cal yr BP, with a decrease in probability during the Medieval Climatic Anomaly (Figure 3-49). Patterns after about 1,000 Cal yr BP diverge and obvious similarities are not apparent.
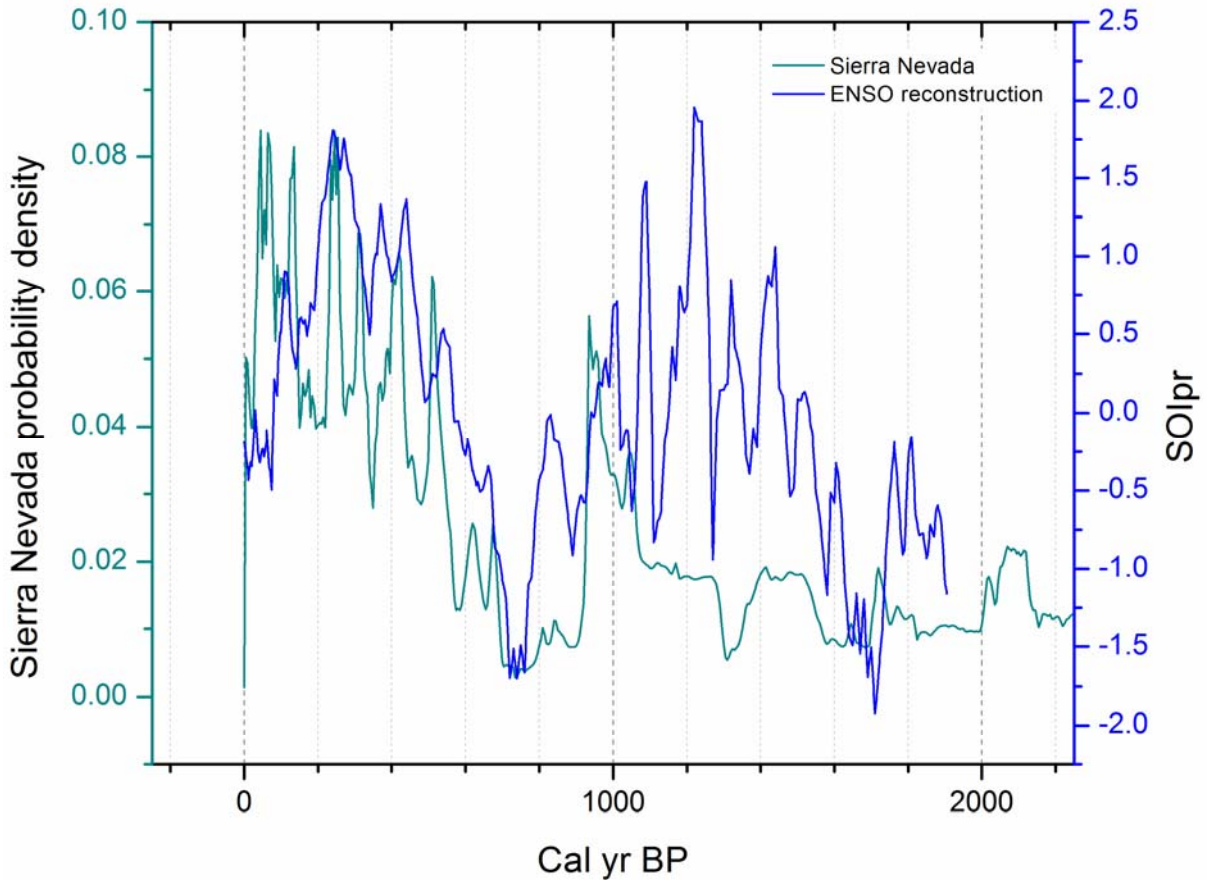
Figure 3-49. Southern Oscillation Index reconstruction (Yan, 2011) is plotted against cumulative probability of radiocarbon ages from the Sierra Nevada region for the last ~2,000 years.

A Pacific Decadal Oscillation (PDO) index from MacDonald and Case (2005) can also be used to compare to the radiocarbon chronology described in this study (Figure 3-50). The PDO reconstruction was based on tree ring chronologies of Pinus flexilis from near Mount San Gorgonio in California and in the Rocky Mountains near Whirlpool Point, Nordegg, Alberta. The reconstruction extends from AD 993-1996, so only the years from AD 993 to 1955 were used in order to plot with the radiocarbon data. MacDonald and Case state that the periodicity of the PDO reconstruction is strong for the past 200 years and exhibits a ~50 to 70 year cycle. Prior to 200 years, they state that the PDO has a strong mode of

variability in only certain time periods. A strong negative signal is apparent during the Medieval Climate anomaly from about AD 993 and 1300 (962-655 Cal yr BP). Comparing the radiocarbon data from the Sierra Nevada with the PDO Index from MacDonald and Case (2005), it is difficult to extract any similarities with the exception of the Medieval Climatic Anomaly, where both PDO index values are negative and cumulative probabilities are low (Figure 3-50). Since PDO index values are positively correlated with precipitation for the southwestern U.S., this would suggest that precipitation is lower during this period, which many other records also suggest. The low number of radiocarbon ages from this period also indicates a period of lower streamflow, or less fluvial deposition. The cool/negative phase of the PDO has an inverse relationship with precipitation in the Pacific Northwest, which may extend into northern California. If the PDO Index from MacDonald and Case (2005) is plotted with the radiocarbon data from northern California, many inverse relationships are apparent, however there are some parts of the PDO Index curve that appear to be in sync with the radiocarbon curve (Figure 3-51). For example, at ~200 Cal yr BP, the curves follow the same trends, whereas at ~400 Cal yr BP, the PDO index is positive and the probability density is low.
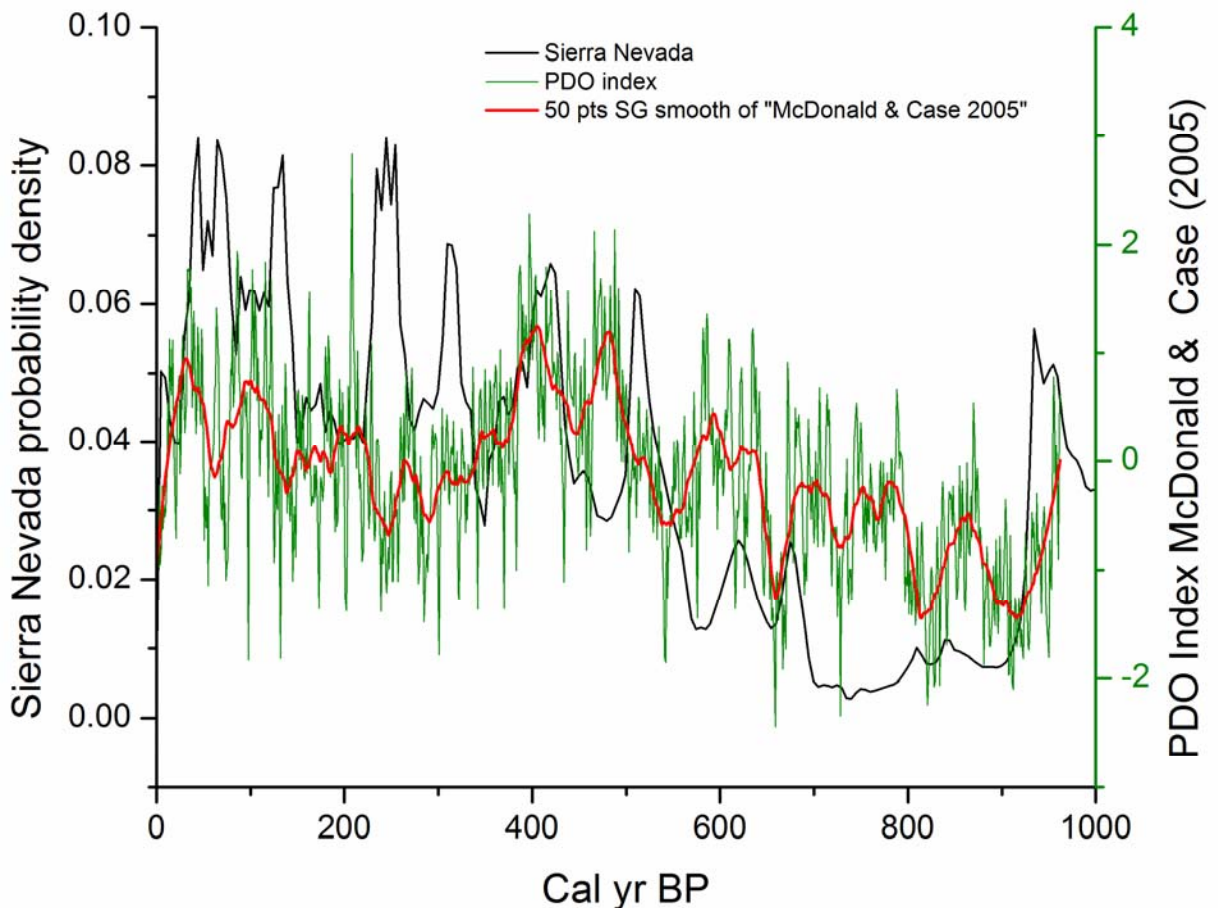
Figure 3-50. PDO Index (MacDonald and Case, 2005) is plotted against cumulative probability of radiocarbon ages from the Sierra Nevada Region for the last ~1,000 years. The PDO index is smoothed using a 50 pt window and the Savitzky-Golay method.
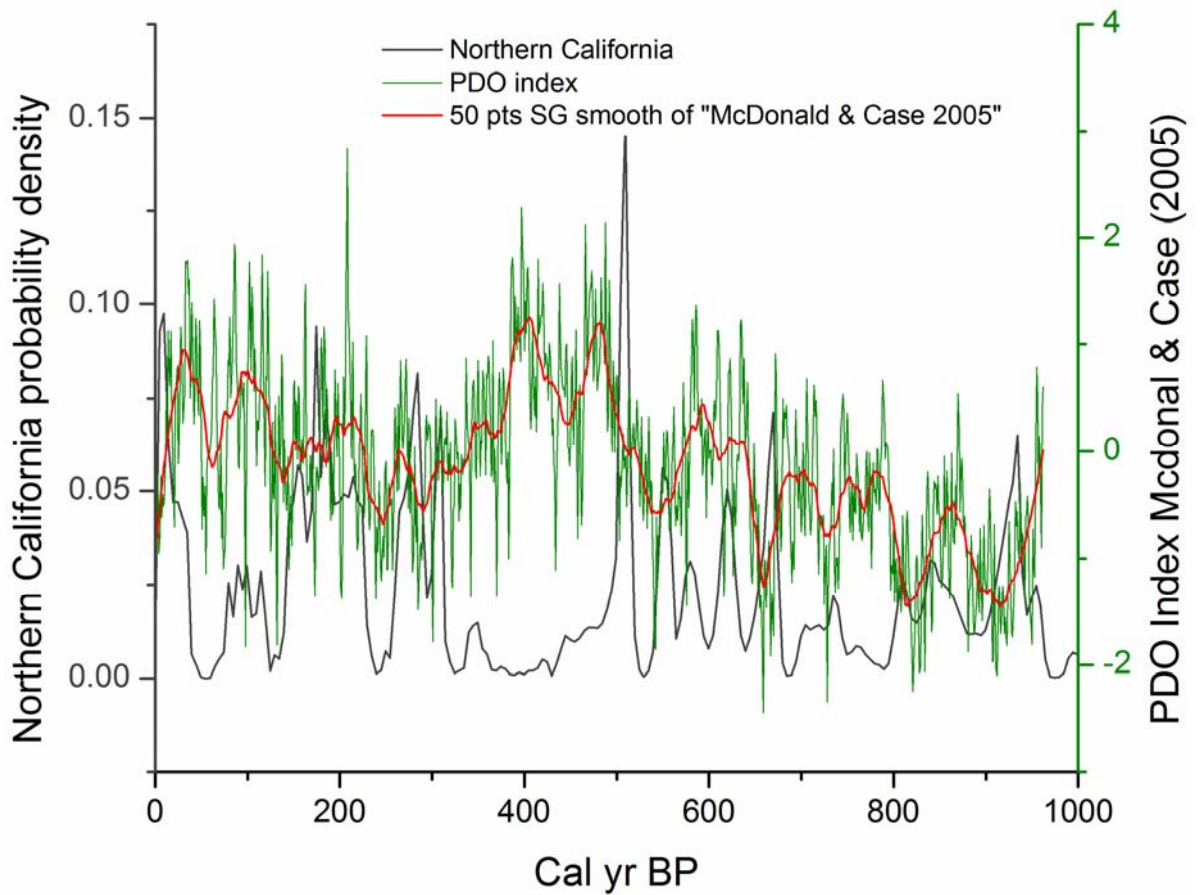
Figure 3-51. PDO Index (McDonald and Case, 2005) is plotted against cumulative probability of radiocarbon ages from the Northern California Region for the last ~1,000 years.

3.4.1 Climate change model scenarios and implications for extreme floods in the Sierra Nevada region

The importance of water supply to California's economy has prompted an abundance of climate change research. Models and projections of future climate conditions are available as well as the anticipated impacts to water supply. There is also research on how extreme precipitation and resultant flooding will change in the state as well. This research is summarized here to provide a comparison to the research in this project comparing paleoflood and paleoenvironmental data. The focus of this investigation is the Sierra Nevada region, which is the source for the majority of runoff within the Sacramento and San Joaquin river basins, and is an important source of water for 6 of 10 agricultural counties (Reclamation, 2011).

From the 2011 SECURE Water Act Report (Reclamation, 2011), Global Circulation (or Climate) models (GCMs) and projections of future greenhouse gas emissions (GHG) for this region project an increase in temperature of approximately 5-6° F during the 21st century. Precipitation is projected to increase slightly in the northern Central Valley (northern Sierra Nevada) and decrease slightly in the southern Central Valley (southern Sierra Nevada). Changes in mean annual runoff include a 2.5% increase in the Sacramento River Basin and a 8.7% decrease in the San Joaquin River Basin by 2050. A greater amount of precipitation is predicted to fall as rain instead of snow at lower elevations, thus increasing winter runoff and decreasing summer runoff. The above projections are generalizations using GCMs and there is considerable uncertainty within the models for this region, which suggests that these basins have about equal chances of becoming wetter or drier. The SECURE Water Act (Reclamation, 2011-citation?) states:

> *Inspection of the underlying ensemble of projection information shows that there is significant variability and uncertainty about these projected conditions both geographically and with time. (p. vii)*

> *…while this report summarizes potential future climate and hydrologic conditions based on best available datasets and data development methodologies, there are a number of analytical uncertainties that are not reflected in this report's characterization of future hydroclimate possibilities. Such uncertainties arise from analyses associated with characterizing future global climate forcings such as greenhouse gas emissions, simulating global climate response to these forcings, correcting global climate model outputs for biases, spatially downscaling global climate model outputs to basin-relevant resolution, and characterizing regional to basin hydrologic response to such downscaled climate projection information. (p. ix)*

These projections were developed in part through the project, West-Wide Climate Assessments: Bias-Corrected and Spatially Downscaled Surface Water Projections (Subhrendu and Pruitt, 2011). This project developed 112 hydrologic projections for basins in the western U.S., including the Sacramento and San

88

Joaquin River basins, using the Variable Infiltration Capacity (VIC) macroscale hydrology model. Climate projections from the World Climate Research Programme Coupled Model Intercomparison Project3 (WCRP CMIP3) were bias-corrected and spatially downscaled. Changes in hydroclimate variables were analyzed for three different time periods: water years 2020-2029, 2050-2059 and 2070-2079. In this report, the authors provide similar projections to those stated above. They specifically note that the lack of calibration of the hydrologic models is a major source of uncertainty that should be addressed before the models are used in future assessments.

The projections above only really provide information regarding the seasonality and volumes of annual runoff. Little information is available in these reports regarding projected changes in extreme events. Work by Dettinger (2011) and Das et al. (2010) attempt to address this question by investigating changes in storm patterns and frequency as a result of climate change. As noted in section 3.1, climate modeling predicts that the frequency and intensity of storms is expected to increase for the Sierra Nevada region, which would result in an increased frequency of high magnitude floods. In addition, more storms are expected to be rainfall driven rather than snowmelt driven as the amount of precipitation falling as rain instead of snow increases at lower elevations (i.e., Dettinger, 2011, Das et al. 2010), which implies that more flow will occur during the winter rather than during spring snowmelt. To arrive at these conclusions, Dettinger et al. (2011) looked at the AR statistics in climate simulations in California under scenarios with greenhouse gas emissions increasing through the 21st century. This scenario was selected because it would have the strongest effect on climate among various scenarios available at the time of the investigation. Their investigation focuses on AR conditions just offshore of the coast of California, since current GCMs lack the detail to portray orographic effects of California's mountain ranges. Their model results show that the number of winters with exceptionally large AR storms increases and the number of AR days increases in most GCMs when compared to historical numbers. On the AR days, the integrated water vapor (IWV) increases in all models. High IWV values are associated with the largest of historical storms and thus suggest that there could be a greater number of storms with extreme precipitation values in the future. Also, since the snowline is also projected to be at higher elevations, more of the basin area will receive rain during the storms, which could also lead to larger magnitude runoff. Although most of the AR days occur during the winter months, Dettinger et al. (2011) mention that in some models, AR days are notably more common in the spring, which could extend the flood season into the spring months.

Although Dettinger's research begins to address the extreme events, an estimated magnitude of the discharge events is lacking and therefore these projections are difficult to compare to the extremes in the paleoflood record and whether they are still within the range of events that have happened during the Holocene. Along some drainages in the Sierra Nevada, paleoflood data indicate that several

prehistorical floods have had larger magnitudes than any historical event (i.e., American River; Klinger and England, 2002). These events as well as non-exceedance information could be used as a reality check on simulated predictions for large magnitude floods if and when they are produced.

3.5 Synthesis of data, Sierra Nevada region

Case study 1 demonstrates how paleoflood data contained within the database can be utilized to investigate the relationship between floods and climate change. The idea behind this study was to link periods of extreme floods or evidence of increased streamflow (greater fluvial deposition) with changes in climate from the paleoclimate record. This type of exercise should aid in the understanding of how floods and climate are linked prior to the historical record and can provide insight regarding hydrologic response given future projections of climate in the state of California.

Radiocarbon data derived from flood deposits and stream terraces were analyzed and plotted to determine the timing of fluvial deposition for regions of interest in California. Although several regions in California were analyzed, the main focus of the study was the Sierra Nevada region because the majority of data was located in this region and because it is the source of many extreme floods in California. The radiocarbon data were compared to proxies of paleoclimate or paleoclimate reconstructions to determine whether any patterns existed between the timing of fluvial deposition and paleoclimate or between the timing of extreme floods and paleoclimate. We would expect that periods with few radiocarbon ages would have less fluvial deposition and therefore lower streamflow on average, whereas periods with numerous radiocarbon ages would have greater fluvial deposition and therefore higher streamflow on average.

Comparison of the radiocarbon data with paleoclimate records in the Sierra Nevada region show some broad relationships that can be defined during the last 1,000 to 2,000 years. During periods of drought (i.e., Medieval Climatic Anomaly, 1000-700 Cal yr BP), the probability density of radiocarbon ages decreases, suggesting lower streamflow in response to dry conditions. There also appears to be a higher probability density of radiocarbon ages during the last 500 or 600 years, a period of cooler, wetter climate, and inferred higher streamflow. Radiocarbon data show broadly similar trends when compared to paleoclimate reconstructions of large scale climate signals such as ENSO or PDO. Even in a transition area such as the Sierra Nevada region where the PDO and SOI indices are not well correlated to the timing of extreme floods, the cumulative probabilities of radiocarbon data show broadly similar trends for the past ~1,000 years especially during the Medieval Climatic Anomaly where cumulative probabilities of radiocarbon ages are low and the PDO index is negative.

Although there are still many unanswered questions regarding the relationship between ENSO and extreme floods, previous research using historical data has generally shown that extreme floods are more likely during periods of El Niño in

southern California and La Niña in northern California. The Pacific Decadal Oscillation (PDO) could also play a similar role in which extreme floods are more likely in southern California during the positive/warm phase of the PDO while in northern California, extreme floods are more likely during the negative/cool phase of the PDO. The Sierra Nevada is an area of transition between the northern jet position and southern jet position, and associated regional relationships with meteorological patterns. Records of extreme paleofloods appear to fall within time periods of both wet and dry climate and do not appear to be related to a specific type of climate in the Sierra Nevada region, at least given the resolution of the data that are currently available. This type of relationship is also shown in Malamud-Roam et al. (2005) over a broader area of California, where records of extreme floods from multiple studies using various methods overlap both periods of drought and wetter intervals.

One of the problems with identifying extreme floods in climate cycles is related to the uncertainty in radiocarbon data, which is larger in some cases than the periodicity of the meteorological patterns. Such is the case with ENSO, which operates on an annual timescale and with PDO which has a decadal timescale. Typically, the analytical error associated with Accelerated Mass Spectrometry (AMS) can range from ± 15 to ± 60 years, but could vary depending on the laboratory and sample. The radiocarbon calibration curve will also return several intervals and associated probabilities for one radiocarbon age. In addition, since most of the precipitation for the annual totals in the Sierra Nevada is derived from a few storms that occur over only a few days, the largest floods could fall within a particularly short wet interval that is obscured by a larger climate pattern, such as a prolonged drought. Tree ring reconstructions are known to be less sensitive to wet periods and more sensitive to drought, which is related to the physiology of trees (i.e., Fritts, 1976). Therefore, streamflow and climate reconstructions based on tree ring data may not be able to capture an extreme wet period whereas they are more likely to accurately extreme dry periods.

There are also questions regarding the applicability of paleoclimate reconstructions of large scale climate signals to the Sierra Nevada region and other regions in California given that the reconstructions utilize data from regions that are geographically distant from the study area. While this question cannot be comprehensively answered in this report, a recent study by Li et al. (2011) found that comparisons of ENSO reconstructions to other proxies of ENSO variability showed broad agreement from their study in the Pacific to nearby regions. In their study, Li et al. (2011) utilized drought reconstructions based on tree ring data from the North America Drought Atlas (NADA) that are annually resolved over a period of 1,100 years. They found that ENSO amplitude had a quasi-regular cycle of about 50-90 years that is "closely coupled to the tropical Pacific mean state".

While extreme floods have been recorded along the length of the Sierra Nevada region, floods that control the envelope curve of historical peak discharge data are

clustered geographically in the southern portion of the Sacramento River Basin. These floods are recorded at gaging stations along rivers that drain the west flank of the Sierra Nevada and include the American River Basin, Yuba River Basin and Feather River Basin. Klinger and England (2002) note that the gap in the Coast Range at San Francisco Bay allows for penetration of large storms inland without confronting the topographic barrier of the Coast Range. It would be expected that since the flood generation in this region is at least partially related to the topography, these basins would continue to generate the largest floods. The smallest floods in terms of unit peak discharge have occurred in the southern Sierra Nevada in drainages such as the Kern River. Several factors including regional physiography, basin relief, shape and orientation, may be responsible for the smaller size floods in these basins.

GCMs are not currently capable of being used to understand the likelihood or extent of future changes in extreme floods. Given the complex topography that plays a substantial role in flood generation and the lack of topographic complexity in these models, it is likely that many of the climate projections are inaccurate and only reflect future conditions on a gross scale. The fact that many models contradict each other and that either outcome, whether wetter or drier, is just as likely at this point renders an exercise using these data as inconsequential. While Dettinger's approach, which uses observations off the coast to avoid the lack of topographic detail in GCMs, is probably a more valid approach to use, his research is still lacking any specific details that might prove useful for linking paleofloods with periods of wetter or drier conditions.

Climate and its associated storm patterns is likely to be the driver behind the hydrologic differences between basins, either through a broad regional change in precipitation, position of storm tracks or the frequency and intensity of storms in various regions of California. Basin parameters, such as soils, rock types, vegetation, elevation, topography, basin shape, aspect, and slope will also be factors in the generation of extreme floods and in some cases will play a significant role. How these factors combine to produce large floods in the Sierra Nevada is a topic worthy of further study. What we can postulate with the current state of knowledge is that the storm types and scenarios that have produced the largest floods historically are likely responsible for generating paleofloods in the pre-historical record and will likely continue to be the mechanisms responsible for extreme floods in the future.

4 CASE STUDY2: COLORADO RIVER BASIN

For the past three years, Reclamation has partially funded paleoflood investigations in the Colorado River Basin through this research project. These investigations have been concentrated in the Upper Colorado River Basin, an area of transition between regions that have been reported to be highly influenced by ENSO conditions in generating extreme floods (Cayan et al. 1999). In the southwestern U.S., extreme floods are predominantly associated with El Niño conditions while the Pacific Northwest experiences more extreme floods during La Niña conditions. The research included in this case study focuses on areas in the transition region where the relationship between floods and ESNO conditions are more poorly understood. Case study 2 includes individual studies that are not compiled into a regional context in this report, and therefore differ from the approach taken in Case study 1. The studies partially funded by this project are summarized in the following sections and include:

- The Moab Mill Project: a paleoflood study on the Colorado River near Moab, Utah

- The Dolores River Basin: a paleoflood study to investigate the paleoflood history

- The Green River: field reconnaissance to determine feasible sites for a paleoflood investigation

4.1 The Moab Mill Project: Paleofloods in the Upper Colorado River near Moab, Utah, May 2006 (Greenbaum et al. 2006)

The Moab Mill Project site is located along the Colorado River near Moab, Utah near uranium tailings piles from the former Atlas Uranium Mine. Studies regarding flood hazards along the Colorado River in this area were initiated due to concern about the stability and potential delivery of tailings into the Colorado River, which would degrade environmental conditions along the river and concerns about DOE plans to cap the tailings in place. As part of this investigation, a paleoflood study was undertaken at a site approximately 17 km (10.6 miles) upstream from Moab to provide long-term estimates of flood hazard (Figure 4-1). While the study was primarily funded by a grant from The Citizens' Monitoring and Technical Assessment Fund (www.mtafund.org), Reclamation funded later components of the study to decrease uncertainty in the hydraulic modeling in the study reach and develop a flood frequency analysis with data from the study site.

To develop flood hazard information, the authors described slackwater stratigraphy at 14 pits at the BLM-TO site, located between Big Bend and Sandy Beach on the Colorado River (Figure 4-2). The pits overlapped each other in elevation down the slope of the deposits in order to correlate between the deposits in each individual pit. This site consisted of two distinct benches of slackwater

deposits and a lower floodplain, inundated by recent flows. Cross sections were surveyed along a 5-km (3.2-mile) long reach with a total station/laser rangefinder. Initially, peak discharges were computed using the slope-area method and were later computed in the HEC-RAS 1D model. A total of 14 OSL ages and 4 radiocarbon ages were determined to develop age estimates for the slackwater units.

Results from the study indicate that at least three floods exceed a peak discharge of 8,500 m^3/s (300,000 ft^3/s) within the past 1410 ± 110 years B.P., while two floods have associated peak discharges that exceed 10,000 m^3/s (350,000 ft^3/s), which exceeds the PMF (300,000 ft^3/s) developed by the USGS for the Moab Valley. HEC-RAS 1D modeling indicates that peak discharges developed from the slope-area method during the initial study may be overestimated; for example the maximum discharge of 10,000 m^3/s developed from slope-area computations is modified to a range of 8,500-10,500 m^3/s when using the HEC-RAS model (Greenbaum et al. 2011).
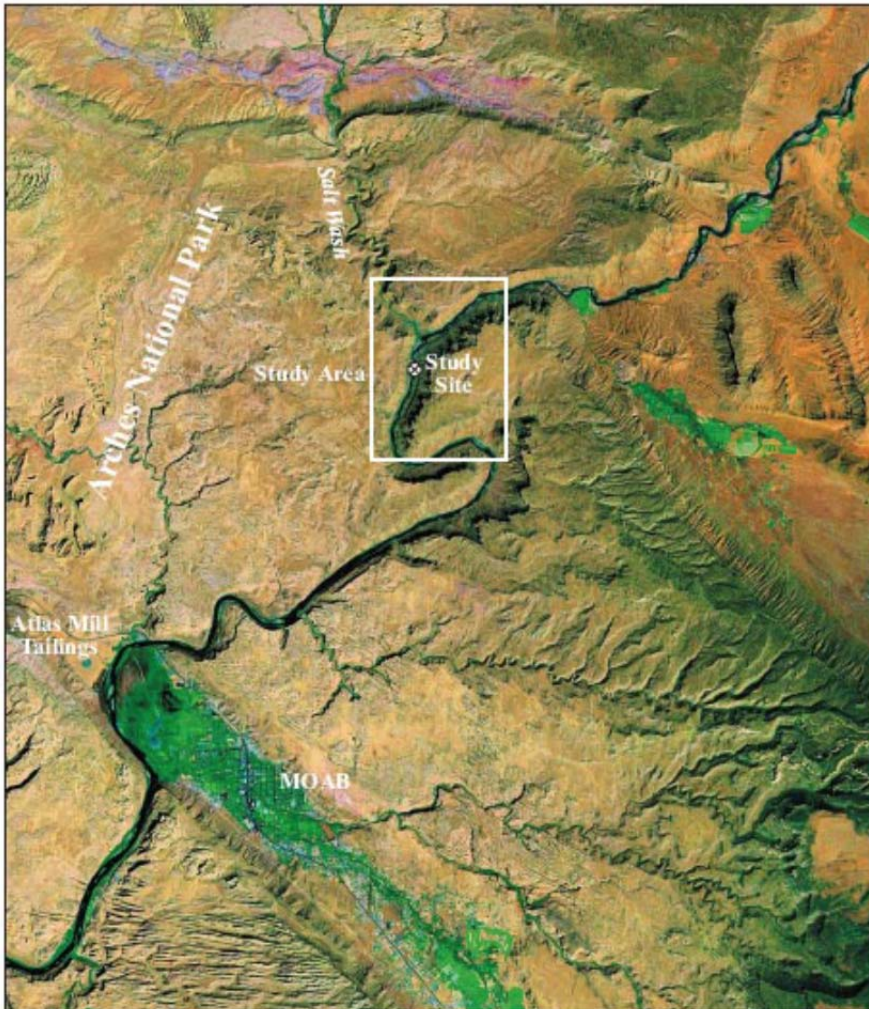
Figure 4-1. Location of the study reach used in Greenbaum et al. 2006 (from Greenbaum et al. 2006).

94

Figure 4-2. BLM-TO study site on the Colorado River near Moab, Utah (from Greenbaum et al. 2006).

4.2 Dolores River Basin: Extreme floods in the Dolores River Basin, Colorado and Utah: Insights from paleofloods, geochronology and hydroclimatic analysis (Cline, 2010)

The Dolores River Basin is a subbasin in the Upper Colorado River basin and drains portions of the San Juan Mountains in southwestern Colorado. With a drainage basin area of 4,574 mi^2 where it joins the Colorado River north of Moab, it is one of the major drainages in the upper Colorado. Many researchers have shown that extreme floods in basins in the southwestern U.S. are strongly correlated with ENSO, specifically El Niño conditions, while extreme floods in basins in the Pacific Northwest are also strongly correlated with El Niño - Southern Oscillation (ENSO), but with La Niña conditions. The Dolores River Basin is located in the transition zone between these two regions and thus could provide some insight regarding flood response and dominant flood mechanisms in an area whose flood producing mechanisms are less well understood. By understanding the link between paleofloods and paleoclimate, this information can also help to inform management decisions regarding how climate change will impact the flood regime in the future.

The Dolores River Basin is located in an area of interest to Reclamation since it is a large part of the Colorado River watershed, where many significant Reclamation

Dams are located. This study can also provide additional flood hazard information for McPhee Dam, located on the Dolores River in the upper portion of the Dolores River basin.

During the course of his research, Cline investigated a total of 10 slackwater sites to develop a paleoflood chronology in the Dolores River Basin (Figure 4-3). Eight of these sites were located on the main stem Dolores River and two on the San Miguel River, a major tributary to the Dolores River. A total of 34 radiocarbon and eight optically-stimulated luminescence (OSL) ages were developed to provide quantitative age estimates of the flood deposits. Hydraulic modeling was a minor component of the study and was performed only at the Tufoni site on the San Miguel River.

Cline's (2010) research has several pertinent results that link extreme floods with hydroclimatic conditions in the paleoclimate record. First, Cline found that the documented paleofloods appear to have been at least 4 times larger than historical floods in the Dolores River Basin. This change in flood regime appears to have occurred about 800 years ago, after which point no flood deposits are recorded at the study sites. Although the magnitude of the paleofloods for the entire basin is much larger than the historical floods, the flood magnitudes in the upper basin fall well below the envelope curve that encompasses floods for the Lower Colorado River Basin (Enzel et al. 1993) (Figure 4-4).

Age estimates for the flood deposits derived from both radiocarbon dating and OSL dating suggest that there are distinct periods of extreme floods. In the Dolores River Basin, periods of multiple extreme floods fall within the 100 A.D. to 1100 A.D. This range overlaps the Medieval Climatic Anomaly (MCA) (950 to 1250 A.D.), a period of severe droughts and widespread wildfire, and suggests that the extreme floods are associated with dry conditions in the watershed. This is in contrast to paleoflood chronologies in the Lower Colorado River Basin, in which extreme floods are documented during cooler, wet periods since about 1000 A.D. in which El Niño conditions are frequent (Ely, 1993; 1997) (Figure 4-5). In the Dolores River Basin, there is a distinct lack of paleoflood deposits from about 1200 A.D. to present, suggesting that the historical flood regime is much different than what was present more than 800 years ago.

Based on analyses of historical floods in the Dolores River Basin, Cline (2010) concludes that floods are most closely associated with the positive phase of the PDO or with shifts in the phase of the PDO. There is a lack of connection between floods in the Dolores River Basin and ENSO, or a poor connection at best, which is consistent with this area being in the transition zone between regions that are highly influenced by ENSO. It should be noted, however that this analysis is performed for moderate size floods in the Dolores River Basin that are generated during the winter months and not for extreme floods, such as those in the paleoflood record. A single large flood in the historical record was recorded during October 1911, and was generated by a dissipating tropical cyclone. This event was excluded from the detailed analysis because it was not a winter flood; if

analyzed, it could provide some useful information regarding extreme storm mechanisms in the Dolores River Basin.
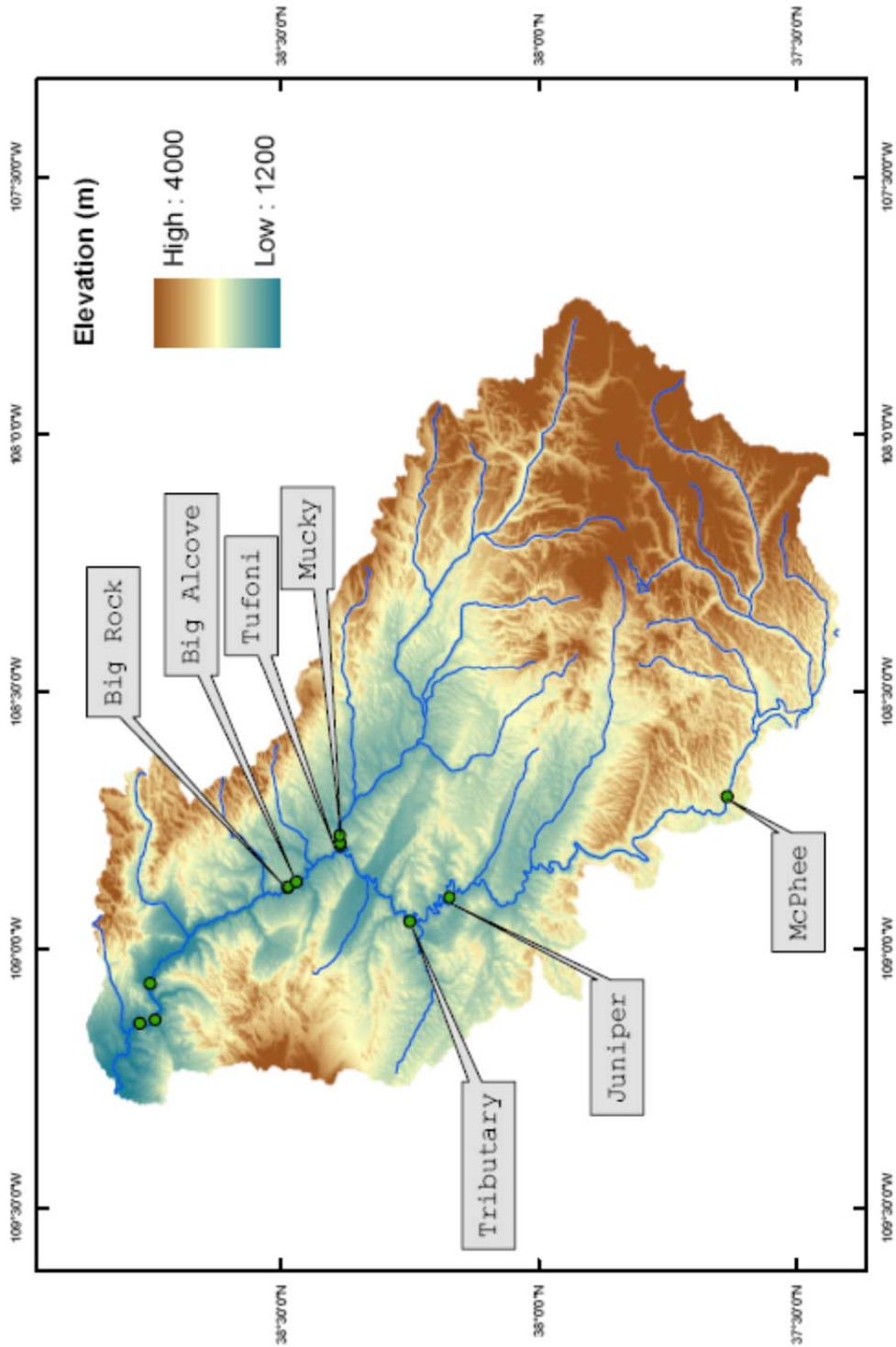
Figure 4-3. Physiography of the Dolores River Basin with paleoflood investigation sites (from Cline, 2010).
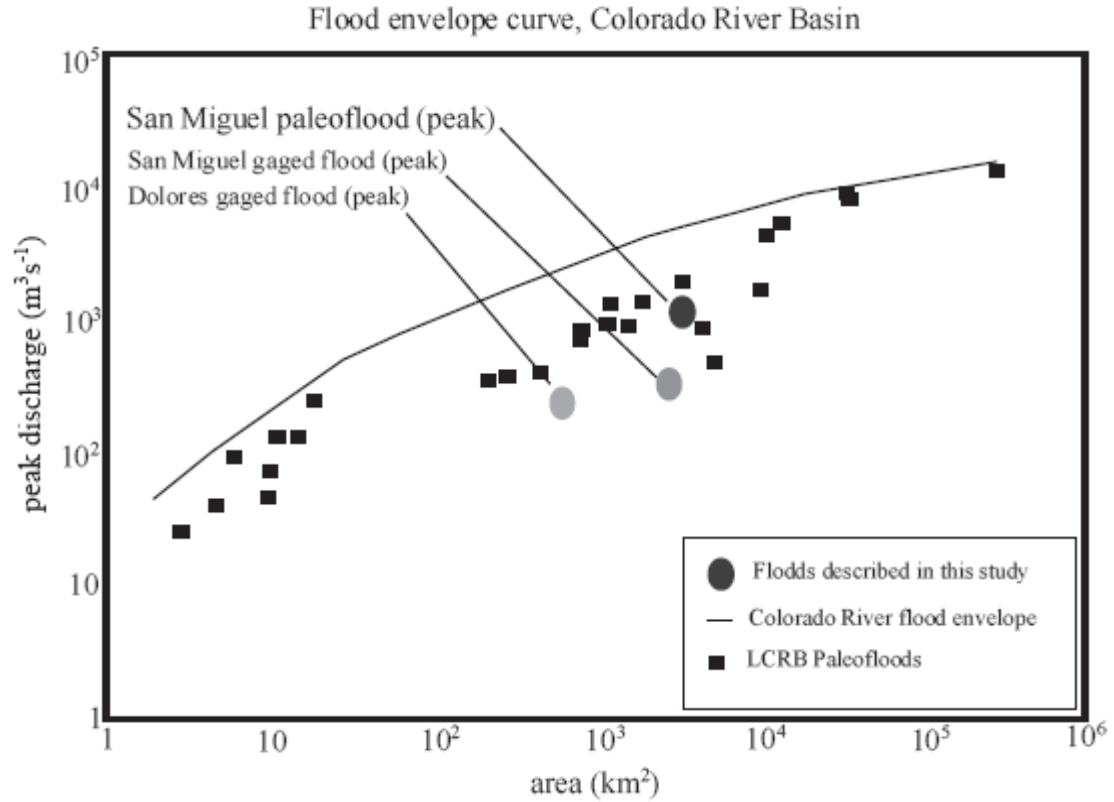
Figure 4-4. Flood envelope curve, Lower Colorado River basin with results from the Dolores River Basin paleoflood study (from Cline, 2010). See Enzel et al. 1993 for the original envelope curve.

Figure labels on chart: Hf1, Hf2, Hf3, Hf5, Hf6a, Hf6b, Hf7a, Hf7b, Hf7c, Hf7d, Hf7e, Hf8, Hf9, Hf10, Hf11, Hf12, Hf13

X-axis values: 9000, 8000, 7000, 6000, 5000, 4000, 3000, 2000, 1000, 0

calibrated years B.P.

☐ Individual flood periods in the DRB

High / Low — Periods of heightened, large magnitude flooding (based on Ely et al., 1993; Ely, 1997)

✱ indicates a linear break in the time scale
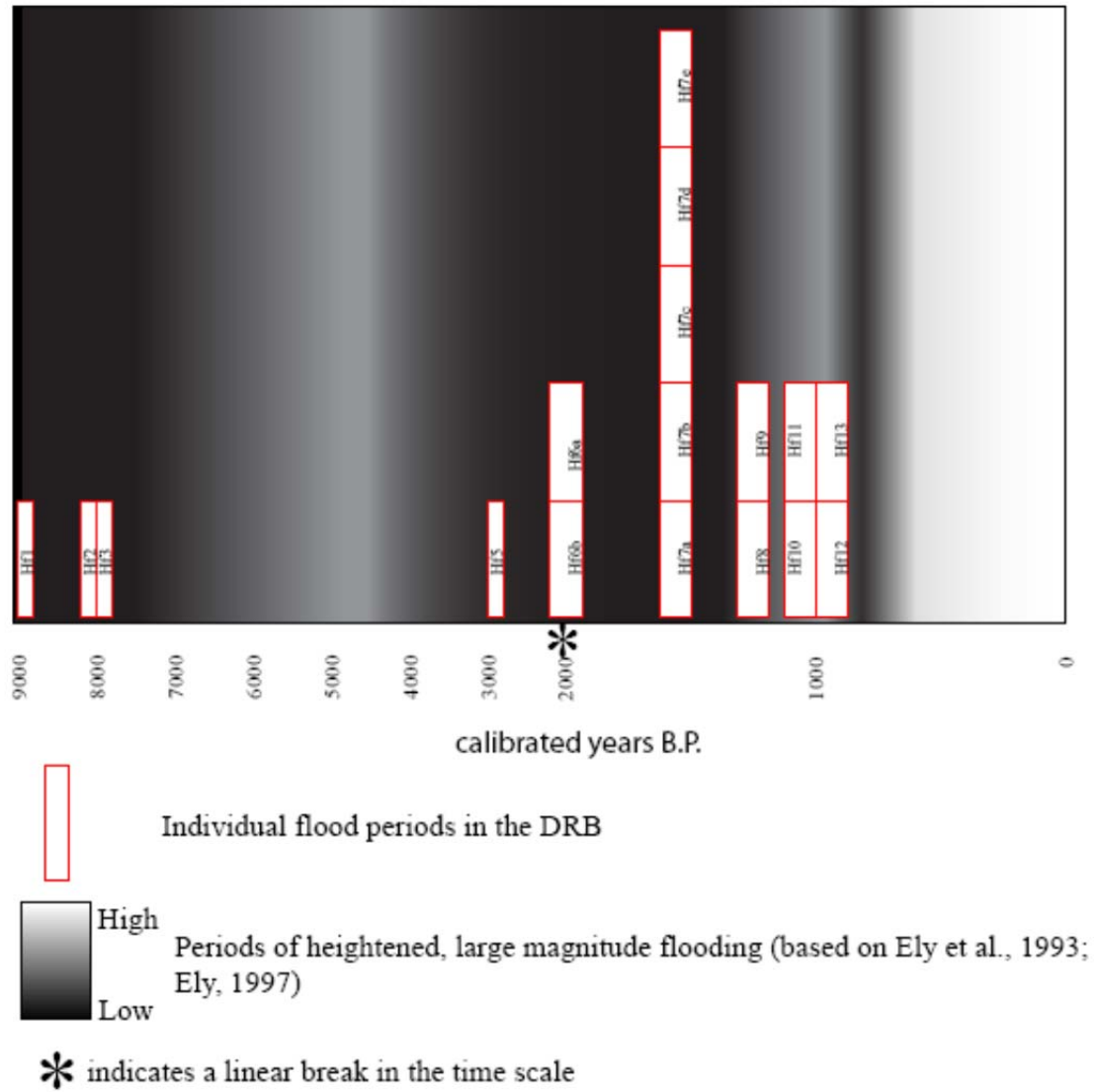
Figure 4-5. Paleoflood chronology of the Dolores River Basin, shown with paleoflood chronology of Ely from the Lower Colorado River Basin (from Cline, 2010).

4.3 Green River Basin: reconnaissance and identification of suitable sites for paleoflood analysis

During July 2012, a team of scientists affiliated with the University of Arizona conducted paleoflood research at six sites along the lower Green River in Stillwater Canyon and at two sites along the Upper Colorado River in Cataract Canyon. The team documented 7 to 9 flood deposits at lower elevation sites and fewer at higher elevations sites. The highest sites were located at 12 to 13.5 m above the water surface in Stillwater Canyon in narrow canyon reaches and 11 to 13.25 m above the water surface in Cataract Canyon in wider canyon settings than those in Stillwater Canyon. Bathymetric surveys near the study sites were

performed as part of this research and will be incorporated into hydraulic modeling at the study sites. Forty (40) samples for OSL analysis and 7 samples for radiocarbon analysis were collected. The OSL samples are currently being processed at the Geological Survey of Israel OSL laboratory in Jerusalem, Israel. This work will complement paleoflood research in the Dolores River basin by Cline (2010) and will hopefully provide further information regarding the relationship between extreme floods and climate in the Upper Colorado River basin.

5 PROJECT SUMMARY AND CONCLUSIONS

This report completes a 2-year study of linkages between extreme floods and climate. During this project, radiocarbon data were compiled for regions in California and were compared to paleoclimate proxies and reconstructions to determine whether any patterns existed between extreme floods and changes in climate. The Sierra Nevada was the main focus of the analyses because many large floods happen in this region and a wealth data exist to conduct a study of extreme floods. The analyses concluded that relationships do exist between records of fluvial deposition and shifts in climate in that less fluvial deposition (or lower streamflow) is occurring during times of drier climate and more fluvial deposition (or higher streamflow) is occurring during times of wetter climate. This relationship can be defined on a broad scale for about the last 1,000 years. Beyond this point, the resolution of paleoclimate data appears to be too coarse in many cases to compare to the radiocarbon data; in addition, more radiocarbon ages may be needed to better define periods of deposition and non-deposition. In any case, the implications for the future are that a drier climate over an extended period will result in smaller annual volumes delivered to Reclamation reservoirs. Therefore, droughts similar to the Medieval Climatic Anomaly will undoubtedly negatively impact Reclamation's water supply.

Paleofloods that have been documented along rivers in the Sierra Nevada appear to fall within both dry and wet periods in the paleoclimate record and therefore suggest that these broad changes in climate may not be able to predict whether extreme floods will happen or not, but rather it is the short term fluctuations in meteorological phenomena within larger climate shifts that will drive extreme floods and where they will increase in severity, or frequency.

This project also funded research in the Upper Colorado River Basin, which was conducted by the University of Arizona and other collaborators. Research is ongoing in the basin and is focusing on the area of transition within the basin where extreme floods are related to El Niño conditions and those where extreme floods are related to La Niña conditions. So far, this research has found that paleofloods fall within dry periods such as the Medieval Climatic Anomaly and are related to the positive phase of the PDO and have a poorly defined relationship with ENSO. This is in contrast to previous research in the Lower

Colorado River Basin by Ely (1993; 1997), where extreme floods appear to fall within wet intervals and are closely associated with El Niño .

Many questions remain unanswered regarding how climate change will impact water supply and extreme floods at Reclamation facilities. This project takes an alternate tact to model simulations of runoff by exploring the relationships between fluvial sedimentation, paleofloods and climate in the recent geologic past. This project has provided an important step in the understanding of this relationship and recommends study in other regions to complement model projections, which still retain considerable uncertainty. Additionally, further stratigraphic studies of the fluvial history on many other rivers should be encouraged so that additional data can be applied to this question.

5.1 Recommendation for further research

While this study focused on California and the Colorado River Basin, radiocarbon ages have been collected along many other rivers in the western U.S. near Reclamation facilities and could be compiled and analyzed for links between paleofloods and paleoclimate. California has benefitted from a large number of research studies over the last 100 years on meteorological phenomena related to extreme precipitation and flooding as well as the many scholars who conduct research regarding paleoclimate. Although research on these topics is available in other regions of the western U.S., it is not as widespread, detailed or recent as the research used in this study. Since California is located along the coast, the link between storms that make landfall and hydrologic response is also more direct than other regions that are further inland, where there is more uncertainty in whether a particular storm is able to penetrate inland and the storm trajectory from the coast to inland areas. This study did not reveal a distinct link between climate and extreme floods; however, this is not necessarily a result that would carry over to other regions, such as the Pacific Northwest or southwestern U.S.

Systems with predominantly more snowmelt floods would perhaps reveal a clearer linkage between wetter/drier intervals because large floods are generally related to the amount of snowpack available to runoff during the spring. However, the relationship may also be complicated by the fact that the largest snowmelt floods are typically preceded by warming trends which allow the snow to ripen and melt off quickly, producing a large peak discharge. So it is also possible that even a large snowpack may not generate a large peak discharge, although it would be likely recorded in fluvial deposition in stream terraces and floodplains along the river channel. More importantly, larger snowpack would likely result in floods with higher volumes, which could be important for operational issues and water storage at Reclamation facilities.

A large number of studies have been conducted in the states of Utah and Colorado that could be used to investigate these kinds of questions. Regions with a combination of storm types may also be interesting to investigate. The Great Plains region combines large frontal storms and thunderstorms as mechanisms for

generating large floods. Some of the largest floods in this region appear to have been generated by AR storms that have penetrated inland into states such as Idaho, generating floods of record (i.e., 1964). Other storms have tracked from the Gulf of Mexico, bringing moisture into Texas and Oklahoma to generate large floods. The radiocarbon database contains many ages from the Great Plains region. Paleoclimate has also been studied in this region, particularly in areas with loess or extensive archeological data. Research is ongoing in the Colorado River Basin through the University of Arizona and other collaborators. Reclamation could continue to contribute to this research by compiling data in subbasins and comparing data to results from ongoing academic research.

6 REFERENCES

Andrews, E.D. (1984): Bed-material entrainment and hydraulic geometry of gravel-bed rivers in Colorado. Geological Society of America Bulletin, 95, 371-378.

Andrews, E.D., R.C. Antweiler, P.J. Neiman, and F.M. Ralph (2004): Influence of ENSO on flood frequency along the California Coast. J. Climate, 17, 337-348.

Atwater, B.F., D.P. Adam, J.P. Bradbury, R.M Forester, R.K. Mark, W.L. Lettis, G.R. Fisher, K.W. Gobalet, and S.W. Robinson (1986): A fan dam for Tulare Lake, California, and implications for the Wisconsin Glacial history of the Sierra Nevada. Bulletin of the Geological Society of America 97, 97–109.

Baker, V.R., and J.E. Costa (1987): Flood power, *in* Mayer, L., and Nash, D., eds., Catastrophic Flooding. Boston, Massachusetts, Allen & Unwin, 1-21.

Barganza, K., J.L. Gergis, S.B. Power, J.S. Risbey, and A.M. Fowler (2009): A multiproxy index of the El Niño -Southern Oscillation, A.D. 1525-1982. J. Geophys. Res (Atmospheres), 1114, D05106.

Barnes, H.H. (1967): Roughness characteristics of natural channels. U.S. Geological Survey Water-Supply Paper 1849, 213.

Biondi, F., Gershunov, A., and D.R. Cayan (2001): North Pacific Decadal Variability since AD 1661. Journal of Climate, 14, 5-10.

Birkeland, P.W. (1999): Soils and Geomorphology. New York, NY, Oxford University Press, 448.

Boggs, S., Jr. (1995): Principles of Sedimentology and Stratigraphy. Prentice Hall, Englewood Cliffs, NJ, 774.

Booth, E.G., J.F. Mount, and J.H. Viers (2006): Hydrologic Variability of the Cosumnes River Floodplain. San Francisco Estuary and Watershed Science, 4 (2), Article 2.

Bradley, R.S. (2003): Climatic forcing during the Holocene, *in*, Mackay, A., Battarbee, R., Birks, H.J.B., and Oldfield, F., eds. Global change in the Holocene. London, UK, Arnold, 1019.

Bronk Ramsey, C., M. Dee, S. Lee, T. Nakagawa, and R. Staff (2010): Developments in the calibration and modeling of radiocarbon dates. Radiocarbon 52(3), 953-961.

Cayan, D.R., K.T. Redmond, and L.G. Riddle (1999): ENSO and hydrologic extremes in the Western United States. Journal of Climate, 12, 2881-2893.

Climate Prediction Center (CPC) (2012): Monitoring Intraseasonal Oscillations, Tropical Intraseasonal Activity (Madden-Julian Oscillation – MJO), Accessed website on May 1, 2012 at http://www.cpc.ncep.noaa.gov/products/intraseasonal/intraseasonal_faq.htm.

Cline, M.L. (2010): Extreme flooding in the Dolores River Basin, Colorado and Utah: Insights from paleofloods, geochronology and hydroclimatic analysis. Ph.D. Dissertation, University of Arizona, Tucson, Arizona, 221.

Conroy, J.L., J.T. Overpeck, J.E. Cole, T.M. Shanahan, and M. Steinitz-Kannan (2008): Holocene changes in eastern tropical Pacific climate inferred from a Galápagos lake sediment record. Quaternary Science Reviews, 27(11-12), 1166-1180.

Cook, E.R., C.A. Woodhouse, C.M. Eakin, D.M. Meko, and D.W. Stahle (2004): Long-term aridity changes in the western United States. Science, 306, 1015-1018.

Cook, E.R., D.M. Meko, D.W. Stahle and M.K. Cleaveland (1999): Drought reconstructions for the continental United States. Journal of Climate, 12, 1145-1162.

Cook, E.R., R.D. D'Arrigo, and K.J. Anchukaitis (2008): ENSO reconstructions from long tree-ring chronologies: Unifying the differences? Conference paper, Reconciling ENSO Chronologies for the Past 500 Years, Moorea, French Polynesia, 2-3 April 2008.

Cook, E.R., (unpublished): On the variability of ENSO over the past six centuries. [submitted to Geophys. Res. Letters in 2005. Information from World Data Center for Paleoclimatology, http://www.ncdc.noaa.gov/paleo/recons.html#hydro.

D'Arrigo, R., and R. Wilson (2006): On the Asian expression of the PDO. Int. J. Climatology, 26, 1607-1617.

D'Arrigo, R., R. Villalba, and G. Wiles (2001): Tree-ring estimates of Pacific decadal climate variability. Climate Dynamics, 18, 219-224.

Das, T., M. Dettinger, D. Cayan, and H. Hidalgo (2010): Potential increase in floods in California's Sierra Nevada under future climate projections. Presentation, California Water and Environmental Modeling Forum, Annual Meeting 2010.

Davis, O.K. (1999): Pollen analysis of Tulare Lake, California: Great Basinlike vegetation in Central California during the full-glacial and early Holocene. Review of Paleobotany and Palynology, 107, 249-257.

Denlinger, R.P., D.R.H. O'Connell, and P.K. House (2002): Robust determination of stage and discharge: An example from an extreme flood on the Verde River, Arizona, *in* House, P.K., Webb, R.H., Baker, V.R., and Levish, D.R., eds., Ancient Floods, Modern Hazards: Principles and Applications of Paleoflood Hydrology. Water Sciences and Application Volume 5, American Geophysical Union, Washington D.C., 127-146.

Dettinger, M. (2004): Fifty-two years of "Pineapple-Express" storms across the West Coast of North America. U.S. Geological Survey, Scripps Institution of

Oceanography for the California Energy Commission, PIER Energy-Related Environmental Research, CEC-500-2005-004.

Dettinger, M. D. (2005): A long-term (~50-yr) historical perspective on flood-generating winter storms in the American River Basin. Proceedings, 2005 California Extreme Precipitation Symposium, April 2, 2005, 62-73.

Dettinger, M. (2011): Climate change, atmospheric rivers, and floods in California – a multimodel analysis of storm frequency and magnitude changes. JAWRA, 47, 514-523.

Dettinger, M. D. and D.R. Cayan (1994): Large-scale atmospheric forcing of recent trends toward early snowmelt runoff in California. Journal of Climate, 8, 606-623.

Dettinger, M., F.M. Ralph, T. Das, P.J. Neiman, and D.R. Cayan (2011): Atmospheric rivers, floods, and the water resources of California. Water 2011, 3, 445-478.

Dubois, N., M. Kienast, C. Normandeau, and T.D. Herbert (2009): Eastern equatorial Pacific cold tongue during the Last Glacial Maximum as seen from alkenone paleothermometry. Paleoceanography, 24, PA4207, doi:10.1029/2009PA001781.

Dubois, N., M. Kienast, S. Kienast, C. Normandeau, S.E. Calvert, T.D. Herbert, and A. Mix (2011): Millennial-scale variations in hydrography and biogeochemistry in the Eastern Equatorial Pacific over the last 100 kyr. Quaternary Science Reviews, 30, 210-223.

Ely, L.L. (1997): Response of extreme floods in the southwestern United States to climatic variations in the late Holocene. Geomorphology, 19 (3-4), 175-201.

Ely, L.L., Y. Enzel, V.R. Baker, and D.R. Cayan (1993): A 5000-year record of extreme floods and climate change in the southwestern United States. Science, 262 (5132), 410-412.

England, J.F. and D.R. Levish (1998): Preliminary Hydrologic Loadings for CFR/PP, Friant, California. Bureau of Reclamation, Technical Services Center, Denver, CO, 10.

Enzel, Y., L.L. Ely, P.K. House, V.R. Baker, and R.H. Webb (1993): Paleoflood evidence for a natural upper bound to flood magnitudes in the Colorado River Basin. Water Resources Research, 29(7), 2287-2297.

Evans, M.N., A. Kaplan and M.A. Cane (2002): Pacific sea surface temperature field reconstruction from coral delta 18O data using reduced space objective analysis. Paleoceanography, 17 (1).

Felis, T., A. Suzuki, H. Kuhnert, N. Rimbu, and H. Kawahata (2010): Pacific Decadal Oscillation documented in a coral record of North Pacific winter temperature since 1873. Geophys. Res. Letters, 37, L14605.

Fritts, H.C. (1976): Tree Rings and Climate. Academic Press, New York, 567.

Galewsky, J., and A. Sobel (2004): Moist dynamics and orographic precipitation in Northern and Central California during the New Year's Flood of 1997. Mon. Wea. Rev., 133, 1594-1612.

Gergis, J.L., and A.M. Fowler (2009): A history of ENSO events since A.D. 1525: implications for future climate change. Climatic Change, 92, 343-387.

Godaire, J.E. and T.R. Bauer (2012): Paleoflood Study, San Joaquin River near Friant Dam, California. Technical Memorandum No. 86-68330-2012-24, Bureau of Reclamation, Denver, CO, 61.

Goman, M. and L. Wells (2000): Trends in river flow affecting the northeastern reach of the San Francisco Bay Estuary over the past 7000 years. Quaternary Research, 54, 206-217.

Goodridge, J. (1996): Data on California's extreme rainfall from 1862-1995. Prepared for the 1996 California Weather Symposium, Rocklin, CA, 33 pp.

Gottschalek, J., V. Kousky, W. Higgins, and M. L'Heureux (2012): Madden-Julian Oscillation. http://www.cpc.ncep.noaa.gov/products/precip/CWlink/MJO/MJO_summary.pdf. Accessed May 2012.

Greenbaum, N., Weisheit, J.S., T. Harden, and J.C. Dohrenwend (2006): Paleofloods in the Upper Colorado River near Moab, Utah, *in* Weisheit, J.S. and S.M. Fields, eds., The Moab Mill Project: A technical report towards reclaiming uranium mill tailings along the Colorado River in Grand County, Utah. Living Rivers, Moab, Utah, p. 13-29.

Greenbaum, N., T. Harden, V.R. Baker, J. Weisheit, M.L. Cline and R. Halevi (2011): Hydraulic analyses of past and present floods along the Upper Colorado River, Moab, Utah. Progress report to U.S. Bureau of Reclamation, Technical Services Center, 9 p.

Haynes, A. (2001): Synoptic pattern typing for historical heavy precipitation events in Southern California. Western Regional Technical Attachment No. 01-15, California Nevada River Forecast Center, November 9, 2001.

Higgins, R.W., J.E. Schemm, W. Shi, and A. Leetmaa (2000): Extreme precipitation events in the Western United States related to tropical forcing. Journal of Climate, 13, 793-820.

Hughes, M.K. and G. Funkhouser (1998): Extremes of moisture availability reconstructed from tree rings for recent millennia in the Great Basin of Western North America, *in* Benniston, M., Innes, J.L., eds., The Impacts of Climate Variability on Forests. Springer-Verlag, Berlin, Lecture notes in Earth Science 74.

Hughes, M.K. and L.J. Graumlich (1996): Multimillennial dendroclimatic studies from the western United States, *in* Jones, P.D., Bradley, R.S., and J. Jouzel, eds. Climatic variations and forcing mechanism of the last 2000 years. Springer-Verlag, Berlin.

Ingram, B.L., and D.J. DePaolo (1993): A 4300 year strontium isotope record of estuarine paleosalinity in San Francisco Bay, California. Earth and Planetary Science Letters, 119 (1-2), p. 103-119.

Jones, C. (2000): Occurrence of extreme precipitation events in California and relationships with the Madden-Julian Oscillation. J. Climate, 13, 3576-3587.

Jones, T.J. and D.J. Kennett (1999): Late Holocene sea temperatures along the central California coast. Quaternary Research, 51, 74-82.

Junker, N.W., R.H. Grumm, R. Hart, L.F. Bosart, K.M. Bell, and F.J. Pereira (2008): Use of normalized anomaly fields to anticipate extreme rainfall in the mountains of Northern California. Wea. Forecasting, 23, 336-356.

Kalnay, E., M. Kanamitsu, R. Kistler, W. Collins, D. Deaven, L. Gandin, M. Iredell, S. Saha, G. White, J. Woollen, Y. Zhu, M. Chelliah, W. Ebisuzaki, W.Higgins, J. Janowiak, K. C. Mo, C. Ropelewski, J. Wang, A. Leetmaa, R. Reynolds, R. Jenne, D. Joseph (1996): The NCEP/NCAR 40-Year Reanalysis Project. Bull. Am. Met. Soc., 77, 437–471.

Kaplan, M.L., C.S. Adaniya, P.J. Marzette, K.C. King, S.J. Underwood, and J.M. Lewis (2009): The role of upstream midtropospheric circulations in the Sierra Nevada enabling leeside (spillover) precipitation, Part II: A secondary atmospheric river accompanying a midlevel jet. J. Hydromet, 10, 1327-1354.

Kienast, M., S.S. Kienast, S.E. Calvert, T.I. Eglinton, G. Mollenhauer, R. François, and A.C. Mix (2006): Eastern Pacific cooling and Atlantic overturning circulation during the last deglaciation. Nature, 443, 846-849.

Klinger, R.E. and T.R. Bauer (2004): Paleoflood study of Los Banos Creek, central California: U.S. Bureau of Reclamation, Technical Services Center, Denver, CO.

Klinger, R.E. and J.F. England, Jr. (2002): Flood Hazard Analysis, Folsom Dam, Central Valley Project, California. Bureau of Reclamation, Flood Hydrology Group, Denver, CO, 128.

Klinger, R.E., R. Hilldale, and T. Harden (in press): Paleoflood study of the Kern and Tule Rivers, California. Bureau of Reclamation, Technical Services Center, Denver, CO.

Kochel, R.C., and V.R. Baker (1988): Paleoflood analysis using slackwater deposits, *in* Baker, V.R., Kochel, R.C., and Patton, P.C., eds. Flood Geomorphology. New York, John Wiley and Sons, 357-376.

Lai, Y.G. (2009): Two-Dimensional Depth-Averaged Flow Modeling with an Unstructured Hybrid Mesh. Journal of Hydraulic Engineering, ASCE, 136 (1), 12-23.

LaMarche, V.C., Jr. (1973): Holocene climatic variations inferred from treeline fluctuations in the White Mountains, California. Quaternary Research, 3 (4), 632-660.

LaMarche, V.C., Jr. (1974): Paleoclimatic inferences from long tree-ring records. Science, 183, 1043-1048.

Leduc, G., L. Vidal, K. Tachikawa, F. Rostek, C. Sonzogni, L. Beaufort, and E. Bard (2007): Moisture transport across Central America as a positive feedback on abrupt climatic changes. Nature, 445, 908-911.

Leverson, V. (2001): Final Report – Los Banos Extreme Rainfall Study: California Coast Ranges. U.S. Bureau of Reclamation, Technical Service Center, Denver, CO, 41.

Levish, D.R. (2002): Paleohydrologic Bounds--Non-Exceedance Information for Flood Hazard Assessment, *in* House, P.K., Webb, R.H., Baker, V.R., and Levish, D.R., eds., Ancient Floods, Modern Hazards, Principles and Applications of Paleoflood Hydrology. Washington, D.C., American Geophysical Union, Water and Science Application 5, 175-190.

Li., J., S.-P. Xie, E.R. Cook, G. Huang, R. D'Arrigo, F. Liu, J. Ma, and X.T. Zheng (2011): Interdecadal modulation of El Niño amplitude during the past millennium. Nature Climate Change, 1, 114-118.

Liu, Z., and T.D. Herbert (2004): High-latitude influence on the eastern equatorial Pacific climate in the early Pleistocene epoch. Nature, 427, 720-723.

MacDonald, G.M., and R.A. Case (2005): Variations in the Pacific Decadal Oscillation over the past millennium. Geophys. Res. Letters, 32, L08703.

Malamud-Roam, F. (2002): A late Holocene history of vegetation change in San Francisco estuary marshes using stable carbon isotopes and pollen analysis. Ph.D. Dissertation, U.C. Berkeley, California.

Malamud-Roam, F. and L. Ingram (2004): Late Holocene δ13C and pollen records of paleosalinity from tidal marshes in the San Francisco estuary. Quaternary Research, 62, 134-145.

Malamud-Roam, F., Dettinger, M., Ingram, B.L., Hughes, M.K., and J.L. Florsheim (2007): Holocene climates and connections between the San Francisco Bay Estuary and its watershed: A Review. San Francisco Estuary and Watershed Science, 5 (1).

Malamud-Roam, F.P., Ingram, B.L., Hughes, M. and J.L. Florsheim (2006): Holocene paleoclimate records from a large California estuarine system and its watershed region: linking watershed climate and bay conditions. Quaternary Science Reviews, 25, 1570-1598.

Mann, M.E., E.P. Gille, R.S. Bradley, M.K. Hughes, J.T. Overpeck, F.T. Keimig, and W.S. Gross (2000): Global temperature patterns in past centuries: an interactive presentation. Earth Interactions, 4, Paper 4.

Mantua, N.J. (2000): PDO Index. http://jisao.washington.edu/pdo/. Accessed May 2012.

Mantua, N.J. (1999): The Pacific Decadal Oscillation - a brief overview for non-specialists. http://jisao.washington.edu/pdo. Accessed May 2012.

Marchitto, T.M., R. Muscheler, J.D. Ortiz, J.D. Carriquiry, and A. van Geen (2010): Dynamical Response of the Tropical Pacific Ocean to Solar Forcing During the Early Holocene. Science, 330, 1378-1381.

McGregor, S., A. Timmermann, and O. Timm (2010): A unified proxy for ENSO and PDO variability since 1650. Climate of the Past, 6, 1-17.

McGlashan, H.D. and R.C. Briggs (1939): Floods of December 1937 in Northern California. U.S. Geological Survey Water-Supply Paper 843, 497.

Meko, D.M., Therrell, M.D., Baisan, C.H., and M.K. Hughes (2001): Sacramento River flow reconstructed to A.D. 869 from tree rings. JAWRA, 37, 1029-1038.

Meko, D.M., Touchan, R., Hughes, M.K., and A.C. Caprio (2002): San Joaquin River flow reconstructed from tree rings [abstract], *in* West, G.J., and N.L. Blomquist, eds., Proceedings of the Nineteenth Annual Pacific Climate Workshop, Sacramento, CA, Interagency Ecological Program for San Francisco Estuary Technical Report 71, 186.

Meyer, R.W. (1993): Potential hazards from flood flows within the John Muir National Historic Site, Franklin Creek drainage basin, California. U.S. Geological Survey WRI 93-4009, 9.

Mo, K.C., and R.W. Higgins (1997): Tropical influences on California precipitation. Journal of Climate, 11, 412-430.

Negrini, R.M., Wigand, P.E., Draucker, S., Gobalet, K., Gardner, J.K., Sutton, M.Q. and R.M. Yohe, II (2006): The Rambla highstand shoreline and the Holocene lake-level history of Tulare Lake, California, USA. Quaternary Science Reviews, 25, 1599-1618.

Oppo, D.W., Y. Rosenthal, and B.K. Linsley (2009): 2,000-year-long temperature and hydrology reconstructions from the Indo-Pacific warm pool. Nature, 460 (7259), 1113-1116, 27 August 2009.

O'Connell, D.R.H. (1999): FLDFRQ3 Three Parameter Maximum Likelihood Flood Frequency Estimation With Optional Probability Regions Using Parameter Grid Integration. Bureau of Reclamation, Technical Service Center, Denver, Colorado.

Parker, G. (1978): Self-formed straight rivers with equilibrium banks and mobile bed. Part 2. The gravel river. Journal of Fluid Mechanics, 89, part 1, 127-146.

Patton, P.C., V.R. Baker, and R.C. Kochel (1979): Slack water deposits-- A geomorphic technique for the interpretation of fluvial paleohydrology, *in* Rhodes, D.D., and Williams, G.P., eds., Adjustments of the fluvial system. Dubuque, Iowa, Kendall/Hunt Publishing Company, 225-253.

Quinn, W.H., and V.T. Neal (1992): The historical record of El Niño events. Published in Climate since AD 1500. Editors R.S. Bradley and P.D. Jones, Routledge, London, 623-648.

Ralph, F.M., P.J. Neiman, G.A. Wick, S.I. Gutmas, M.D. Dettinger, D.R. Cayan, and A.B. White (2006): Flooding on California's Russian River: Role of atmospheric rivers. Geophys. Res. Letters, 33, L13801.

Ralph, F.M., P.J. Neiman, and G.A. Wick (2004): Satellite and CALJET aircraft observations of atmospheric rivers over the eastern North-Pacific Ocean during the winter of 1997/98. Mon. Wea. Rev., 132, 1721-1745.

Ralph, F.M., P.J. Neiman, and R. Rotunno (2005): Dropsonde observations in low-level jets over the northeastern Pacific Ocean from CALJET-1998 and PACJET-2001: Mean vertical-profile and atmospheric-river characteristics. Mon. Wea. Rev., 133, 889-910.

Reclamation (2011): SECURE Water Act Section 9503(c)-Reclamation Climate Change and Water 2011 Section 7 - Basin Report: Sacramento and San Joaquin Rivers.

Schimmelmann, A., Lange, C.B., and B.J. Meggers (2003): Paleoclimatic and archaeological evidence for a ~200-yr recurrence of floods and droughts linking California, Mesoamerica and South America over the past 2000 years. The Holocene, 13, 763-778.

Seaber, P.R., Kapinos, F.P., and G.L. Knapp. (1994): Hydrologic Unit Maps. U.S. Geological Survey Water-Supply Paper 2294.

Shen, C., W.-C. Wang, W. Gong, and Z. Hao (2006): A Pacific Decadal Oscillation record since 1470 AD reconstructed from proxy data of summer rainfall over eastern China. Geophys. Res. Letters, 33, L03702.

Slack, J. R., and J.M. Landwehr. (1992): HCDN: A U.S. Geological Survey streamflow data set for the United States for the study of climate variations, 1874 – 1988. U.S. Geological Survey Open-File Report 92-129.

Soil Survey Division Staff (1993): Soil Survey Manual. U.S. Department of Agriculture Handbook No. 18, 437.

Stahle, D.W., R.D. D'Arrigo, P.J. Krusic, M.K. Cleaveland, E.R. Cook, R.J. Allan, J.E. Cole, R.B. Dunbar, M.D. Therrell, D.A. Gay, M.D. Moore, M.A. Stokes, B.T. Burns, J. Villanueva-Diaz and L.G. Thompson (1998): Experimental dendroclimatic reconstruction of the Southern Oscillation. Bull. American Meteorological Society, 79, 2137-2152.

Stine, S. (1990): Late Holocene fluctuations of Mono Lake, eastern California. Paleogeography, Paleoclimatology, and Paleoecology, 78, 333-381.

Stine, S. (1994): Extreme and persistent drought in California and Patagonia during mediaeval time. Nature, 369, 546-549.

Subhrendu, G. and T. Pruitt (2011): West-wide climate risk assessments: Bias-corrected and spatially downscaled surface water projections. Technical Memorandum No. 86-68210-2011-01. Bureau of Reclamation, Denver, CO, 122.

Sullivan, D.G. (1982): Prehistoric flooding in the Sacramento Valley: stratigraphic evidence from Little Packer Lake, Glenn County, California. M.S. Thesis, University of California, Berkeley.

Swetnam, T.W., C.H. Baisan, A.C. Caprio, P.M. Brown, R. Touchan, R.S. Anderson and D.J. Hallett (2009): Multi-millennial fire history from the Giant Forest, Sequoia National Park. California Fire Ecology, 5, 120-150.

Underwood, S.J., M.L. Kaplan, and K.C. King (2009): The role of upstream midtropospheric circulations in the Sierra Nevada enabling leeside (spillover) precipitation, Part I: A synoptic-scale analysis of spillover precipitation and flooding in a leeside basin. J. Hydromet., 10, 1309-1326.

Webb, R.H., and R.D. Jarrett (2002): One-dimensional estimation techniques for discharges of paleofloods and historical floods, *in* House, P.K., Webb, R.H., Baker, V.R., and Levish, D.R., eds., Ancient Floods, Modern Hazards, Principles and Applications of Paleoflood Hydrology. American Geophysical Union, Water and Science Application 5, Washington, D.C., 111-125.

Yan, H., L. Sun, Y. Wang, W. Huang, S. Qiu, and C. Yang. (2011): A record of the Southern Oscillation Index for the past 2,000 years from precipitation proxies. Nature Geoscience, DOI: 10.1038/NGEO1231.

Zhang, Y., J.M. Wallace, and D.S. Battisti (1997): ENSO-like interdecadal variability: 1900-93. Journal of Climate, 10, 1004-1020.

ATTACHMENT A: FLOOD FREQUENCY CURVES

NF Feather River at USGS gage 11404500
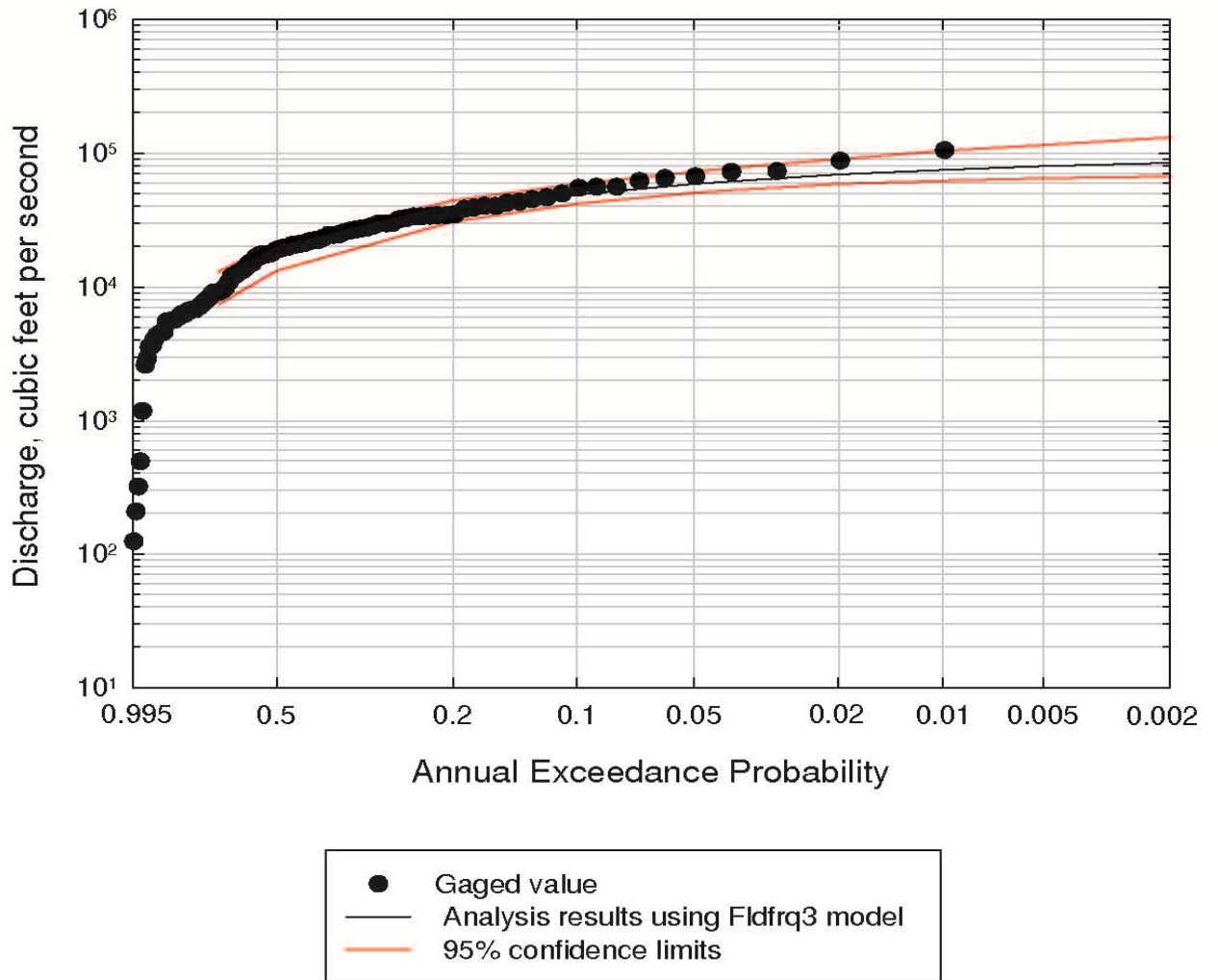
Yuba River at USGS gage no. 11418000

Legend:
- ● Gaged value
- —— Analysis results using Fldfrq3 model
- —— 95% confidence limits

NF American River at USGS gage no. 11427000

MF American River at USGS gage no. 11433500
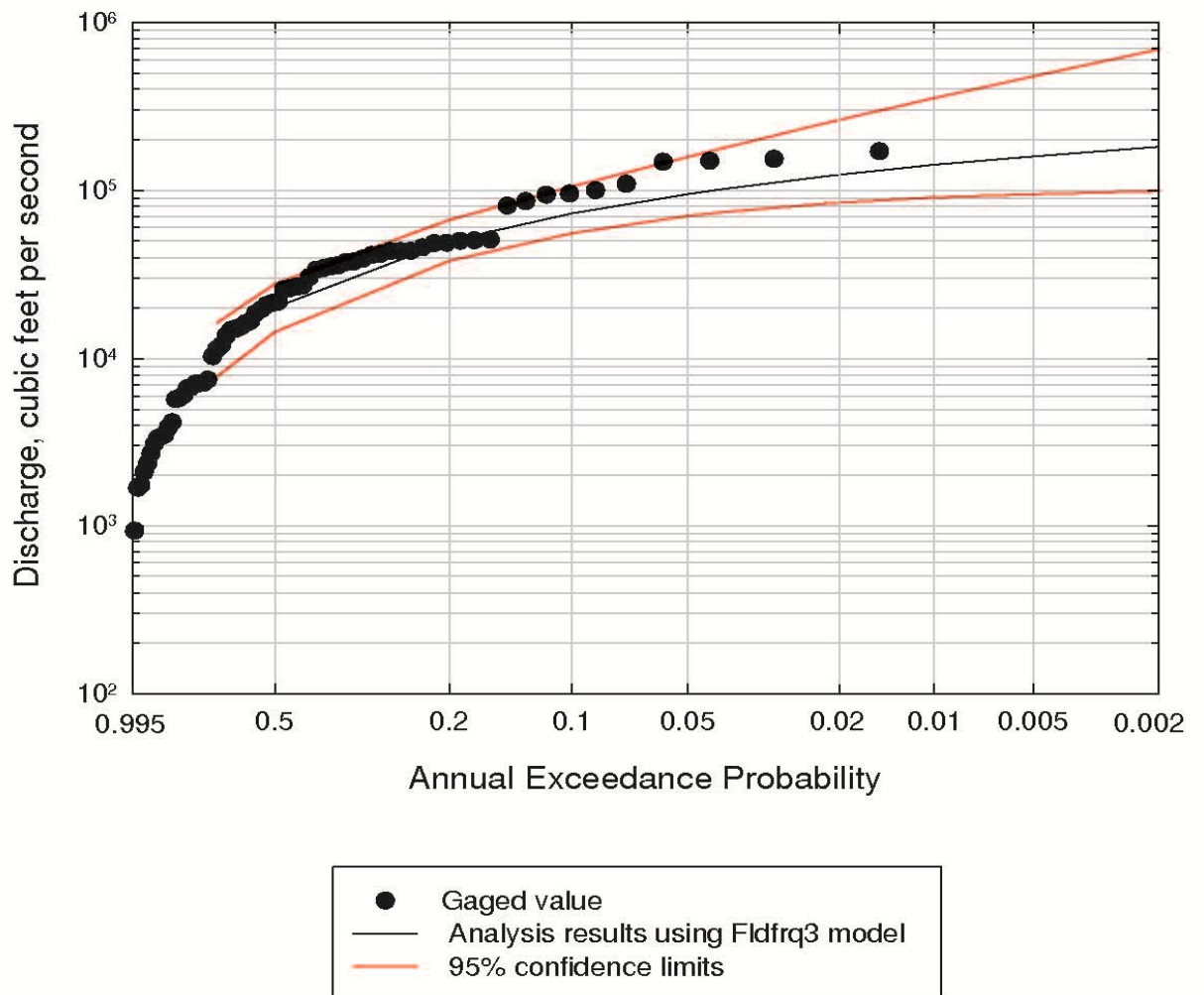
SF American River at USGS gage no. 11443500
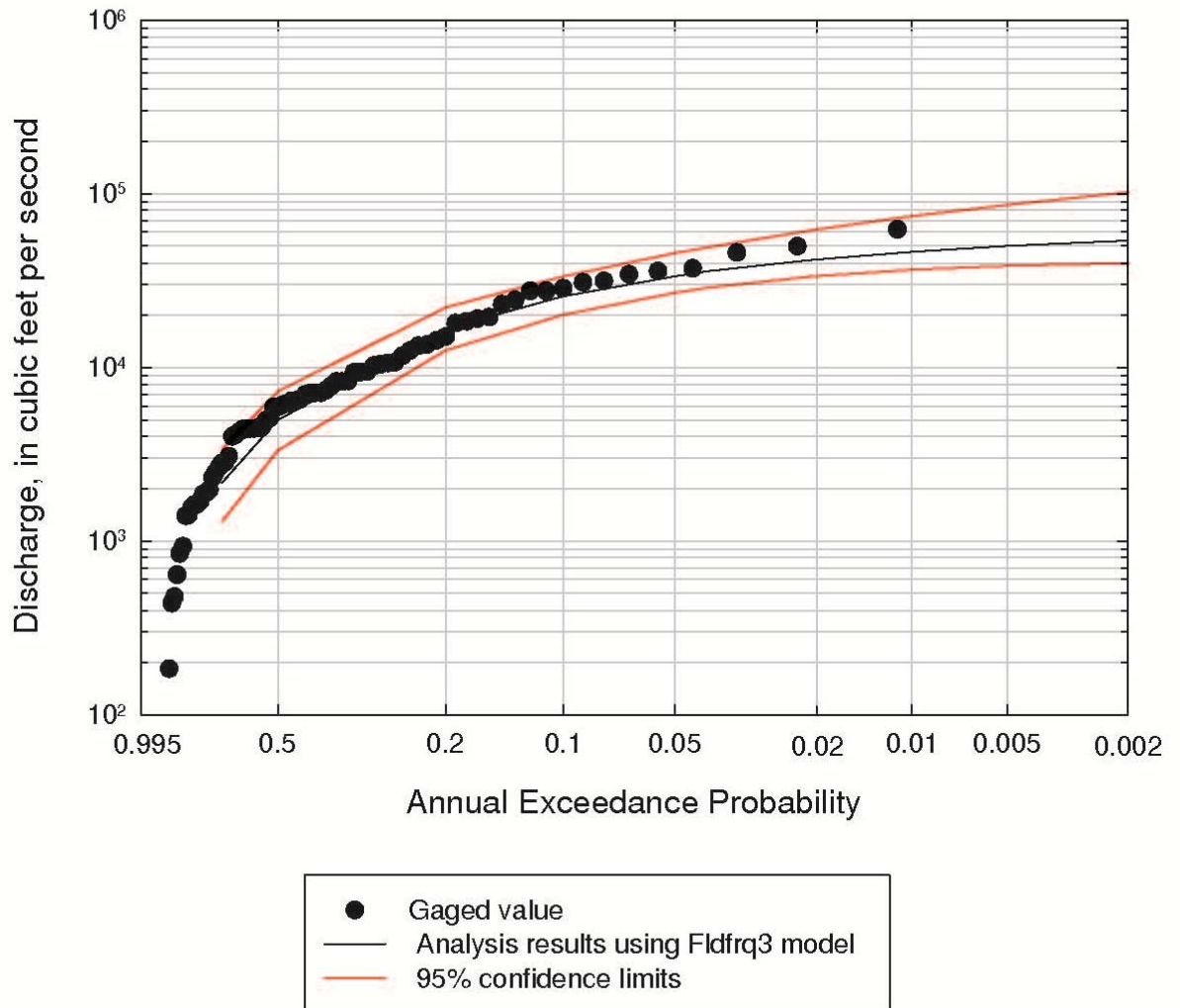
Cosumnes River at USGS gage no. 11335000
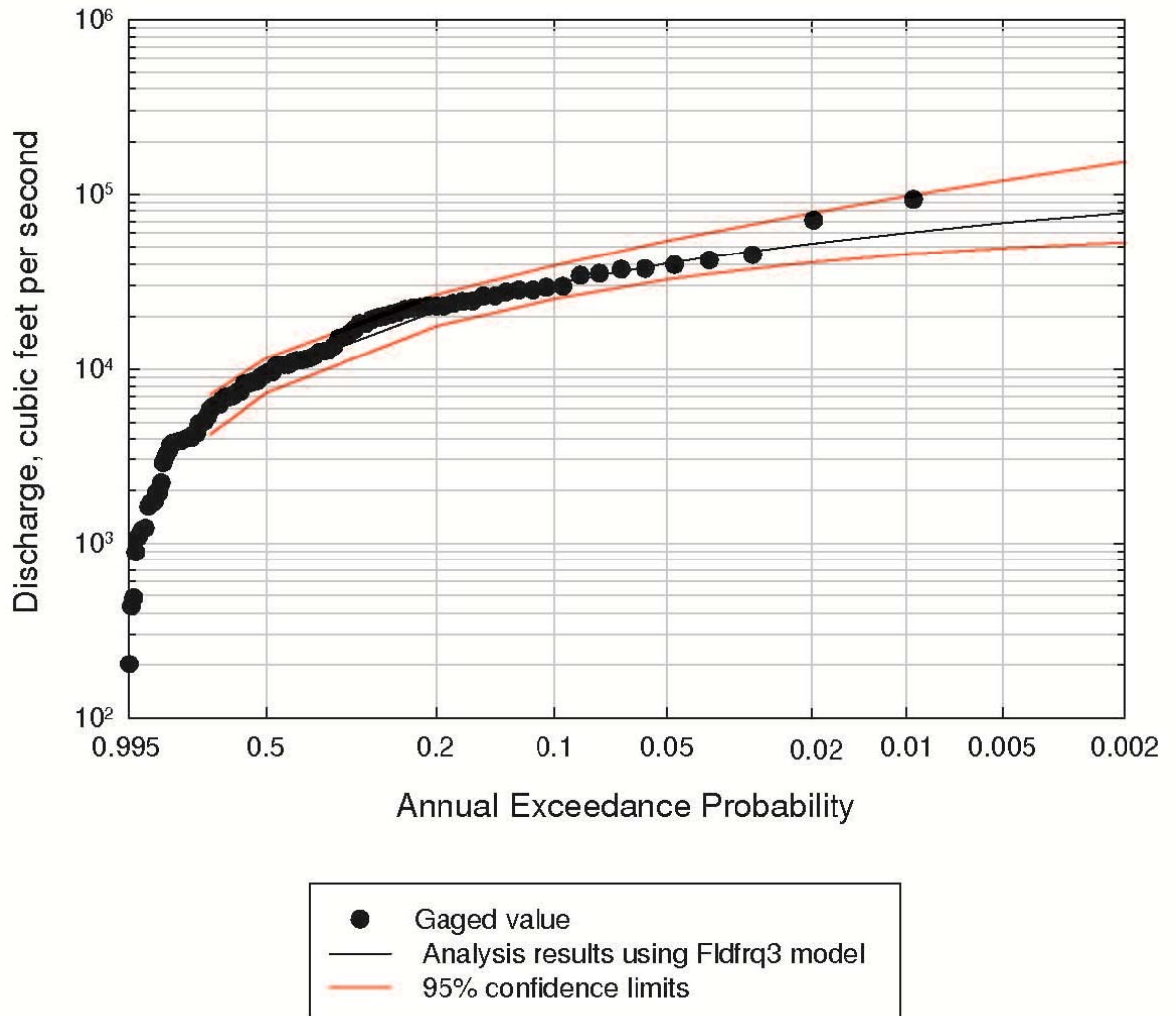
Mokelumne River at USGS gage no. 11319500
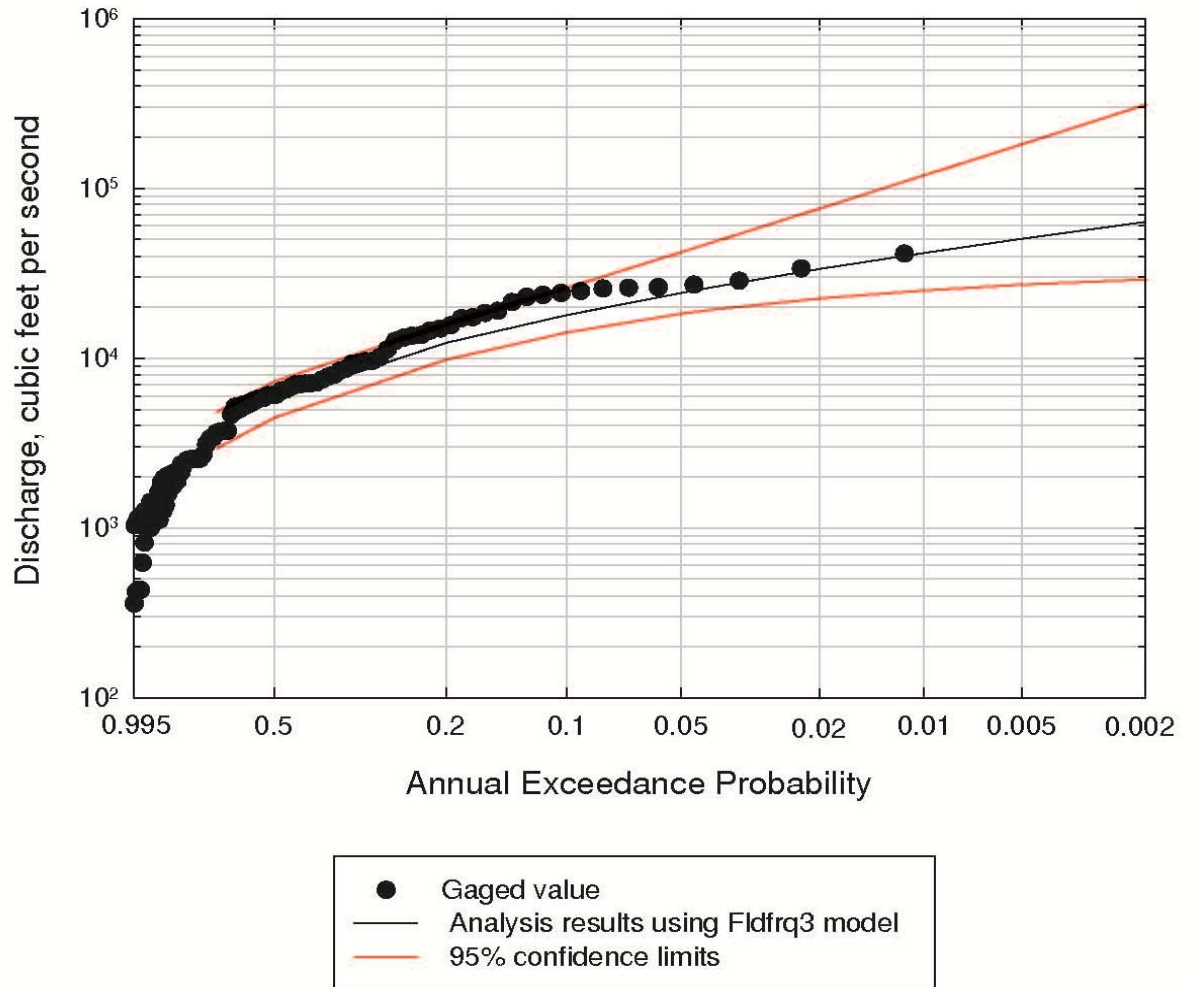
NF Stanislaus River at USGS gage no. 11294500
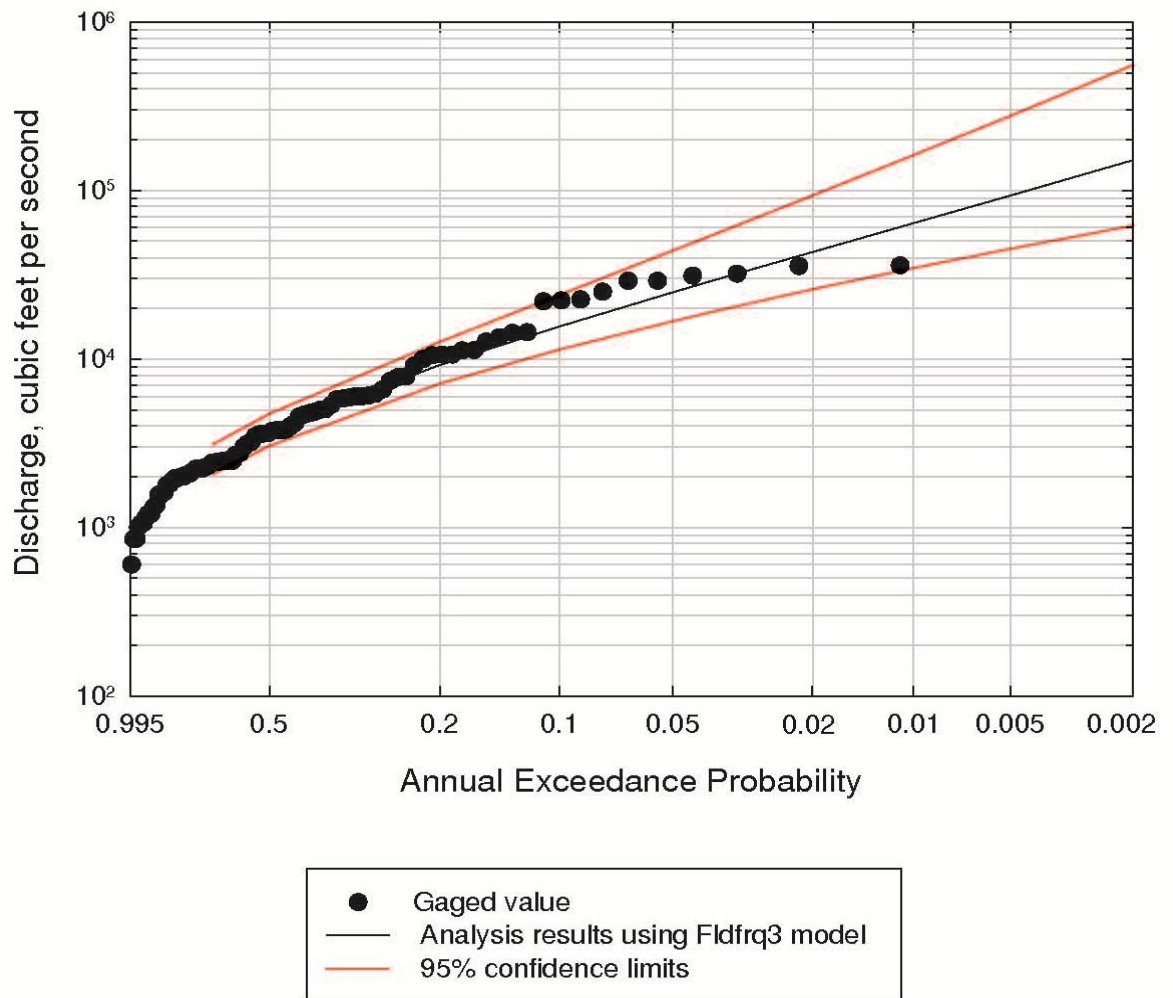
MF Stanislaus River at USGS gage no. 11292700
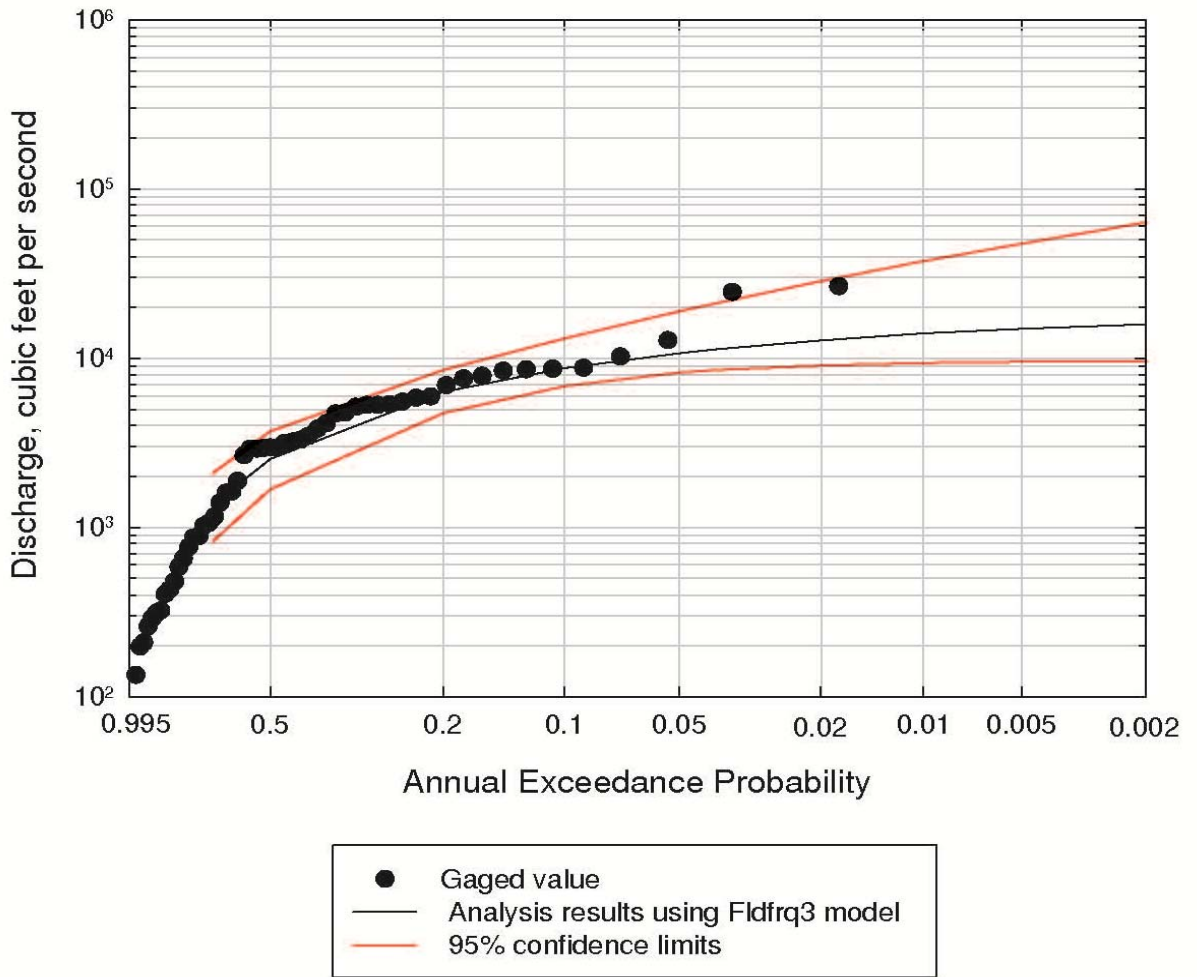
SF Tuolumne River at USGS gage no. 11281000
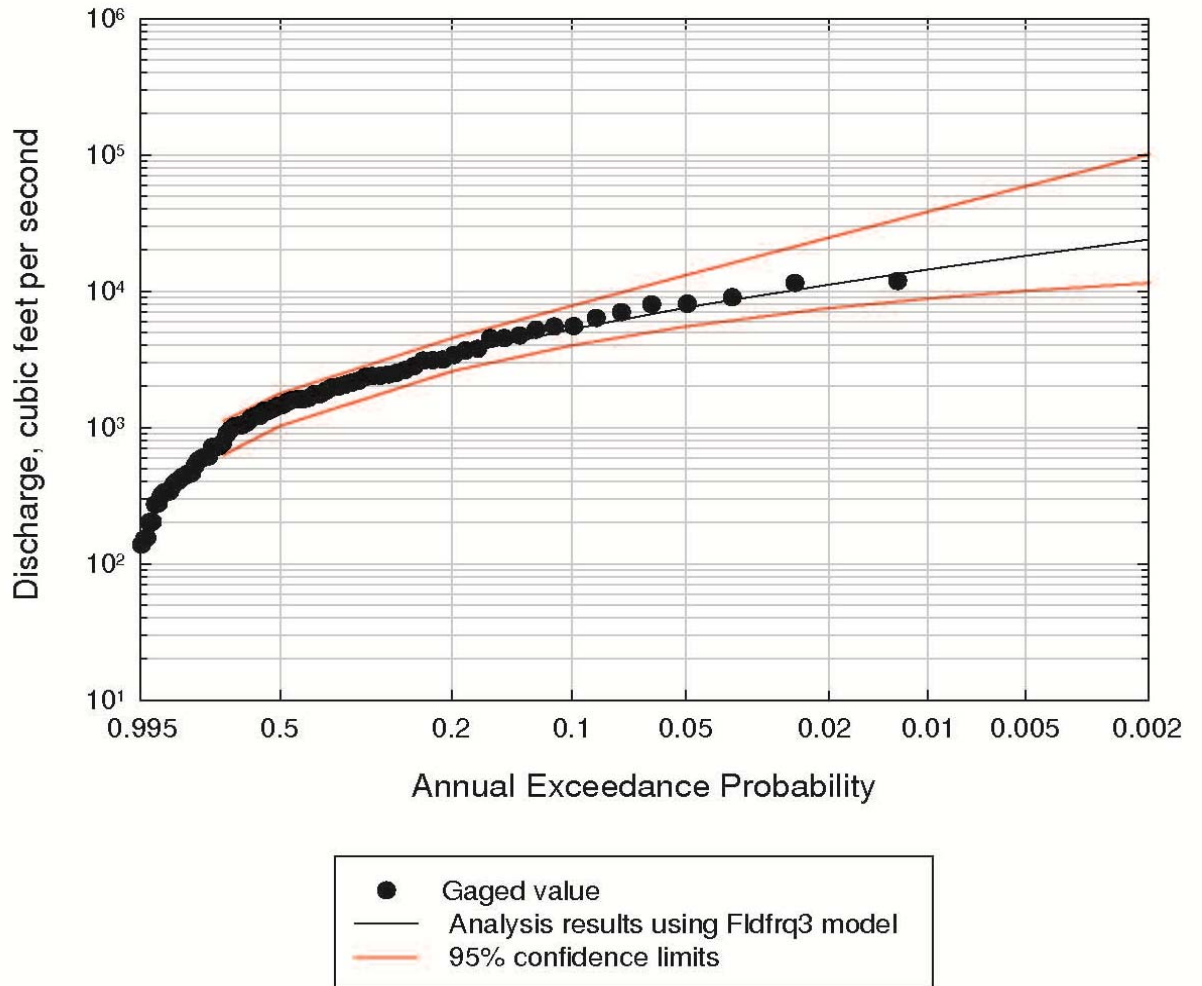
Merced River at USGS gage no. 11266500
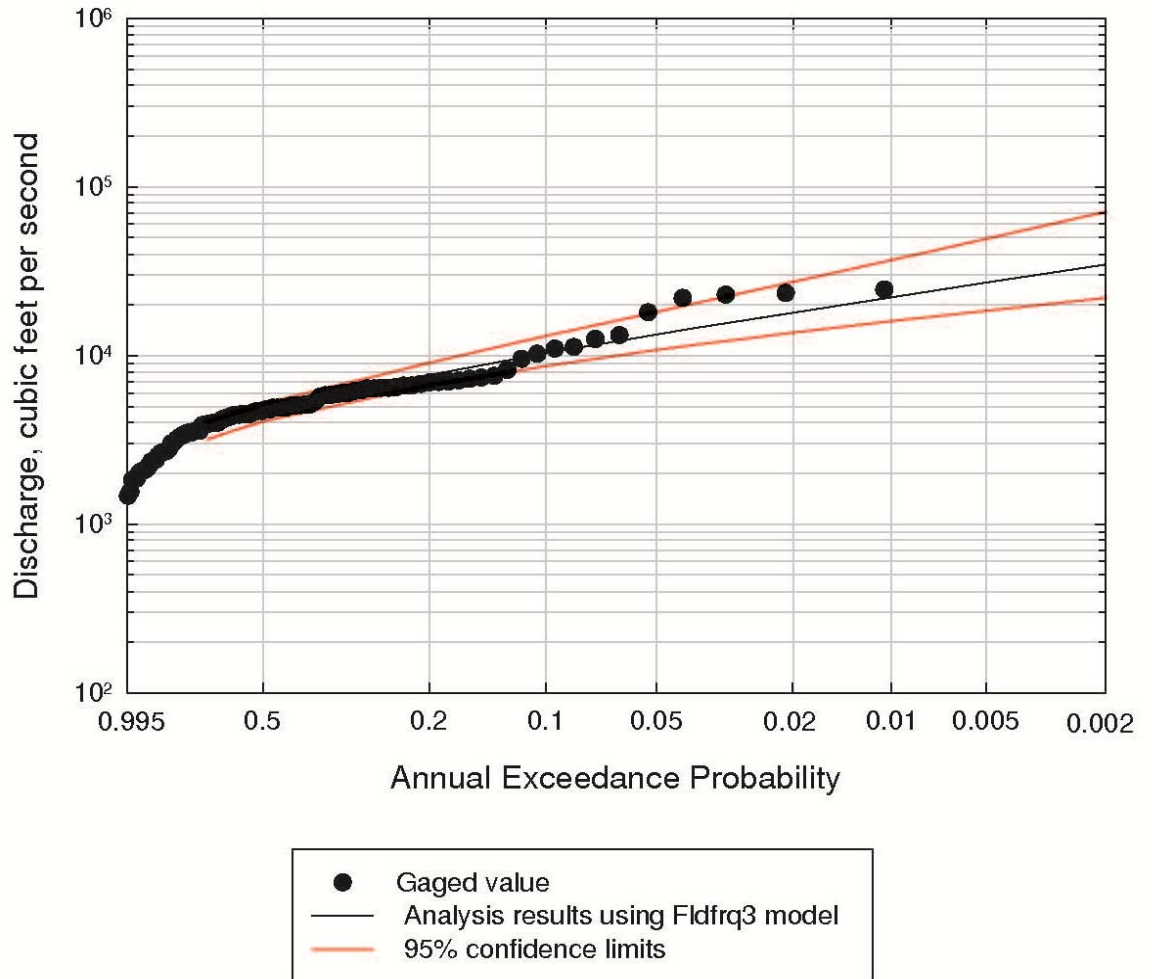
San Joaquin River at USGS gage no. 11242000

Legend:
- ● Gaged value
- —— Analysis results using Fldfrq3 model
- —— 95% confidence limits
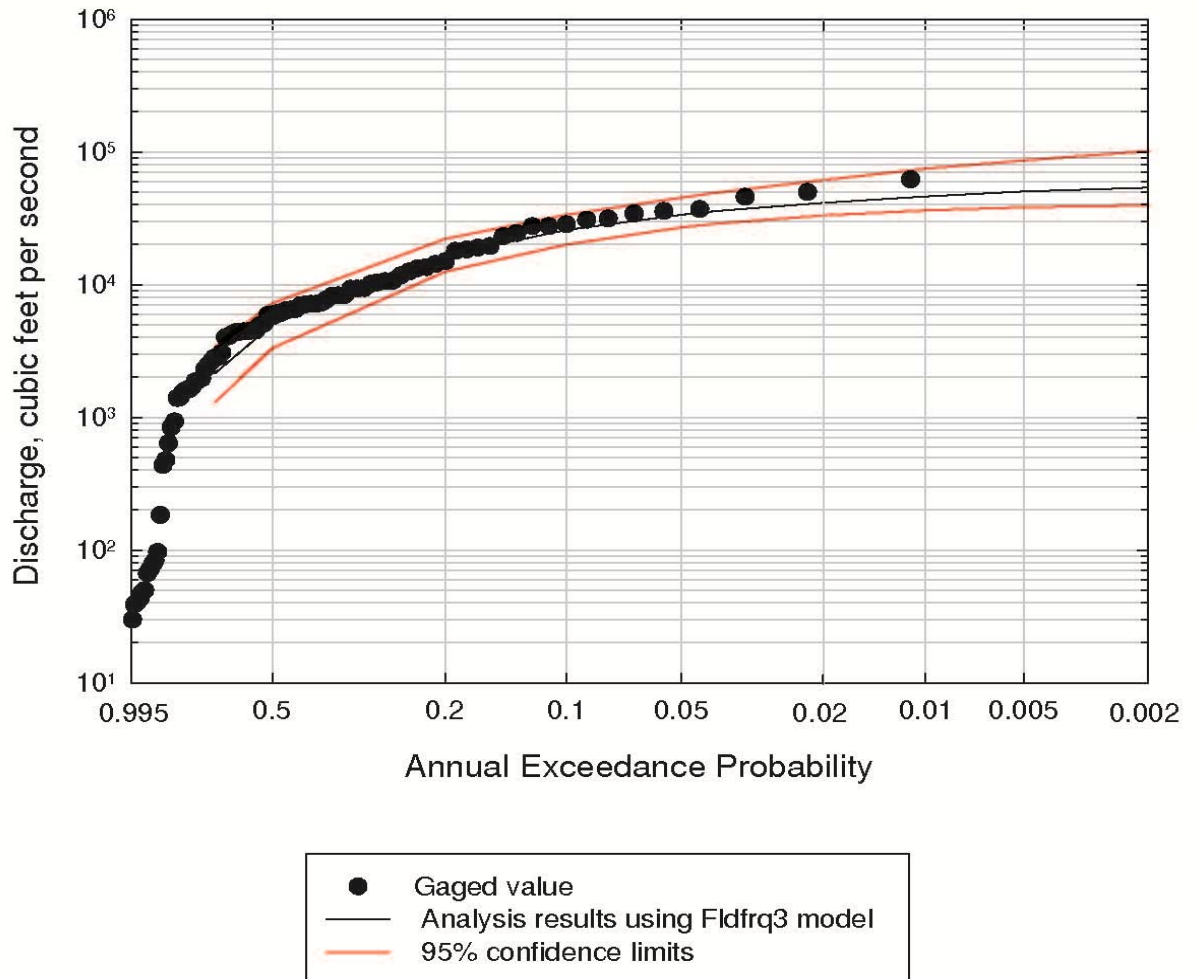
Kings River at USGS gage no. 11213500

Kaweah River at USGS gage no. 11210500
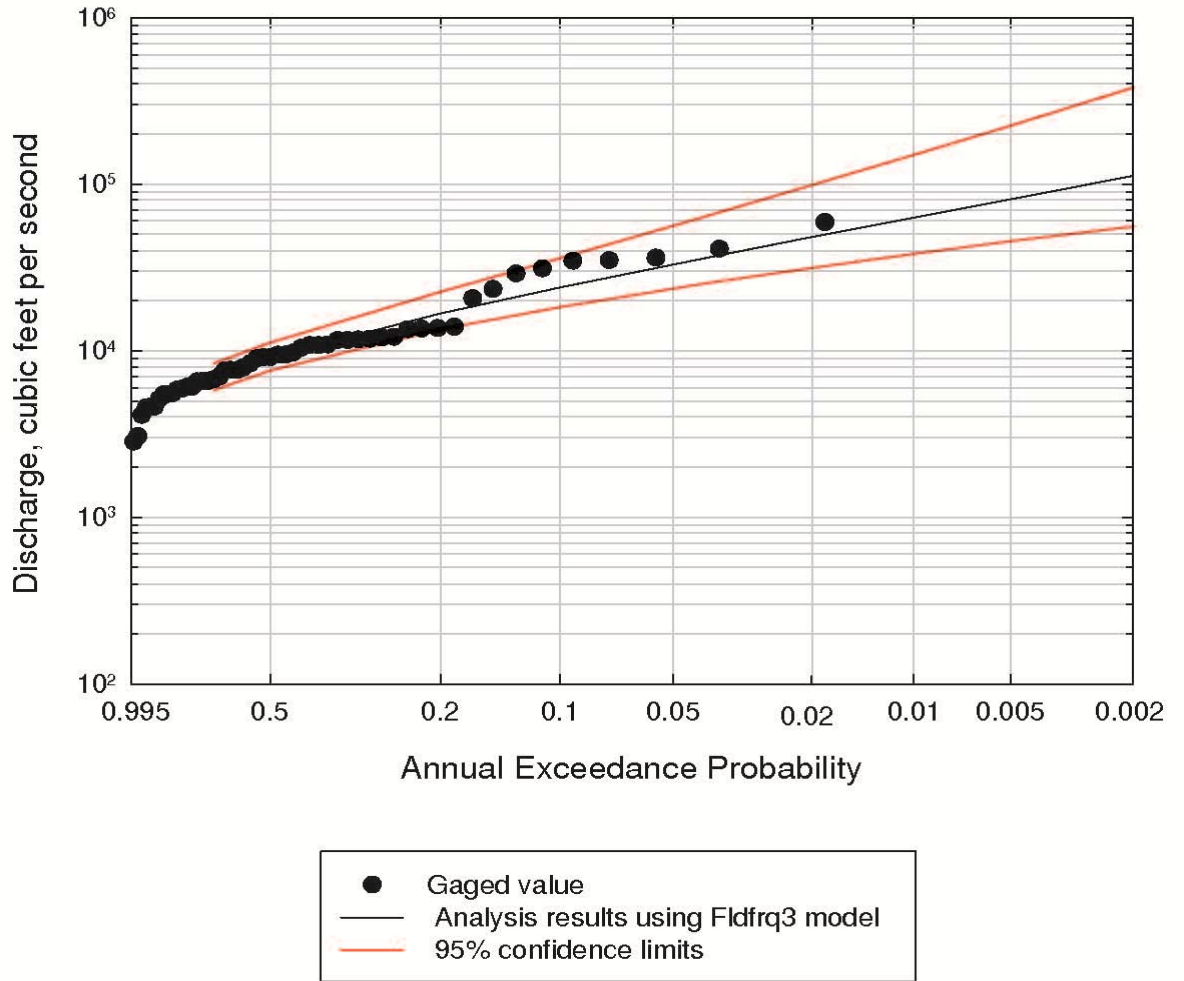
Tule River at USGS gage no. 11203500

Kern River at USGS gage no. 11186000
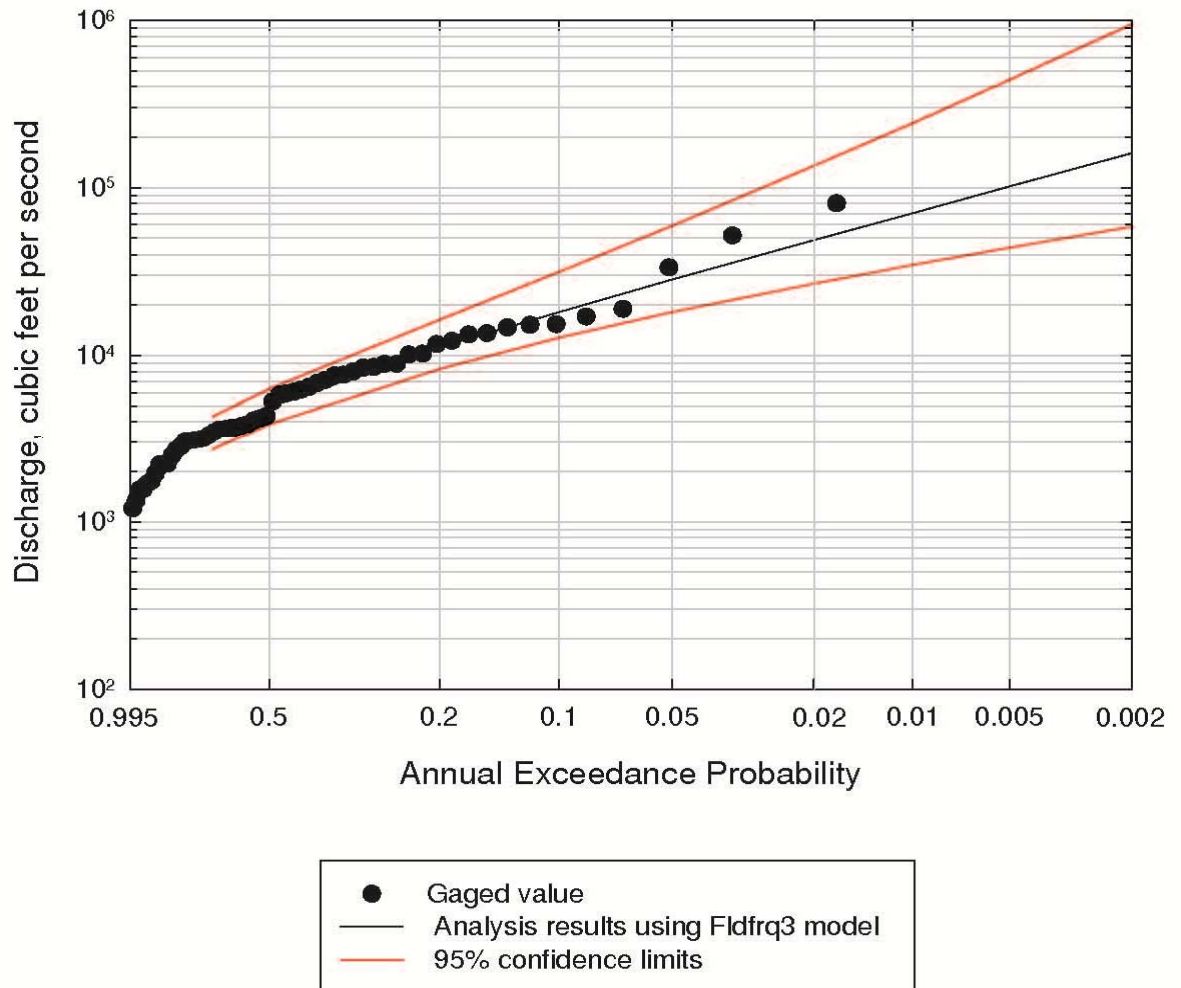
SF Kern River at USGS gage no. 11189500
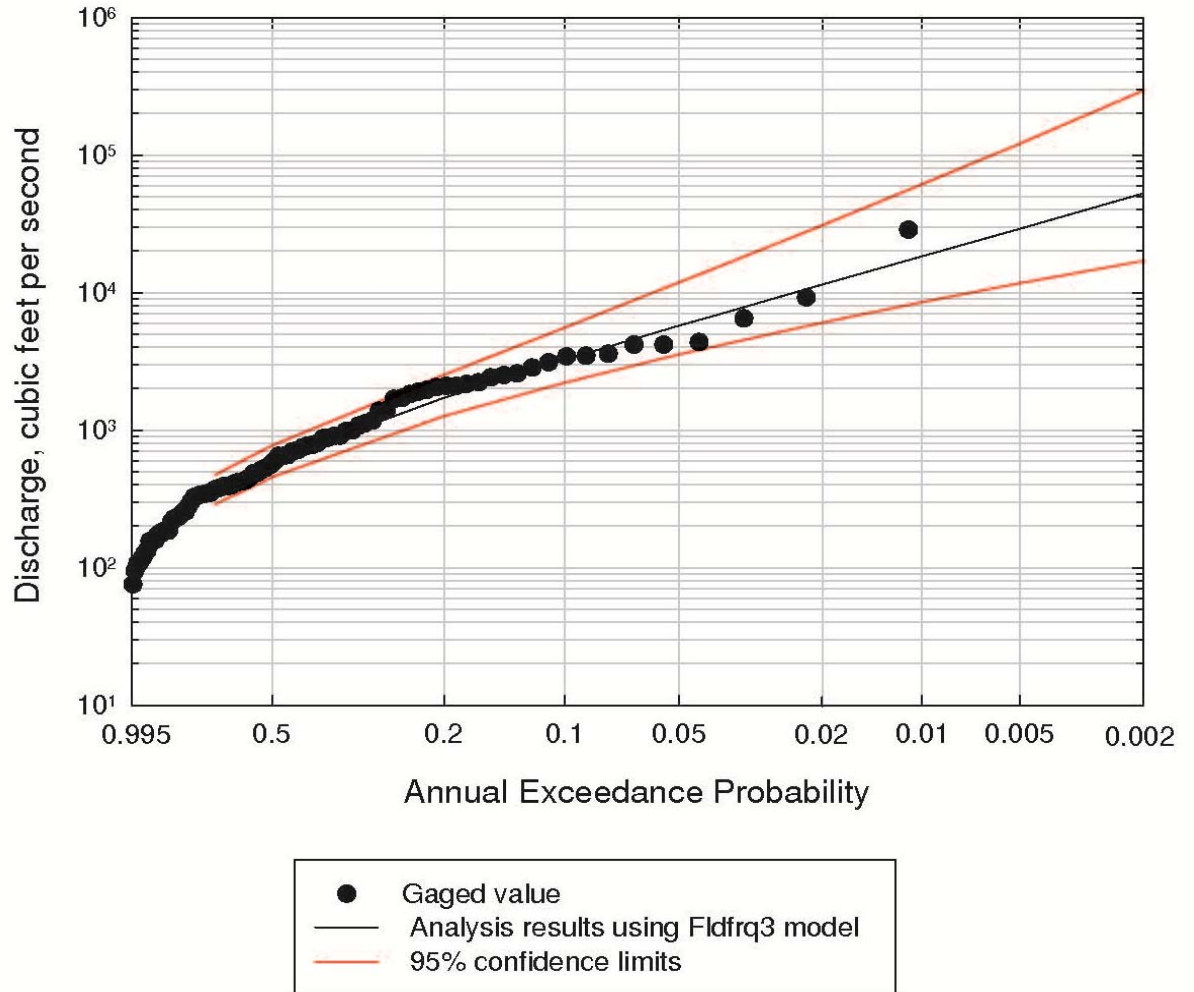
ATTACHMENT B: CALIBRATED RADIOCARBON AGES
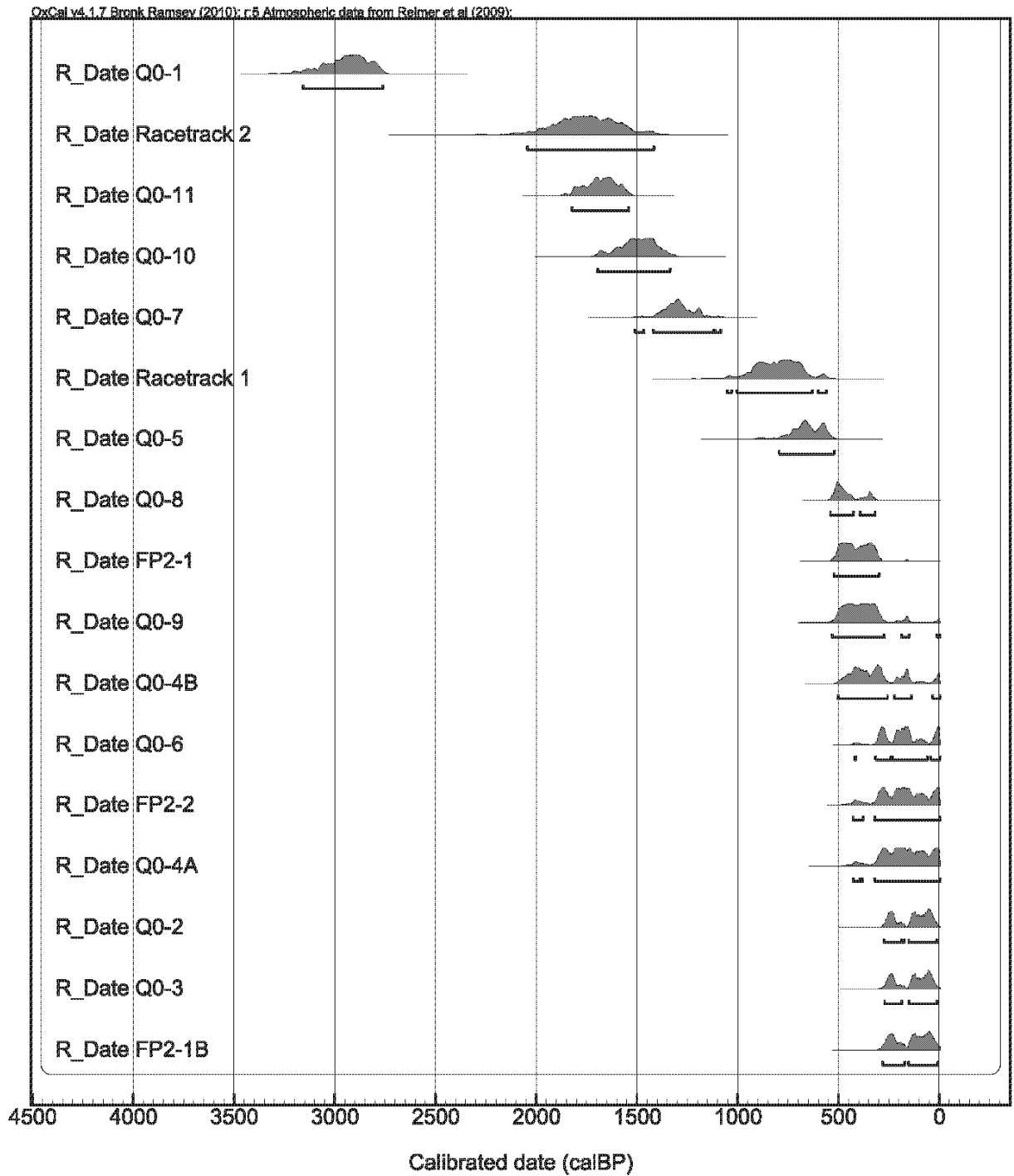
Southern California Calibrated Radiocarbon Ages

OxCal v4.1.7 Bronk Ramsey (2010); r:5 Atmospheric data from Reimer et al (2009);

R_Date Q0-1
R_Date Racetrack 2
R_Date Q0-11
R_Date Q0-10
R_Date Q0-7
R_Date Racetrack 1
R_Date Q0-5
R_Date Q0-8
R_Date FP2-1
R_Date Q0-9
R_Date Q0-4B
R_Date Q0-6
R_Date FP2-2
R_Date Q0-4A
R_Date Q0-2
R_Date Q0-3
R_Date FP2-1B

4500 4000 3500 3000 2500 2000 1500 1000 500 0

Calibrated date (calBP)

Sierra Nevada Calibrated Radiocarbon Ages

OxCal v4.1.7 Bronk Ramsey (2010); r:5 Atmospheric data from Reimer et al (2009);

R_Date SF1-1-3AC

R_Date CR1-1-1RH

R_Date SF2-1-3AL

R_Date CF1-1-4VIS

R_Date MF2-2PIN

R_Date CF1-1-1PIB

R_Date CF1-2-1PI

R_Date MF2-2RH

R_Date MF1-2-4PI

R_Date SF1-3-2ACS

R_Date CF1-1-3PIW

R_Date SF1-1-2COB

600   500   400   300   200   100   0

Calibrated date (calBP)

131
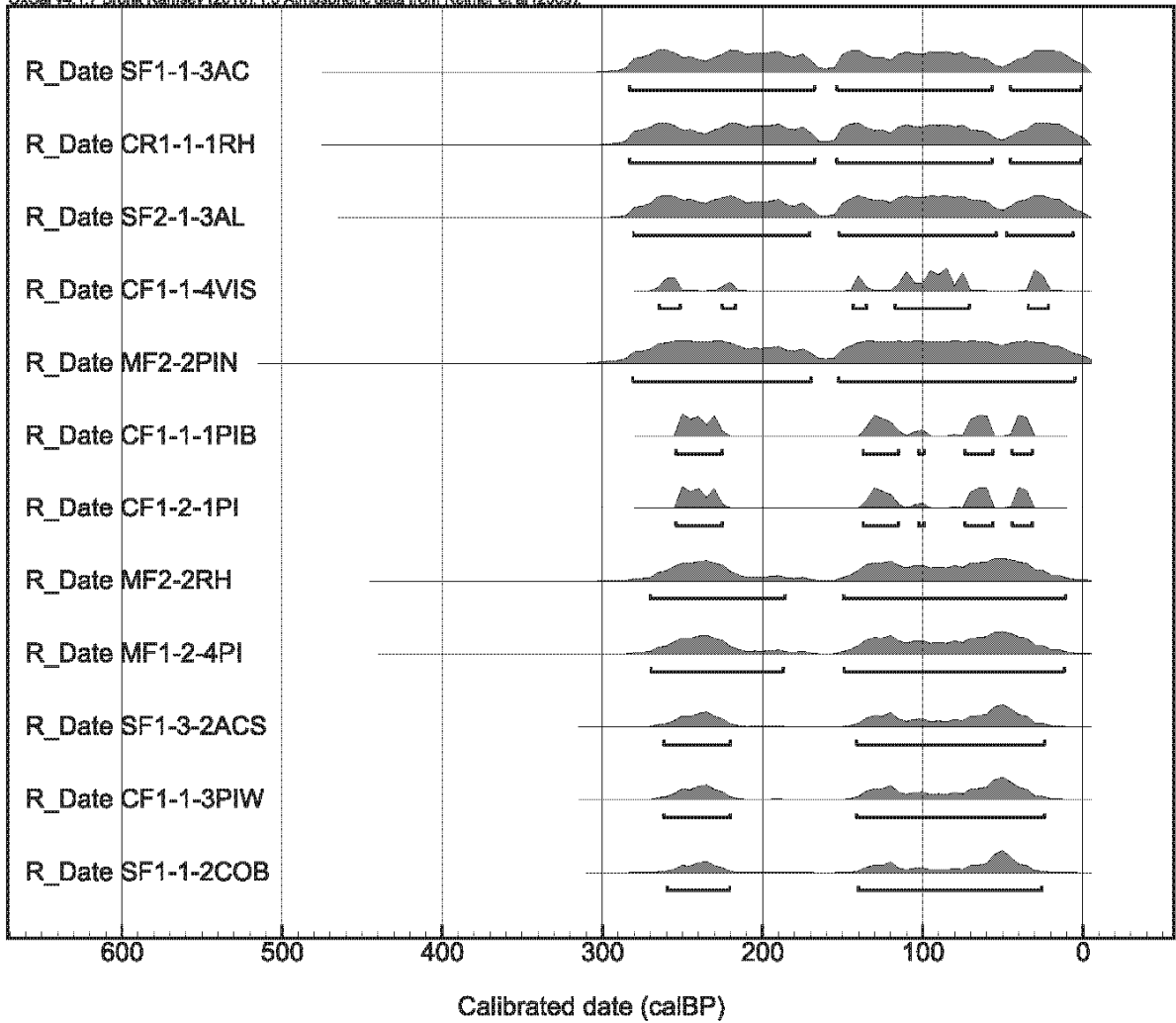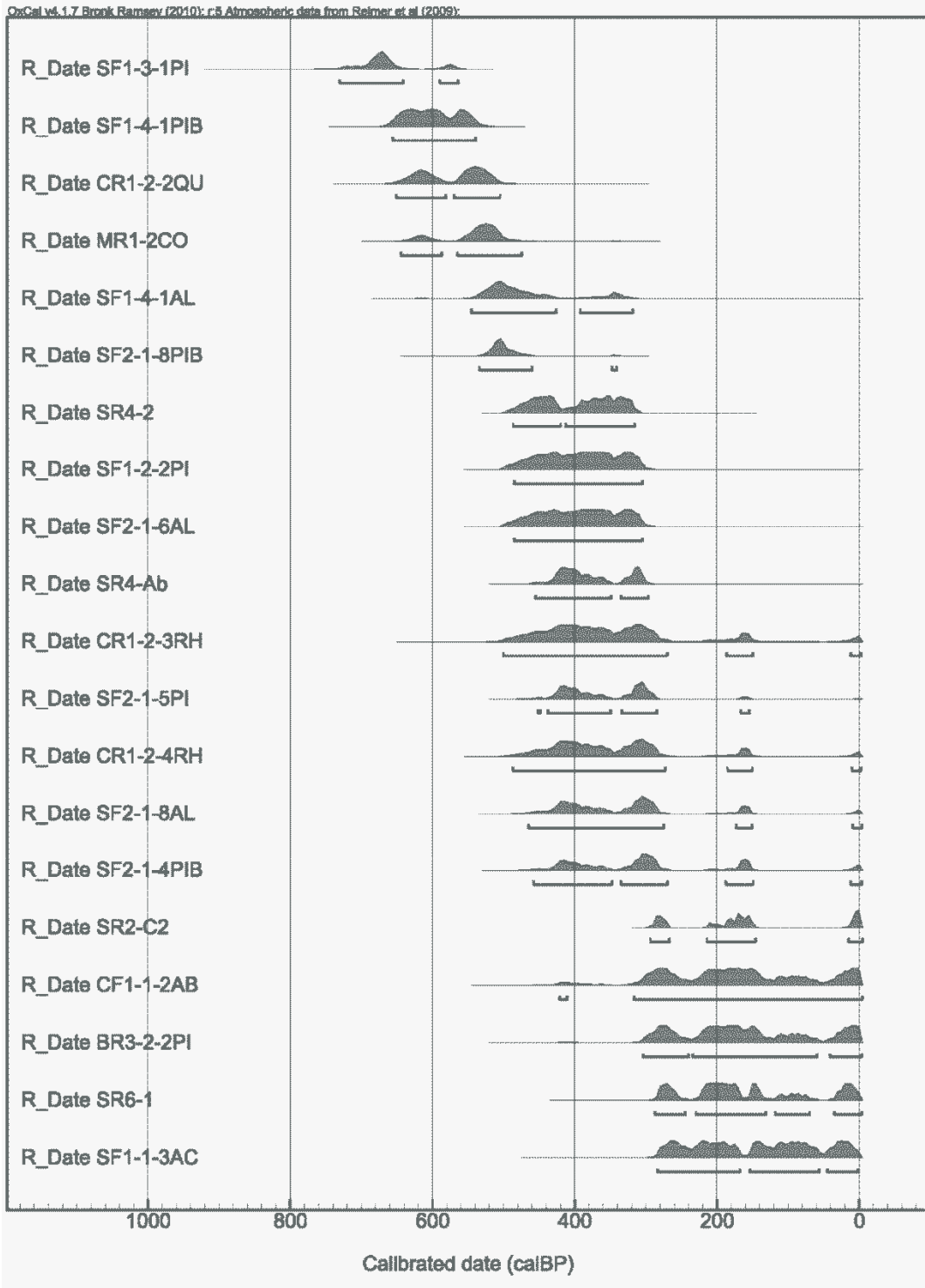
Sierra Nevada Calibrated Radiocarbon Ages (cont.)

Sierra Nevada Calibrated Radiocarbon Ages (cont.)

OxCal v4.1.7 Bronk Ramsey (2010); r:5 Atmospheric data from Reimer et al (2009);

R_Date BR3-1-1QU
R_Date CR1-2-3QU
R_Date SR1-C2
R_Date AC1-5AL
R_Date SF1-2-3PI
R_Date BR1-3-3QU
R_Date SF1-4-2PI
R_Date CR1-2-2RH
R_Date BR1-2-1QU
R_Date BR1-2-3QU
R_Date CF1-4-1CO
R_Date SR3-Bw2
R_Date BR1-3-2QU
R_Date SF1-2-3AC
R_Date BR1-2-2QU
R_Date CR1-2-1RH
R_Date AC1-6PIC
R_Date SR5-2
R_Date BR2-2-2PI
R_Date SF1-3-1PI

2500   2000   1500   1000   500

Calibrated date (calBP)

Sierra Nevada Calibrated Radiocarbon Ages (cont.)

OxCal v4.1.7 Bronk Ramsey (2010); r:5 Atmospheric data from Reimer et al (2009);

R_Date BR3-1-4QU
R_Date BR2-1-3PI
R_Date BR2-2-2QU
R_Date BR2-1-2QU
R_Date BR1-3-1QU
R_Date RR1-2SXW
R_Date RR1-2PIB
R_Date BR1-1-3QU
R_Date SR1-2-2PIB
R_Date BR2-1-1MIX
R_Date AC1-8AL
R_Date AC1-8TS
R_Date BR1-1-2QU
R_Date SR1-2-3CO
R_Date SF1-4-1PI
R_Date SR1-C3
R_Date SR3-Bw3
R_Date SF1-3-2PIB
R_Date CF1-4-2QU
R_Date BR3-1-1QU

8000   7000   6000   5000   4000   3000   2000

Calibrated date (calBP)

Westside San Joaquin Valley Calibrated Radiocarbon Ages

OxCal v4.1.7 Bronk Ramsey (2010); r:5 Atmospheric data from Reimer et al (2009);

R_Date LB3-3QU

R_Date SC3A-1AC

R_Date LG2-1-4MIX

R_Date LB1-3FR

R_Date CC4-2AC

R_Date LB1-1PL

R_Date SC3B-1AT

R_Date LB3-7AS

R_Date LG2-1-2AC

R_Date LB2-4PL

700   600   500   400   300   200   100   0

Calibrated date (calBP)

Westside San Joaquin Valley Calibrated Radiocarbon Ages (cont.)

OxCal v4.1.7 Bronk Ramsey (2010); r:5 Atmospheric data from Reimer et al (2009);

R_Date CC6-3PI
R_Date CC6-4RH
R_Date CC5-2AT
R_Date CC7-1AT
R_Date LPC1-5Y
R_Date CC5-1MIX
R_Date SC3C-2MIX
R_Date SC2-4AC
R_Date CC1-2MIX
R_Date CC2-7AC
R_Date SC2-3AC
R_Date LPC1-7Y
R_Date LPC1-1Y
R_Date CC3-2AC
R_Date SC2-2MIX
R_Date CC2-5RH
R_Date CC2-2AC
R_Date CC2-3AT
R_Date CC3-3SX
R_Date CC3-4SX

5000   4000   3000   2000   1000   0

Calibrated date (calBP)

Northern California Calibrated Radiocarbon Ages

OxCal v4.1.7 Bronk Ramsey (2010); r:5 Atmospheric data from Reimer et al (2009);

Calibrated date (calBP)

Northern California Calibrated Radiocarbon Ages (cont.)

OxCal v4.1.7 Bronk Ramsey (2010); r:5 Atmospheric data from Reimer et al (2009);

R_Date ECR4-6

R_Date ECR2-4

R_Date TP5-1RO

R_Date TP5-2RO

R_Date SBC2-2

R_Date ECR1-3

R_Date ECR1-7

R_Date ECR2-6

R_Date LS3-6

R_Date SBC1-5

R_Date SK1-5AE

R_Date ECR4-4

R_Date LS3-2

R_Date ECR1-6

R_Date LOW2-5

R_Date SK1-3AC

R_Date LOW2-3

R_Date TP2-1QU

R_Date TP2-8PS

R_Date LS4-6

6000   5000   4000   3000   2000   1000

Calibrated date (calBP)

ATTACHMENT C: RADIOCARBON DATA

Sample name	Date	Error	Cal yr B.P. (oldest age)	Cal yr B.P. (youngest age)	Sample depth (cm)	Sample weight (g)	Material	Landform	soil horizon	Date relevance	Site name	River name	No. of floods	Bound age (max)	Bound age (min)	Bound Qmax (ft³/s)	Bound Qmin (ft³/s)	Facility	Level of study
										Sierra Nevada region									
AC1-5AL	1740	50	1810	1520	8-12 (below datum)	0.06	Alnus charcoal	terrace	Cb2	flood deposit	Alder Creek	South Fork American River	1 or more	1650	1380	81000	67000	Folsom Dam	Detailed
AC1-6PIC	1020	50	1060	780	at datum	0.03	Pinus cone scale (charred)	terrace	Ab3	flood deposit	Alder Creek	South Fork American River	1 or more	1125	650	81000	67000	Folsom Dam	Detailed
AC1-8AL	2850	50	3070	2850	50-60 (below datum)	0.07	Alnus charcoal	terrace	Bw3	flood deposit	Alder Creek	South Fork American River		not used to develop bound				Folsom Dam	Detailed
BR1-1-2QU	2430	50	2725	2340	62-72	0.02	Quercus charcoal	terrace	3Bw2	flood deposit	Old Rock Bridge	American River	1 or more	1600	1000	254000	170000	Folsom Dam	Detailed
BR1-1-3QU	3120	50	3440	3215	80-95	0.01	Quercus charcoal	terrace	3Cox	flood deposit	Old Rock Bridge	American River	1 or more	1600	1000	254000	170000	Folsom Dam	Detailed
BR1-2-1QU	1310	50	1300	1095	35-45	0.02	Quercus charcoal	terrace	Btj	flood deposit	Old Rock Bridge	American River	1 or more	1600	1000	254000	170000	Folsom Dam	Detailed
BR1-2-2QU	1100	40	1070	935	65-85	0.05	Quercus charcoal	terrace	BC	flood deposit	Old Rock Bridge	American River	1 or more	1600	1000	254000	170000	Folsom Dam	Detailed
BR1-2-3QU	1280	70	1305	1055	94-105	0.07	Quercus charcoal	terrace	BC2	flood deposit	Old Rock Bridge	American River	1 or more	1600	1000	254000	170000	Folsom Dam	Detailed
BR1-3-1QU	3440	70	3860	3485	25-45	0.01	Quercus charcoal	terrace	2Bt	flood deposit	Old Rock Bridge	American River	1 or more	1600	1000	254000	170000	Folsom Dam	Detailed
BR1-3-2QU	1120	60	1165	930	55-70	<0.01	Quercus charcoal	terrace	2Bt2	flood deposit	Old Rock Bridge	American River	1 or more	1600	1000	254000	170000	Folsom Dam	Detailed
BR1-3-3QU	1580	60	1570	1330	80-94	<0.01	Quercus charcoal	terrace	3Cox	flood deposit	Old Rock Bridge	American River	1 or more	1600	1000	254000	170000	Folsom Dam	Detailed
BR2-1-1MIX	2860	50	3170	2840	28-62	0.012	mixed pinus bark (charred) and conifer charcoal	terrace	Bw	flood deposit	Old Rock Bridge	American River	3 or less	1105	152	254000	170000	Folsom Dam	Detailed
BR2-1-2QU	3510	70	3980	3630	62-95	0.01	Quercus charcoal	terrace	Cox	flood deposit	Old Rock Bridge	American River	3 or less	1105	152	254000	170000	Folsom Dam	Detailed
BR2-1-3PI	4620	90	5600	5000	100	0.01	Pinus charcoal	terrace	2Cox	flood deposit	Old Rock Bridge	American River	3 or less	1105	152	254000	170000	Folsom Dam	Detailed
BR2-2-2QU	3750	60	4350 / 4300	4330 / 3910	28	0.03	Quercus charcoal	terrace	Bw	flood deposit	Old Rock Bridge	American River	3 or less	1105	152	254000	170000	Folsom Dam	Detailed
BR2-2-2PI	910	50	930	720	24-44	0.01	Pinus charcoal	terrace	Bw	flood deposit	Old Rock Bridge	American River	3 or less	1105	152	254000	170000	Folsom Dam	Detailed
BR3-1-1QU	1970	50	2060	1810	35-60	0.03	Quercus charcoal	terrace	Bw	flood deposit	Old Rock Bridge	American River		not used to develop bound				Folsom Dam	Detailed
BR3-1-4QU	6030	60	7150 / 7020 / 6700	7130 / 6720 / 6680	155-180	0.013	Quercus charcoal	terrace	2Coxb2	Flood deposit & colluvium	Old Rock Bridge	American River		not used to develop bound				Folsom Dam	Detailed

Sample name	Date	Error	Cal yr B.P. (oldest age)	Cal yr B.P. (youngest age)	Sample depth (cm)	Sample weight (g)	Material	Landform	soil horizon	Date relevance	Site name	River name	No. of floods	Bound age (max)	Bound age (min)	Bound Qmax (ft³/s)	Bound Qmin (ft³/s)	Facility	Level of study
BR3-2-2PI	180	50	310 40	60 10	125	0.007	Pinus charcoal	terrace	Btj	Flood deposit & colluvium	Old Rock Bridge	American River	not used to develop bound					Folsom Dam	Detailed
AC1-8TS	2640	80	2940	2460	50-60 (below datum)	0.17	Tsuga charcoal	terrace	Bwb	Flood deposit	Alder Creek	South Fork American River	not used to develop bound					Folsom Dam	Detailed
SF1-1-2COB	30	40	125 70	115 35	35-43	0.03	Conifer bark (charred)	terrace	Abb	flood deposit	Sand Flat	South Fork American River	2 to 5	650	na	49000	32000	Folsom Dam	Detailed
SF1-1-3AC	140	40	285	0	53-60	0.06	Arctostaphylos charcoal	terrace	Cb	flood deposit	Sand Flat	South Fork American River	2 to 5	650	na	49000	32000	Folsom Dam	Detailed
SF1-2-2PI	330	40	490	295	42	0.13	Pinus charcoal	terrace	Bwb2	flood deposit	Sand Flat	South Fork American River	1 or more	1125	650	81000	67000	Folsom Dam	Detailed
SF1-2-3AC	1110	40	1075	940	74-82	0.03	Arctostaphylos charcoal	terrace	Bw2b2	flood deposit	Sand Flat	South Fork American River	1 or more	1125	650	81000	67000	Folsom Dam	Detailed
SF1-2-3PI	1630	40	1580	1410	74-82	0.12	Pinus charcoal	terrace	Bw2b2	flood deposit	Sand Flat	South Fork American River	not used to develop bound					Folsom Dam	Detailed
SF1-3-1PI	720	40	700 585	640 575	29-35	0.06	Pinus charcoal	terrace	AB	flood deposit	Sand Flat	South Fork American River	1 or more	1125	650	81000	67000	Folsom Dam	Detailed
SF1-3-2ACS	50	40	255 135	225 30	35-50	0.01	Arctostaphylos seed (charred)	terrace	2AB	flood deposit	Sand Flat	South Fork American River	1 or more	1125	650	81000	67000	Folsom Dam	Detailed
SF1-3-2PIB	2100	40	2145	1945	35-50	0.01	Pinus bark scale (charred)	terrace	2AB	flood deposit	Sand Flat	South Fork American River	not used to develop bound					Folsom Dam	Detailed
SF1-4-1PIB	600	40	605	530	40-55	0.05	Pinus bark scale (charred)	terrace	Bwb	flood deposit	Sand Flat	South Fork American River	1 or more	1650	1380	81000	67000	Folsom Dam	Detailed
SF1-4-1AL	440	50	550	310	40-50	<0.01	Alnus charcoal	terrace	Bwb	flood deposit	Sand Flat	South Fork American River	1 or more	1650	1380	81000	67000	Folsom Dam	Detailed
SF1-4-1PI	2220	40	2330	1775	40-50	0.11	Pinus charcoal	terrace	Bwb	flood deposit	Sand Flat	South Fork American River	1 or more	1650	1380	81000	67000	Folsom Dam	Detailed
SF1-4-2PI	1540	40	1520	1330	65-85	0.05	Pinus charcoal	terrace	Coxb	flood deposit	Sand Flat	South Fork American River	1 or more	1650	1380	81000	67000	Folsom Dam	Detailed
SF2-1-3AL	130	40	280	0	26	0.3	Alnus charcoal	terrace	ABb	flood deposit	Sand Flat	South Fork American River	2 to 5	650	na	49000	32000	Folsom Dam	Detailed

Sample name	Date	Error	Cal yr B.P. (oldest age)	Cal yr B.P. (youngest age)	Sample depth (cm)	Sample weight (g)	Material	Landform	soil horizon	Date relevance	Site name	River name	No. of floods	Bound age (max)	Bound age (min)	Bound Qmax (ft³/s)	Bound Qmin (ft³/s)	Facility	Level of study
SF2-1-4PIB	260	40	430 320 180 10	380 275 150 0	32	4.77	Pinus bark (charrred)	terrace	Coxb	flood deposit	Sand Flat	South Fork American River	2 to 5	650	na	49000	32000	Folsom Dam	Detailed
SF2-1-5PI	280	30	430 320	380 285	37	<0.01	Pinus charcoal	terrace	Coxb/Bwb2 contact	flood deposit	Sand Flat	South Fork American River	2 to 5	650	na	49000	32000	Folsom Dam	Detailed
SF2-1-6AL	330	40	490	295	43-44	0.02	Alnus charcoal	terrace	Coxb2	flood deposit	Sand Flat	South Fork American River	2 to 5	650	na	49000	32000	Folsom Dam	Detailed
SF2-1-8PIB	440	30	525	465	44-64	1.4	Pinus bark (charred)	terrace	Coxb2	flood deposit	Sand Flat	South Fork American River	2 to 5	650	na	49000	32000	Folsom Dam	Detailed
SF2-1-8AL	270	40	435 325 175 5	365 375 150 0	44-64	0.22	Alnus charcoal	terrace	Coxb2	flood deposit	Sand Flat	South Fork American River	2 to 6	650	na	49000	32000	Folsom Dam	Detailed
RR1-2PIB	3260	60	3630	3360	150-170	6.34	Pinus bark	terrace	C?	Soil	Hell Hole Dam	Rubicon River	not used to develop bound					Folsom Dam	Detailed
RR1-2SXW	3350	60	3710	3400	150-170	0.89	Salix wood	terrace	C?	soil	Hell Hole Dam	Rubicon River	not used to develop bound					Folsom Dam	Detailed
MF1-2-4PI	60	50	270 150	200 10	125-130 (below datum)	0.1	Pinus charcoal	terrace	--	flood deposit	Oak Tree	Middle Fork American River	not used to develop bound					Folsom Dam	Detailed
MF2-2RH	70	50	270 145	195 10	180	<0.01	Rhamnus charcoal	terrace	Unit 4	flood deposit	Oak Tree	Middle Fork American River	not used to develop bound					Folsom Dam	Detailed
MF2-2PIN	110	60	285	0	180	<0.01	Pinus needle and pinus charcoal	terrace	Unit 4	flood deposit	Oak Tree	Middle Fork American River	not used to develop bound					Folsom Dam	Detailed
CR1-1-1RH	140	40	285	0	14-25	0.81	Rhamnus charcoal	terrace	AB	soil	Michigan Bar	Consumnes River	not used to develop bound					Folsom Dam	Detailed
CR1-2-1RH	1060	40	1055	920	45-60	0.11	Rhamnus charcoal	terrace	Bt2	soil	Michigan Bar	Consumnes River	not used to develop bound					Folsom Dam	Detailed
CR1-2-2QU	540	50	640	500	45-75	0.01	Quercus charcoal	terrace	Bt2	soil	Michigan Bar	Consumnes River	not used to develop bound					Folsom Dam	Detailed
CR1-2-2RH	1490	50	1500	1295	45-75	0.03	Rhamnus charcoal	terrace	Bt2	soil	Michigan Bar	Consumnes River	not used to develop bound					Folsom Dam	Detailed
CR1-2-3QU	1880	50	1905	1705	75-90	0.01	Quercus charcoal	terrace	Bt2	soil	Michigan Bar	Consumnes River	not used to develop bound					Folsom Dam	Detailed

Sample name	Date	Error	Cal yr B.P. (oldest age)	Cal yr B.P. (youngest age)	Sample depth (cm)	Sample weight (g)	Material	Landform	soil horizon	Date relevance	Site name	River name	No. of floods	Bound age (max)	Bound age (min)	Bound Qmax (ft³/s)	Bound Qmin (ft³/s)	Facility	Level of study
CR1-2-3RH	290	60	490 / 195 / 10	270 / 145 / 0	75-90	0.03	Rhamnus charcoal	terrace	Bt2	soil	Michigan Bar	Consumnes River	not used to develop bound					Folsom Dam	Detailed
CR1-2-4RH	280	50	465 / 180 / 10	275 / 150 / 0	90-125	0.03	Rhamnus charcoal	terrace	BC	soil	Michigan Bar	Consumnes River	not used to develop bound					Folsom Dam	Detailed
MR1-2CO	500	50	650	460	--	0.01	Conifer charcoal	terrace	--	soil	Mokelumne Hill	Mokelumne River	not used to develop bound					Folsom Dam	Detailed
CF1-1-1PIB	100.1	0.6	Modern	Modern	22	0.88	Pinus bark	terrace	C	soil	Clarks Flat	Middle Fork Stanislaus River	not used to develop bound					Folsom Dam/New Melones Dam	Detailed
CF1-1-2AB	190	60	310	0	52	0.13	Abies charcoal	terrace	3B	soil	Clarks Flat	Middle Fork Stanislaus River	not used to develop bound					Folsom Dam/New Melones Dam	Detailed
CF1-1-3PIW	50	40	255 / 135	225 / 30	41-50	26.76	Pinus wood	terrace	3B	soil	Clarks Flat	Middle Fork Stanislaus River	not used to develop bound					Folsom Dam/New Melones Dam	Detailed
CF1-1-4VIS	125.3	0.6	Modern	Modern	41-76	?	Vitis seed	terrace	3B	soil	Clarks Flat	Middle Fork Stanislaus River	not used to develop bound					Folsom Dam/New Melones Dam	Detailed
CF1-2-1PI	99.9	0.6	Modern	Modern	30-53	0.49	Pinus charcoal	terrace	2Bb	soil	Clarks Flat	Middle Fork Stanislaus River	not used to develop bound					Folsom Dam/New Melones Dam	Detailed
CF1-4-1CO	1230	60	1280	990	23-47	0.03	Conifer charcoal	terrace	Ab	soil	Clarks Flat	Middle Fork Stanislaus River	not used to develop bound					Folsom Dam/New Melones Dam	Detailed
CF1-4-2QU	2070	60	2290 / 2150	2270 / 1870	47-78	0.05	Quercus charcoal	terrace	Bwb	soil	Clarks Flat	Middle Fork Stanislaus River	not used to develop bound					Folsom Dam/New Melones Dam	Detailed
SR1-2-2PIB	2890	60	3210	2850	20-25	0.13	Pinus bark	terrace	A2b	soil	Clarks Flat	Stanislaus River	not used to develop bound					Folsom Dam/New Melones Dam	Detailed
SR1-2-3CO	2360	50	2750	2150	40-45	0.02	Conifer charcoal	terrace	Bwb	soil	Clarks Flat	Stanislaus River	not used to develop bound					Folsom Dam/New Melones Dam	Detailed
SR1-C2	1799	22	1820 / 1660	1690 / 1630	48-65	--	Microcharcoal	terrace	C2	soil	Coyote Reach	San Joaquin River	0	2400	1000	140000	105000	Friant Dam	Detailed
SR1-C3	2208	45	2340	2120	65-85	--	Microcharcoal	terrace	C3	soil	Coyote Reach	San Joaquin River	0	2400	1000	140000	105000	Friant Dam	Detailed
SR2-C2	197	17	290 / 220 / 20	270 / 140 / -11	40-70	0.0041	Salicaceae charcoal	terrace	C2	soil	Skaggs Bridge Reach	San Joaquin River	not used to develop bound					Friant Dam	Detailed
SR2-5	1.5468	0.0049	Modern	Modern	140	1.559	Pseudotsuga menziesii wood	terrace	C4	soil	Skaggs Bridge Reach	San Joaquin River	not used to develop bound					Friant Dam	Detailed

Sample name	Date	Error	Cal yr B.P. (oldest age)	Cal yr B.P. (youngest age)	Sample depth (cm)	Sample weight (g)	Material	Landform	soil horizon	Date relevance	Site name	River name	No. of floods	Bound age (max)	Bound age (min)	Bound Qmax (ft³/s)	Bound Qmin (ft³/s)	Facility	Level of study
SR3-Bw2	1187	38	1180	1060	35-70	--	Microcharcoal	terrace	Bw2	soil	Skaggs Bridge Reach	San Joaquin River	0	0	2400	1000	140000	Friant Dam	Detailed
SR3-Bw3	2106	19	2125	2045	70-110	--	Microcharcoal	terrace	Bw3	soil	Skaggs Bridge Reach	San Joaquin River	0	0	2400	1000	140000	Friant Dam	Detailed
SR4-Ab	297	25	460	290	79-110	0.0021	Salicaceae charcoal	terrace	Ab	flood deposit	Coyote Reach	San Joaquin River	1	1050	900	110000	44000	Friant Dam	Detailed
SR4-2	347	24	490	310	110	0.0019	Salicaceae charcoal	terrace	Ab	flood deposit	Coyote Reach	San Joaquin River	6	550	350	110000	44000	Friant Dam	Detailed
SR5-2	1014	24	980 / 850	900 / 830	60-80	0.0007	Conifer charcoal	Slackwater bench	Cox	flood deposit	Horseshoe Bend	San Joaquin River	1	1040	890	110000	73000	Friant Dam	Detailed
SR6-1	162	28	290 / 230 / 120 / 40	240 / 130 / 70 / -11	160-170	0.0026	Salicaceae charcoal	Slackwater bench	Ab	flood deposit	Horseshoe Bend	San Joaquin River		not used to develop bound				Friant Dam	Detailed
Northern California region																			
TP1-1PI	145	15	280 / 230 / 150 / 40	250 / 170 / 130 / 10	58	0.17	Pinus charcoal	colluvium	C	colluvium	Clear Creek at Tower House	Clear Creek		not used to develop bound				Whiskeytown Dam	Detailed
TP1-6SA	130	15	270 / 150	180 / 10	22	0.067	Salicaceae charcoal	colluvium	C	colluvium	Clear Creek at Tower House	Clear Creek		not used to develop bound				Whiskeytown Dam	Detailed
TP2-1QU	645	15	670 / 600	630 / 560	29	0.061	Quercus charcoal	terrace	2C	flood deposit	Clear Creek at Tower House	Clear Creek	1 or more	700	500	22000	22000	Whiskeytown Dam	Detailed
TP2-8PS	565	15	635 / 565	595 / 535	40	0.022	Pseudotsuga menziesii charcoal	terrace	2C	flood deposit	Clear Creek at Tower House	Clear Creek	1 or more	700	500	22000	22000	Whiskeytown Dam	Detailed
TP4-3PI	195	15	290 / 190 / 20	270 / 150 / 11	80	0.087	Pinus charcoal	terrace	2Cb2	soil	Clear Creek at Peltier Campground	Clear Creek		not used to develop bound				Whiskeytown Dam	Detailed
TP4-6BK	140	15	280 / 160 / 40	170 / 60 / 1	43	1.14	rounded, slightly charred bark	terrace	B2	soil	Clear Creek at Peltier Campground	Clear Creek		not used to develop bound				Whiskeytown Dam	Detailed
TP5-1RO	3970	15	4520 / 4450	4470 / 4410	45	0.015	Rosaceae charcoal	terrace	B2	soil	Clear Creek at NEED Camp	Clear Creek	0	4500	3300	46000	35000	Whiskeytown Dam	Detailed
TP5-2RO	3095	15	3370	3260	70	0.037	Rosaceae charcoal	terrace	B2	soil	Clear Creek at NEED Camp	Clear Creek	0	4500	3300	46000	35000	Whiskeytown Dam	Detailed

Sample name	Date	Error	Cal yr B.P. (oldest age)	Cal yr B.P. (youngest age)	Sample depth (cm)	Sample weight (g)	Material	Landform	soil horizon	Date relevance	Site name	River name	No. of floods	Bound age (max)	Bound age (min)	Bound Qmax (ft^3/s)	Bound Qmin (ft^3/s)	Facility	Level of study
TP6-2QU	365	15	500 / 380	420 / 320	36	0.025	Quercus charcoal	colluvium	2Bt2	soil	Clear Creek at NEED Camp	Clear Creek		not used to develop bound				Whiskeytown Dam	Detailed
ECR1-6	950	15	930 / 880	890 / 790	18	0.058	Quercus charcoal	terrace	Bt	soil	Eagle Creek Ranch	Trinity River	0	2720	790	56500	44500	Trinity Dam	Detailed
ECR1-3	2490	15	2720	2480	40	0.646	Quercus charcoal	terrace	Bt2b	soil	Eagle Creek Ranch	Trinity River	0	2720	790	56500	44500	Trinity Dam	Detailed
ECR1-7	2475	15	2710 / 2620	2630 / 2460	60	0.013	Quercus charcoal	terrace	Cox	soil	Eagle Creek Ranch	Trinity River	0	2720	790	56500	44500	Trinity Dam	Detailed
ECR2-4	4005	15	4520 / 4455	4460 / 4420	36	0.064	Pinus charcoal	terrace	B2	soil	Eagle Creek Ranch	Trinity River	0	4520	2120	53500	42000	Trinity Dam	Detailed
ECR2-6	2175	15	2310 / 2190	2230 / 2120	22-26	0.046	Pinus charcoal	terrace	B2	soil	Eagle Creek Ranch	Trinity River	0	4520	2120	53500	42000	Trinity Dam	Detailed
ECR4-4	1015	15	965	920	32	0.023	Fraxinus charcoal	terrace	Bt	soil	Eagle Creek Ranch	Trinity River	0	5020	920	50500	40500	Trinity Dam	Detailed
ECR4-6	4455	15	5280	5160	34	0.009	Alnus charcoal	terrace	Bt2	soil	Eagle Creek Ranch	Trinity River	0	5020	920	50500	40500	Trinity Dam	Detailed
LOW1-2	430	15	520	480	30	0.011	Pinus charcoal	terrace	A/Cox contact	flood deposit	Lowden Ranch	Trinity River	1	520	480	71600	71600	Trinity Dam	Detailed
LOW2-3	690	15	680 / 590	650 / 560	43	0.016	Cercocarpus charcoal	terrace	C (unit 1)	soil	Lowden Ranch	Trinity River		not used to develop bound				Trinity Dam	Detailed
LOW2-5	920	15	920	790	23	0.006	Conifer charcoal	terrace	2C	soil	Lowden Ranch	Trinity River		not used to develop bound				Trinity Dam	Detailed
STF1-2	195	15	290	260	24	0.004	Quercus charcoal	terrace	Bt1	soil	Steiner Flat	Trinity River		not used to develop bound				Trinity Dam	Detailed
SBC1-5	1300	15	1290 / 1210	1230 / 1180	33	0.005	Quercus charcoal	terrace	Bt1	soil	Steel Bridge Campground	Trinity River	0	1290	1180	97000	90000	Trinity Dam	Detailed
SBC2-2	2685	15	2845 / 2800	2805 / 2750	92-117	0.02	Conifer charcoal	terrace	BC	soil	Steel Bridge Campground	Trinity River		not used to develop bound				Trinity Dam	Detailed
JCC1-2	265	15	430 / 320	400 / 280	51	0.005	Pinus bark scale charcoal	terrace	3Ab	soil	Junction City Campground	Trinity River	1	430	280	71600	71600	Trinity Dam	Detailed
JCC1-3	195	15	290 / 220 / 20	260 / 140 / -11	31	0.085	Pseudotsuga menziesii charcoal	terrace	2C	soil	Junction City Campground	Trinity River		not used to develop bound				Trinity Dam	Detailed
JCC1-5	190	20	290 / 220 / 20	260 / 140 / -11	13	0.019	Asteraceae charcoal	terrace	C	soil	Junction City Campground	Trinity River		not used to develop bound				Trinity Dam	Detailed
LS1-6	160	15	290 / 230 / 30	250 / 130 / -1	40	0.0046	Rosaceae twig charcoal	T3 terrace	Cb	flood deposit	LS1	Little Stony Creek	3	120	40	10000	8000	East Park Dam	Intermed

Sample name	Date	Error	Cal yr B.P. (oldest age)	Cal yr B.P. (youngest age)	Sample depth (cm)	Sample weight (g)	Material	Landform	soil horizon	Date relevance	Site name	River name	No. of floods	Bound age (max)	Bound age (min)	Bound Qmax (ft³/s)	Bound Qmin (ft³/s)	Facility	Level of study
LS1-7	135	15	280 150 40	170 60 10	75	0.0447	Salix charcoal	T3 terrace	Cb	flood deposit	LS1	Little Stony Creek	3	120	40	10000	8000	East Park Dam	Intermed
LS1-1	190	15	290 220 20	260 140 -11	210	0.0176	Cercocarpus charcoal	T3 terrace	2Cb	flood deposit	LS1	Little Stony Creek	3	120	40	10000	8000	East Park Dam	Intermed
LS3-2	975	15	940 870	900 800	50	0.0017	Rhamnaceae charcoal	T2 terrace	Bw	soil	LS3	Little Stony Creek	0	1360	860	48000	42000	East Park Dam	Intermed
LS3-6	1320	15	1290	1260	120	0.0043	Quercus charcoal, vitrified	T2 terrace	Bt	soil	LS3	Little Stony Creek	0	1360	860	48000	42000	East Park Dam	Intermed
LS4-2	435	15	520	485	30	0.0024	Asteraceae charcoal	T1 terrace	B1	soil	LS4	Little Stony Creek	not used to develop bound					East Park Dam	Intermed
LS4-6	565	15	635 565	595 535	38	0.0487	Juniperus charcoal	T1 terrace	B2	soil	LS4	Little Stony Creek	not used to develop bound					East Park Dam	Intermed
SK1-3AC	825	20	775	685	72	0.025	Arctostaphylos charcoal	terrace	2Btb	soil	SK1	Sacramento River	not used to develop bound					Keswick/Shasta Dam	Recon
SK1-5AE	1145	15	1130 1090	1100 970	55	0.019	Acer charcoal	terrace	Bt2b	soil	SK1	Sacramento River	not used to develop bound					Keswick/Shasta Dam	Recon
										Southern California Region									
Q0-1	2810	80	3150 3120 3090	3130 3090 2760	470	--	Detrital charcoal	slackwater deposit in trib	4C	soil?	Buell Flat t1	Santa Ynez River	0	3190	2800	104000	70000	Bradbury Dam	Detailed
Q0-2	60	60	270 150	180 10	40	--	Detrital charcoal	slackwater deposit in trib	A2	flood deposit	Buell Flat t1	Santa Ynez River	not used to develop bound					Bradbury Dam	Detailed
Q0-3	50	60	270 150	200 10	40	--	wood	slackwater deposit in trib	A2	flood deposit	Buell Flat t1	Santa Ynez River	not used to develop bound					Bradbury Dam	Detailed
FP2-2	190	70	430 320	390 0	155-173	--	Detrital charcoal	fp2 surface	C (UNIT 5)	soil	Acin fp2	Santa Ynez River	not used to develop bound					Bradbury Dam	Detailed
FP2-1	370	70	530	290	27-67	--	Detrital charcoal	fp2 surface	C (UNIT 5)	soil	Acinfp2	Santa Ynez River	not used to develop bound					Bradbury Dam	Detailed
FP2-1B	50	80	280 160	160 0	27-67	--	Detrital charcoal	fp2 surface	C (UNIT 5)	soil	Acinfp2	Santa Ynez River	not used to develop bound					Bradbury Dam	Detailed
Q0-4A	170	80	430	390	15-20	--	Detrital charcoal	fp2 surface	A1	soil	Rizzoli fp2 test pit 1	Santa Ynez River	not used to develop bound					Bradbury Dam	Detailed
Q0-4B	270	70	490 230 30	260 130 0	15-20	--	Detrital charcoal	fp2 surface	A1	soil	Rizzoli fp2 test pit 1	Santa Ynez River	not used to develop bound					Bradbury Dam	Detailed

Sample name	Date	Error	Cal yr B.P. (oldest age)	Cal yr B.P. (youngest age)	Sample depth (cm)	Sample weight (g)	Material	Landform	soil horizon	Date relevance	Site name	River name	No. of floods	Bound age (max)	Bound age (min)	Bound Qmax (ft³/s)	Bound Qmin (ft³/s)	Facility	Level of study
Q0-5	700	90	780	530	85-110	--	Detrital charcoal	low terrace?	2C	flood deposit	Shannon fp2 test pit 3	Santa Ynez River	1	820	570	81000	60000	Bradbury Dam	Detailed
Q0-6	200	50	310 / 40	60 / 0	130-142	--	Detrital charcoal	floodplain bar fp2	A2b	soil	Crawford fp2 bar test pit	Santa Ynez River	not used to develop bound					Bradbury Dam	Detailed
Q0-7	1380	80	1410	1160	120-135	--	Detrital charcoal	t1 terrace	C1	soil	Crawford hay barn t1 test pit	Santa Ynez River	not used to develop bound					Bradbury Dam	Detailed
Q0-8	430	50	540 / 390	430 / 320	85	--	Detrital charcoal	t1 terrace	Bt2	soil	Crawford t1 test pit	Santa Ynez River	not used to develop bound					Bradbury Dam	Detailed
Q0-9	340	80	520 / 180 / 10	270 / 150 / 0	105	--	Detrital charcoal	t1 terrace	Bt3	soil	Crawford t1 test pit	Santa Ynez River	not used to develop bound					Bradbury Dam	Detailed
Q0-10	1600	80	1690 / 1630	1650 / 1310	160-190	--	Detrital charcoal	t1 terrace	Bt3	soil	Crawford t1 test pit	Santa Ynez River	not used to develop bound					Bradbury Dam	Detailed
Q0-11	1760	60	1820	1530	160-190	--	Detrital charcoal	t1 terrace	Bt3	soil	Crawford t1 test pit	Santa Ynez River	not used to develop bound					Bradbury Dam	Detailed
Racetrack 1	855	125	980 / 610	630 / 560	--	--	Bulk sample	fp2 surface	?	soil	Rancho Chahuchu fp2	Santa Ynez River	not used to develop bound					Bradbury Dam	Detailed
Racetrack 2	1820	130	2010	1410	--	--	Bulk sample	fp2 surface	?	soil	Rancho Chahuchu fp2	Santa Ynez River	not used to develop bound					Bradbury Dam	Detailed
Westside San Joaquin Valley Region																			
LB1-1PL	180	40	300 / 230 / 40	240 / 70 / 0	24	0.012	Platanus racemosa charcoal	T3 deposit	Bk	flood deposit	LB1	Los Banos Creek	1	300	150	13700	10800	Los Banos Dam	Detailed
LB1-3FR	240	40	420 / 320 / 200 / 20	390 / 270 / 150 / 0	55-67	0.026	Fraxinus charcoal	T3 deposit	Bkb (hearth)	flood deposit	LB1	Los Banos Creek	1	300	150	13700	10800	Los Banos Dam	Detailed
LB2-4PL	110	40	280 / 150	170 / 0	45-50	0.01	Platanus racemosa charcoal	T3 deposit	Bkb	flood deposit	LB2	Los Banos Creek	1	300	150	13700	10800	Los Banos Dam	Detailed
LB3-3QU	330	40	490	300	62	0.004	Quercus charcoal	T3 deposit	2Bkb	flood deposit	LB3	Los Banos Creek	1	300	150	13700	10800	Los Banos Dam	Detailed
LB3-7AS	160	40	290	0	55-60	0.03	Asteraceae twig charcoal	T3 deposit	2Bkb	flood deposit	LB3	Los Banos Creek	1	300	150	13700	10800	Los Banos Dam	Detailed
LPC1-1Y	890	40	920	710	75	0.021	gastropod shell	terrace	Bk3/Ab contact	soil	LPC1	Little Panoche Creek	not used to develop bound					Little Panoche Dam	Recon
LPC1-5Y	2580	40	2760 / 2560	2710 / 2540	240	0.087	gastropod shell	terrace	Cb2?	soil	LPC1	Little Panoche Creek	not used to develop bound					Little Panoche Dam	Recon

Sample name	Date	Error	Cal yr B.P. (oldest age)	Cal yr B.P. (youngest age)	Sample depth (cm)	Sample weight (g)	Material	Landform	soil horizon	Date relevance	Site name	River name	No. of floods	Bound age (max)	Bound age (min)	Bound Qmax (ft³/s)	Bound Qmin (ft³/s)	Facility	Level of study
LPC1-7Y	1010	40	970 / 850	900 / 810	90	0.064	gastropod shell	terrace	Bkb	soil	LPC1	Little Panoche Creek	not used to develop bound					Little Panoche Dam	Recon
CC1-2MIX	1140	60	1180	930	70-80	<0.02	Arctostaphylos and Rhamnus charcoal	T3y deposit	Abk	soil	Bench Mark 819	Cantua Creek	0	1000	500	9890	6360	Cantua Stream Group	Detailed
CC2-2AC	530	60	650	470	45-50	0.05	Arctostaphylos charcoal	T3y deposit	AB	soil	Bench Mark 819	Cantua Creek	0	1000	500	9890	6360	Cantua Stream Group	Detailed
CC2-3AT	410	60	530	310	70-75	0.02	Atriplex charcoal	T3y deposit	BCk	soil	Bench Mark 819	Cantua Creek	0	1000	500	9890	6360	Cantua Stream Group	Detailed
CC2-5RH	570	60	660	510	140-145	0.06	Rhamnus charcoal	T3y deposit	C	soil	Bench Mark 819	Cantua Creek	0	1000	500	9890	6360	Cantua Stream Group	Detailed
CC2-7AC	1130	60	1170	930	265-270	0.04	Arctostaphylos charcoal	T3y deposit	C	soil	Bench Mark 819	Cantua Creek	0	1000	500	9890	6360	Cantua Stream Group	Detailed
CC3-2AC	870	60	920	670	60-75	0.02	Arctostaphylos charcoal	T3y deposit	C	soil	Bench Mark 819	Cantua Creek	0	1000	500	9890	6360	Cantua Stream Group	Detailed
CC3-3SX	410	60	530	310	92-94	0.08	Salix charcoal	T3y deposit	Bkb	soil	Bench Mark 819	Cantua Creek	0	1000	500	9890	6360	Cantua Stream Group	Detailed
CC3-4SX	390	60	520	300	111-113	0.37	Salix charcoal	T3y deposit	C	soil	Bench Mark 819	Cantua Creek	0	1000	500	9890	6360	Cantua Stream Group	Detailed
CC4-2AC	210	60	430 / 320	390 / 0	73-81	0.27	Arctostaphylos charcoal	T4 deposit	C	soil	Bench Mark 819	Cantua Creek	many	not used to develop bound				Cantua Stream Group	Detailed
CC5-1MIX	2070	70	2310 / 2160	2240 / 1830	30-45	<0.01	Arctostaphylos and Rhamnus charcoal	T3o deposit	BCk	soil	Cantua gage	Cantua Creek	0	2800	1500	14130	11300	Cantua Stream Group	Detailed
CC5-2AT	2650	60	2880 / 2630	2700 / 2490	60-75	0.02	Atriplex charcoal	T3o deposit	Bkb	soil	Cantua gage	Cantua Creek	0	2800	1500	14130	11300	Cantua Stream Group	Detailed
CC6-3PI	3530	60	3980 / 3930	3950 / 3630	100-115	0.04	Pinus charcoal	T2 deposit	3Bkb2	soil	Bench Mark 819	Cantua Creek	not used to develop bound					Cantua Stream Group	Detailed
CC6-4RH	3350	60	3710 / 3430	3450 / 3400	118-123	0.02	Rhamnus charcoal	T2 deposit	3Bkb2/ 3CBkb	soil	Bench Mark 819	Cantua Creek	not used to develop bound					Cantua Stream Group	Detailed
CC7-1AT	2590	60	2800	2460	67	0.02	Atriplex charcoal	T3o deposit	Bkb	soil	Roadcut	Cantua Creek	not used to develop bound					Cantua Stream Group	Detailed

Sample name	Date	Error	Cal yr B.P. (oldest age)	Cal yr B.P. (youngest age)	Sample depth (cm)	Sample weight (g)	Material	Landform	soil horizon	Date relevance	Site name	River name	No. of floods	Bound age (max)	Bound age (min)	Bound Qmax (ft³/s)	Bound Qmin (ft³/s)	Facility	Level of study
SC2-2MIX	790	60	910 / 840 / 590	860 / 640 / 570	45-60	<0.03	Arctostaphylos, Atriplex and Rhamnus charcoal	T3y deposit	BCk	soil	Salt Creek I damsite	Salt Creek	0	1000	500	4940	2830	Cantua Stream Group	Detailed
SC2-3AC	1030	60	1060	780	85-95	0.01	Arctostaphylos charcoal	T3y deposit	Acb	soil	Salt Creek I damsite	Salt Creek	0	1000	500	4940	2830	Cantua Stream Group	Detailed
SC2-4AC	1270	60	1300	1060	138	0.01	Arctostaphylos charcoal	T3y deposit	CBkb2	soil	Salt Creek I damsite	Salt Creek	0	1000	500	4940	2830	Cantua Stream Group	Detailed
SC3A-1AC	300	50	480 / 170 / 10	270 / 150 / 0	78	0.05	Arctostaphylos charcoal	T4 deposit	BCk	soil	Meanders	Salt Creek	many	not used to develop bound				Cantua Stream Group	Detailed
SC3B-1AT	160	50	290	0	53-54	0.03	Atriplex charcoal	T4 deposit	?	soil	Meanders	Salt Creek	many	not used to develop bound				Cantua Stream Group	Detailed
SC3C-2MIX	1760	60	1820	1530	50-75	<0.03	Arctostaphylos, Atriplex, and Rhamnus charcoal	T3y deposit	Bk/Bkz	soil	Meanders	Salt Creek	0	not used to develop bound				Cantua Stream Group	Detailed
LG2-1-2AC	150	50	290	0	35-50	0.01	Arctostaphylos charcoal	T4 deposit	CBkb3	soil	Chevron property	Los Gatos Creek	many	not used to develop bound				Cantua Stream Group	Detailed
LG2-1-4MIX	270	50	470	270	55-73	<0.03	Arctostaphylos and Atriplex charcoal	T4 deposit	C	soil	Chevron property	Los Gatos Creek	many	not used to develop bound				Cantua Stream Group	Detailed